UNIVERSITÀ DEGLI STUDI FIRENZE

DOTTORATO DI RICERCA

INTERNATIONAL DOCTORATE IN STRUCTURAL BIOLOGY

CICLO XXVII

COORDINATORE Prof. Claudio Luchinat

Expression and purification of potential amyloidogenic proteins: Aβ peptides and hSOD1 to investigate the mechanisms of fibrils formation.

Settore Scientifico Disciplinare CHIM/03

Dottorando

Dott. Magdalena Korsak

Tutore

Dr. Tatiana Kozyreva

Coordinatore

Prof. Claudio Luchinat

Anni 2012/2014

This thesis has been approved by the University of Florence, the University of Frankfurt and the Utrecht University

Universiteit Utrecht

CERM Firenze

FRANKFURT AM MAIN

Contents

Preface

One of the major paradigms in structural biology, according to which a rigid well-folded 3D structure is required for protein function, has clearly changed over the last decades. Recent studies show that some proteins despite the absence of a stable secondary or tertiary structure, play important roles in a number of biological processes, such as differentiation, transcription regulation, DNA condensation, mRNA processing, and apoptosis. Such proteins are known as intrinsically disordered proteins (IDPs) and are characterized by high flexibility and plasticity, that facilitate their interactions with a broad range of binding partners, such as proteins, membranes, nucleic acids and other molecules of biological relevance. (Uversky & Dunker, 2010). Intrinsically disordered proteins are also prone to misfolding and tend to evade normal clearance pathways. In turn, the combination of misfolding and lack of clearing mechanisms can result in aberrant processes, often associated with the onset of pathologies. In these cases, it is common to observe progressive protein aggregation into intracellular and/or extracellular deposits. The consequence is a diverse group of neurodegenerative disorders, each of which entails the aggregation of particular proteins in characteristic patterns and locations (Jucker & Walker, 2013).

Under some particular conditions (e.g. environmental change or mutation) even native folded proteins might lose theirs stable, biochemically functional forms, and for this reason they can be investigated by the same methodologies used for IDPs. Examples of such proteins are beta amyloid peptide (Aβ) (intrinsically disordered in the monomeric form) associated to the Alzheimer's disease (AD), and superoxide dismutase (SOD1) (which is intrinsically disordered in the reduced apo form) related to amyotrophic lateral sclerosis (ALS). These proteins are the main topics of this thesis.

In this work we will present detailed structural characterization of Aβ prefibrillar and fibrillar assemblies by Solid State Nuclear Magnetic Resonance (SSNMR) that is crucial for understanding Aβ precise mechanism aggregation pathways and identifying toxic Aβ species involved in Alzheimer's disease.

This thesis will demonstrate also attempt of reverting side effects caused by cisplatin, that is effectie drug strongly inhibiting process of SOD1 oligomerization. That could open a way toward a novel therapeutic strategies in amyotrophic lateral sclerosis (ALS), since the

clinical use of cisplatin is still limited cause of the development of neurotoxicity and others undesirable effects.

Chapter 1 Introduction

1.1 Neurodegenerative diseases. Protein folding and misfoding

Neurodegenerative diseases are defined as hereditary and sporadic conditions that leads to progressive dysfunction of nervous system. Progression in atrophy of the affected central or peripheral structures of the nervous system is slow and steady, with symptoms visible when many cells degenerate and die or fail to function properly. According to their phenotypic effects they can be divided into two subclasses: one related to problems with movements, and another one linked with deterioration of the memory, leading to dementia. These subclasses encompass such diseases as Alzheimer's disease and other dementias, brain cancer, degenerative nerve diseases, encephalitis, epilepsy, genetic brain disorders, head and brain malformations, hydrocephalus, stroke, Parkinson's disease, amyotrophic lateral sclerosis (ALS or Lou Gehrig's Disease), Huntington's disease, prion diseases and Hallervorden–Spatz disease.

Many of the well-known neurodegenerative diseases represent a set of proteinopathies. A common pathological feature of these neurodegeneration is deposition within neurons or in the brain parenchyma of pathogenic aggregates. These deposits are composed largely of misfolded specific proteins, in the form of amyloid fibrils or plaques, and seem to be directly related to neurotoxicity. Protein deposition diseases can be sporadic (85%), hereditary (10%) or transmissible (5%). The general principle of these disorders arise from the failure of a specific peptide or protein to adopt its native physiological function by changing their conformation, size or their three-dimensional shape resulting in self-association, elongation and precipitation in distinct brain areas. As a consequence of misfolding, the protein aggregates, losses native functions and becomes pathologically active. The risk of self-association and aggregation is associated with a genetic defect, aging, persistently high concentrations of the protein and it is greatly increased with proteins characterized by a high level of intrinsic disorder, that facilitates radical changes in their conformation (Bayer, 2013; Carrell & Lomas, 1997; Uversky, 2010).

Although progress in neuroscientific research is noticeable in the substantial understanding of the molecular bases of this devastating diseases, still the main question - what is the cause of neurodegeneration and how we cope with it? - remains unclear.

1.1.1 From Alzheimer's Disease to amyloid-β

Alzheimer's disease (AD) is a progressive neurodegenerative disorder named after the German physician Alois Alzheimer who first described the disease (Alzheimer, 1907).

A major pathological feature of AD is the accumulation of two types of proteinaceous inclusions: extracellular amyloid deposits – senile plaques in the cerebral cortex and vasculature – and intracellular neurofibrillary tangles in medial temporal lobe. Neurofibrillary tangles are composed of hyperphosphorylated tau (Grundke-Iqbal et al. 1986), while amyloid plaques contain in 90% the amyloid β-peptide (Aβ) (Glenner & Wong, 1984; Masters et al. 1985). The remaining 10% of amyloid plaques are composed of proteins from the apolipoprotein E class, lipids from membranes of degenerated portions of the intercommunicated nerve extensions called axons, metal ions such as Cu (I /II), Zn (II), Fe (II /III) and Al (III), and traces of other components from the extracellular liquid. Amyloid plaques fall into two broad morphological categories: diffuse and neuritic. Both plaque types are detectable with anti-Aβ antibodies, but only neuritic plaques are prominently stained by sheet-binding dyes such as Congo red and thioflavin S. Neuritic dystrophies are swollen and distorted processes of axonal or dendritic origin that radiate from the core of a neuritic plaque. They are detectable with antibodies against the amyloid precursor protein (APP), phospho-tau, neurofilaments and ubiquitin, indicating a disruption of protein transport and attempts to degrade this blockage. Progressive neuritic plaque deposition is a hallmark of AD. Neuritic plaque formation commonly begins in the neocortex and later affects the hippocampus and amygdala. By the end stage of the disease, neuritic plaques are present in the brainstem and other subcortical structures. It has been suggested that the presence and a substantial increase in diffuse plaque is associated with the preclinical stages of AD.

Surprisingly, amyloid plaques have been also found in cognitively normal individuals, where plaque burden does not correlate with memory decline. Although asymptomatic elderly people develop amyloid plaques, the quantity of amyloid is generally less than in AD patients (Aizenstein et al. 2008). This unexpected observation that Aβ is produced constantly throughout life as a physiologically normal metabolite generated in healthy people changed the common concept of AD (Hardy & Selkoe, 2002).

Several genetic factors have been found to be associated with AD. Missense mutations in the genes which encode for amyloid precursor protein, presenlin-1, presenlin-2 have been found to be linked with familial Alzheimer's disease. These observations led to the so-called "amyloid cascade hypothesis" (fig. 1), which proposes that the deposition of Aβ, principally

of Aβ42, that has a high tendency to aggregate by forming beta-sheet structures, would be the central trigger of the pathological changes observed in the brains of AD patients (Hardy & Higgins, 1992; Herrup, 2010). The amyloid cascade hypothesis proposes that accumulation in the brain of Aβ aggregates lead to a series of downstream events such as loss of neurons and white matter, oxidative and inflammatory damage, the cascade of tau-hyperphosphorylation, increased cytoskeleton flexibility, which in turn lead to energy failure and synaptic dysfunction and neuronal death.

Although the direct involvement of Aβ peptides in AD is well documented, the precise molecular mechanism of the neurotoxic effects and the mechanism of generation and oligomerization of Aβ peptides remains unclear. Moreover, there is still a significant gap between the site-specific structural information and the complex structural diversity of Aβ amyloids. All these uncertainties complicate identifying therapeutic targets for AD and cause that this disease is relentless and incurable. The current limited number of treatments for Alzheimer's disease merely address symptoms rather than the root causes.

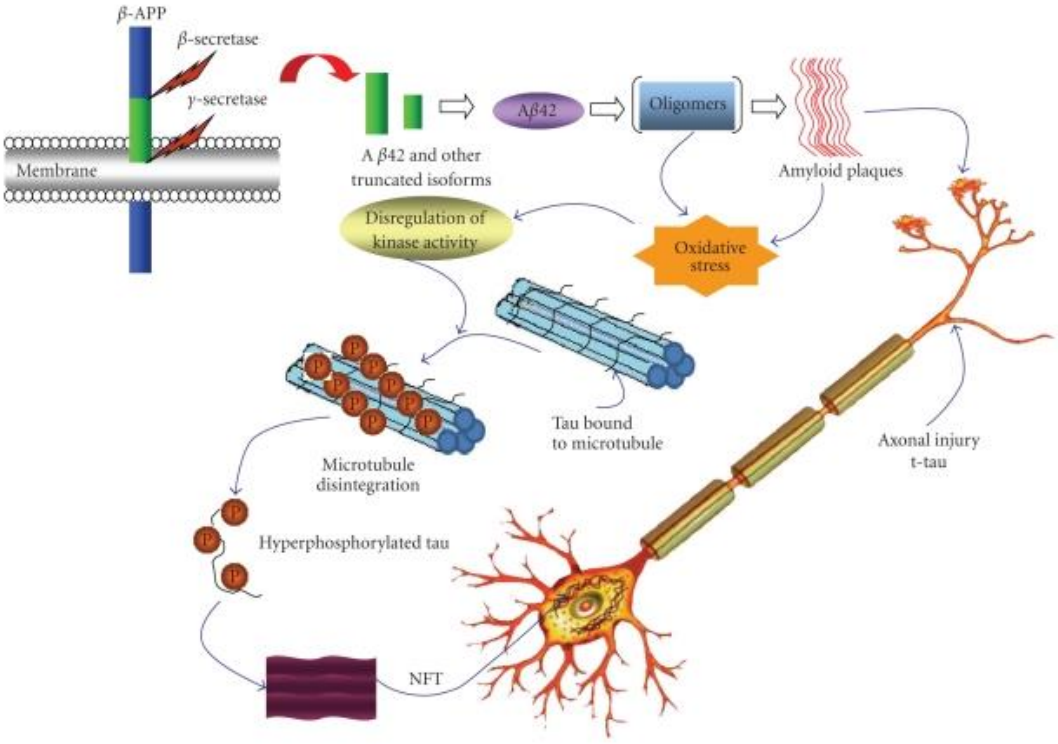

Figure 1. Pathological cascades hypothesis and potential biomarkers of AD. Adapted from (Anoop et al. 2010).

1.1.2 Pathology of ALS and implication to hSOD1

Amyotrophic lateral sclerosis (ALS or Lou Gehrig's Disease) is a neurodegenerative disorder characterized by the progressive dysfunction and degeneration of upper and lower motor neurons, which results in fatal paralysis.

The occurrence of ALS is predominantly (90%) sporadic without an obvious etiology. Approximately 10% of cases are referred as familial (fALS) and are inherited in a dominant manner. In 1993 it was suggested by the first time link between fALS and mutations in the gene that encodes the antioxidant enzyme copper-zinc superoxide dismutase (Rosen, 1993), and over 100 fALS-linked mutations, distributed throughout the SOD1 gene, are now associated with roughly 20% of the fALS cases (Andersen et al. 2006; Bruijn et al. 2004; Valentine et al. 2005). Sporadic and familial ALS deteriorate the same neurons with similar pathology and cause progressive muscle weakness, spasticity, hyperreflexia, muscle atrophy, and paralysis.

Although the causes of motor neuron death in ALS are poorly understood, a prominent hypothesis for SOD1-linked familial ALS involves the formation of protein aggregates containing misfolded hSOD1 as the main component in amyloid-like deposits. These components have been widely found both in the spinal cords of ALS patients (Jonsson et al 2004; Shibata et al. 1996) and in transgenic mice developing ALS (Bruijn et al. 1997; Johnston et al. 2000; Wang et al. 2002; Watanabe et al. 2001). The precursors of these protein aggregates are believed to be soluble oligomeric intermediates of the hSOD1 aggregation process. These oligomers are thought to be responsible for gain of toxic function, similar to what has been proposed for other neurodegenerative diseases (Mulligan & Chakrabartty 2013; Ross & Poirier 2004). Althought mechanism regard to cytotoxicity of SOD1 aggregates is not fully clear, various hypotheses include mitochondrial dysfunction (Hervias et al. 2006), impairment of axonal transport, oxidative stress, perturbations in Ca^{2+} homeostasis and glutamate excitotoxicity (Tortarolo et al. 2006).

However it is still an open question, whether the protein aggregates are the primary cause of ALS or a consequence and represent a defensive response aimed at protecting cells from the more toxic oligomeric species (Polymenidou & Cleveland, 2011).

1.2 Amyloid beta (Aβ) peptides

Amyloid beta (Aβ) peptides are a group of 37 to 43 amino acids peptides that are derived from the intramembranous proteolytic cleavage of the amyloid precursor protein (APP) (Haass & Selkoe, 2007). APP is a member of an evolutionarily conserved gene family with two mammalian homologs, amyloid precursor-like proteins (APLP) 1 and 2 (Wasco et al. 1992, 1993). These proteins contain highly similar sequences in their ectodomains and intracellular carboxy-termini, but the transmembrane region comprising the Aβ peptide is unique to APP (Bayer et al. 1999). Although its primary physiological function remains unclear, APP has been implicated in a variety of processes such as intracellular signalling, synapse adhesion, trophic support, axon remodelling and apoptosis (Zheng & Koo, 2011).

APP is processed via two major pathways that utilize different enzymes and result in distinct cleavage products (fig. 2). The non-amyloidogenic pathway precludes the formation of Aβ due to constitutive α-secretase-mediated cleavage in the middle of the Aβ domain (Esch et al. 1990). Alpha-cleavage of APP occurs mainly at the plasma membrane, releasing a soluble α-APP fragment (sAPPα) into the lumen/extracellular space and creating a membrane-bound, 83-residue C-terminal fragment (C83) (Sisodia, 1992). The presence of sAPPα is associated with normal synaptic signalling and results in synaptic plasticity, learning and memory, emotional behaviors and neuronal survival. Subsequent intramembranous cleavage of C83 by γ-secretase liberates a soluble, 3 kDa fragment (p3) and the APP intracellular domain (AICD) (Zheng & Koo, 2011). The p3 fragment is rapidly degraded, while the AICD may act as a transcriptional regulator.

The amyloidogenic processing of APP primarily occurs in the endocytic pathway. β-secretase initiates the sequence of amyloidogenic cleavage events. Cleavage of APP at the β-site generates a soluble amino-terminal fragment (sAPPβ) and a membrane-associated, 99-residue C-terminal fragment (C99). γ-secretase then performs a stepwise, intramembrane cleavage of the C99 fragment, releasing various isoforms of Aβ and the AICD. The most common Aβ isoforms are Aβ40, a 40 residues peptide, and Aβ42 which contains an extra isoleucine and alanine residues on the C-terminus. Aβ40 form is the more common of the two - under physiological conditions, the ratio of Aβ42 to Aβ40 is about 1:9, but Aβ42 has more hydrophobic nature, and thus its aggregative ability and neurotoxicity are much greater than those of Aβ40 (Jan et al. 2010; Walsh et al. 2009). Both of these forms (Aβ40 and Aβ42) are targets of intense study.

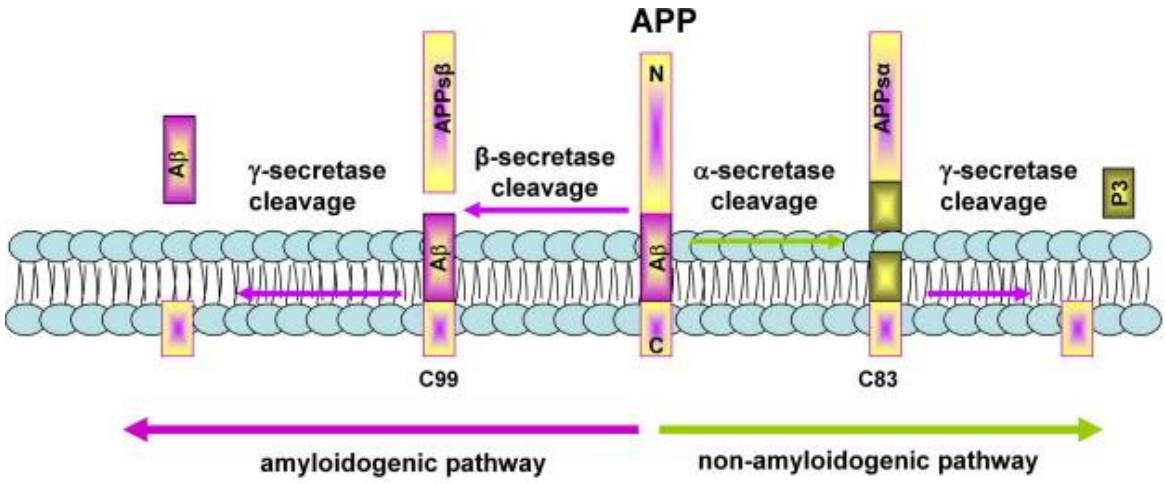

Figure 2. APP metabolism by the secretase enzymes. Adapted from (Barrantes et al. 2010).

1.2.1 Aβ polymorphism

Aβ is a heterogeneous mixture of peptides which exist in a complex equilibrium, sensitive to numerous external factors. Under distinct conditions Aβ molecules can spontaneously self-aggregate *in vitro* into different species, which are having different solubility, stability and biological and toxic properties (Jan et al. 2010) (fig. 3). Aβ peptides can form soluble oligomers and protofibrils, which could be intermediates of a fibrillation process (Benilova et al. 2012). Recent studies have revealed the high neurotoxicity of these species and their close links with AD, showing e.g. that soluble Aβ oligomers extracted from Alzheimer's disease brains potently impair synapse structure and function (Benilova et al. 2012; Chimon et al. 2007; Hoshi et al. 2003; Krafft & Klein, 2010; Kirkitadze et al. 2002; Lambert et al. 1998; Lesne´ et al. 2006; Noguchi et al. 2009; Selkoe, 2008; Shankar *et al*. 2008). Instead, the formation of amyloidal deposits consisting of Aβ fibrils is a pathological hallmark of AD. Although mature amyloid fibrils are sometimes described as being predominantly neutral (Aksenov et al. 1996), there is evidence in some recent reports that Aβ fibrils are also neurotoxic and that the progression of AD symptoms is correlated with the amount of these insoluble Aβ assemblies (Chimon et al. 2007; Lorenzo et al. 1994; Meyer-Luehmannet al. 2008; Petkova et al. 2005; Qiang et al. 2012; Selkoe et al. 2004; Walsh et al. 1999). In brain tissue, Aβ fibrils may initiate inflammation (Cameron & Landreth, 2010; Glass et al., 2010) or oxidative damage (Sultana et al., 2009; Tougu et al., 2011). Additionally fibrillar oligomers (which may be fibril fragments), but not non-fibrillar

oligomers, have been reported to be elevated in AD patients (Tomic et al. 2009), that highlights likely causative role of Aβ fibrils in AD. On the other hand, it is commonly reported that asymptomatic elderly people develop amyloid plaques, while only about 30% of octagenerians develop AD, suggesting that amyloid fibrils alone might not destroy neurons (Tycko, 2011). Therefore the identity of Aβ aggregates that contribute most to neurotoxicity and neurodegeneration in AD and their pathogenic mechanisms is still a subject of controversy.

Besides the different types of aggregates, the morphology of the same type of Aβ assemblies can also vary significantly depending on different aggregation conditions. This phenomenon is called polymorphism and has also been found in samples derived from AD patient brain tissues (Paravastu et al. 2009; Lu et al. 2013). Tissue from two Alzheimer's disease (AD) patients contained a single predominant 40-residue Aβ (Aβ40) fibril structure in each patient, but the structures in the two patients were different. A molecular structural model developed for Aβ40 fibrils from one patient reveals features that distinguish *in vivo* from *in vitro* fibrils (Lu et al. 2013). Furthermore, it has been shown that different structures of Aβ fibrils can cause changes in neurotoxicity, which clearly highlights that polymorphism, revealed as structural variations, is extremely pathological relevant (Petkova et al. 2005).

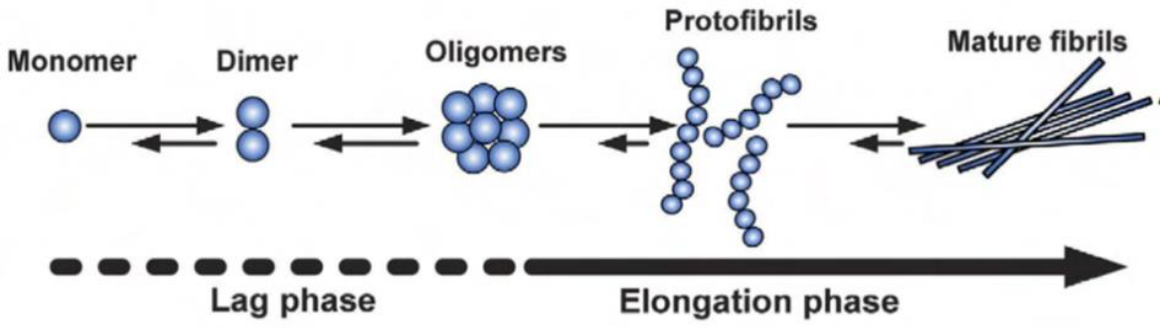

Figure 3. A putative schematic of aggregation of Aβ with two kinetic phases. In the lag phase monomers slowly form oligomers (dashed lines). In the elongation phase oligomers via protofibrils promote fibril formation (straight line). Adapted from (Kumar et al. 2011).

1.2.2 Overview of polymorphism and structural models of amyloidal fibrils

Mature amyloid fibrils, the terminal stage of the fibrillogenic pathway, largely exhibit polymorphism, which is demonstrated in variations in shapes at mesoscopic scale, as well as at the microscopic and supramolecular level. The polymorphism of Aβ fibrils was determined *in vitro* by numerous different structural studies. Cryo-electron microscopy (cryo-EM) (Fändrich et al. 2011; Meinhardt et al. 2009), and solid-state nuclear magnetic resonance (SSNMR) (Benzinger et al. 1998; Bertini et al. 2011a; Lansbury et al. 1995; Paravastu et al. 2008; Petkova et al. 2002, 2005, 2006; Qiang et al. 2011) in particular, revealed a large spectrum of Aβ40 fibrils polymorphisms, with molecular structures that depend on aggregation conditions. Aβ40 amyloid fibrils have been widely investigated and several structural models have recently been proposed using SSNMR (Bertini et al. 2011a, Paravastu et al. 2008; Petkova et al. 2002, 2006). A structural model of Aβ42 fibrils was proposed based on solution NMR and mutagenesis (Lührs et al. 2005).

In all these fibrillar assemblies Aβ molecules are densely packed in extended β-sheets (ladders), but exhibit polydispersed morphology and differ from one another in lengths and bundle widths. Mature fibrils possess a long, straight and highly regular morphology and are characterized by a specific filamentous structure and usually contain 2–6 protofilaments that are more than 1 μm long and 8–12 nm in diameter. They display a cross-β X-ray fiber diffraction pattern as well as stainability with Congo red, resulting in green birefringence and exhibit positive Thioflavin-T binding response (Merz et al. 1983; Petkova et al. 2005; Serpell, 2000). It is widely accepted that amyloid fibrils are insoluble deposits, but recent studies have shown that many biochemical factors, e.g. biological lipids, are able to efficiently revert the fibrillation process and convert these insoluble assemblies into soluble, highly toxic intermediate species (Martins et al. 2008).

Experiment-based, several different Aβ40 and Aβ42 fibrils models demonstrate that the distinct polymorphism of fibrillar assemblies is reflected in variations in the overall structural symmetry (twofold vs. threefold), differences in specific aspects of structural elements, conformations and various residue sites, as well as in the nature of β-sheet structures including topologies of the β1-turn-β2 motif and inter-protofilament contacts (Ahmed et al. 2010; Bertini et al. 2011a; Lührs et al. 2005; Paravastu et al. 2008; Petkova et al. 2006) (fig. 4). All this models suggest that the Aβ molecule adopts a U-shaped protofilament structure, which hydrogen-bonds with identical molecules to form a pair of inregister, parallel β-sheets. However, the models differ in the precise location of the U-turn

in the sequence, as well as in the specific interactions between distal regions. The inter-β-strand contacts within the U-shaped β-strand-turn-β-strand motif might be shifted in each fibril models, demonstrating that polymorphism is present at the protofilament level (Colletier et al. 2011). Recent studies have also shown that, in Aβ fibrils carrying mutants, both parallel and anti-parallel registry can occur (Qiang et al. 2011). Although the structural polymorphism of Aβ40 fibrils was initially described as taking place mainly at the supramolecular level (Paravastu et al. 2008), a recent structural model of mature Aβ fibrils (Bertini et al. 2011a) suggests that polymorphism can already originate at the level of the N-terminal conformation. The N-terminal part of the peptide in the fibril model can adopt β_N-strand, but there is also evidence in the literature that a disordered conformation on the N-terminal part in some other Aβ fibrils is also possible (Paravastu et al. 2008; Petkova et al. 2006; Sachse et al. 2008, 2010). Therefore the N-terminal part of Aβ40 peptides can adopt distinct conformations and thereby also contribute to structural diversity.

It is reasonable to speculate that the folding of the monomer, the coexistence of multiple nucleation processes (each leading to a different fibril structure), and supramolecular packing (within and among protofilaments) are linked or even define the different morphology of amyloid fibrils through structural duplication/propagation along the fibril axis similar to the growth of 1D nanomaterials (Bertini et al. 2011a). Polymorphism of Aβ fibrils formation might be also attributed to the comparably high thermodynamic stabilities of distinct polymorphs, and the low rates of dissociation of peptide monomers or soluble species from fibrils (Qiang et al. 2013). Finally it is worth to mention that such multiplicity of Aβ species is derived not only from native biological variation, but also from the different techniques used to generate such species *in vitro* or to isolate them from brain tissue. The predominant discrepancies in morphology in Aβ40 fibril samples can be result of changes in growth conditions, specifically the presence or absence of gentle agitation of the peptide solution during fibril formation. Quiescent growth leads to fibrils with the morphology of "twisted pairs" (Paravastu et al. 2008), instead gentle agitation results in striated ribbons (Petkova et al. 2006) (fig. 5). The overall symmetry with which cross-β units are arranged is the difference between them. The "twisted pair" protofilament contains three cross-β units, related by an approximate three-fold rotational symmetry axis, whereas the "striated ribbon" protofilament contains two cross-β units, related by an approximate two-fold rotational symmetry axis that coincides with the long axis of the protofilament. Difference is also

observable in the conformation of 23-29 residues and sidechain-sidechain contacts between cross-β units (Tycko, 2011).

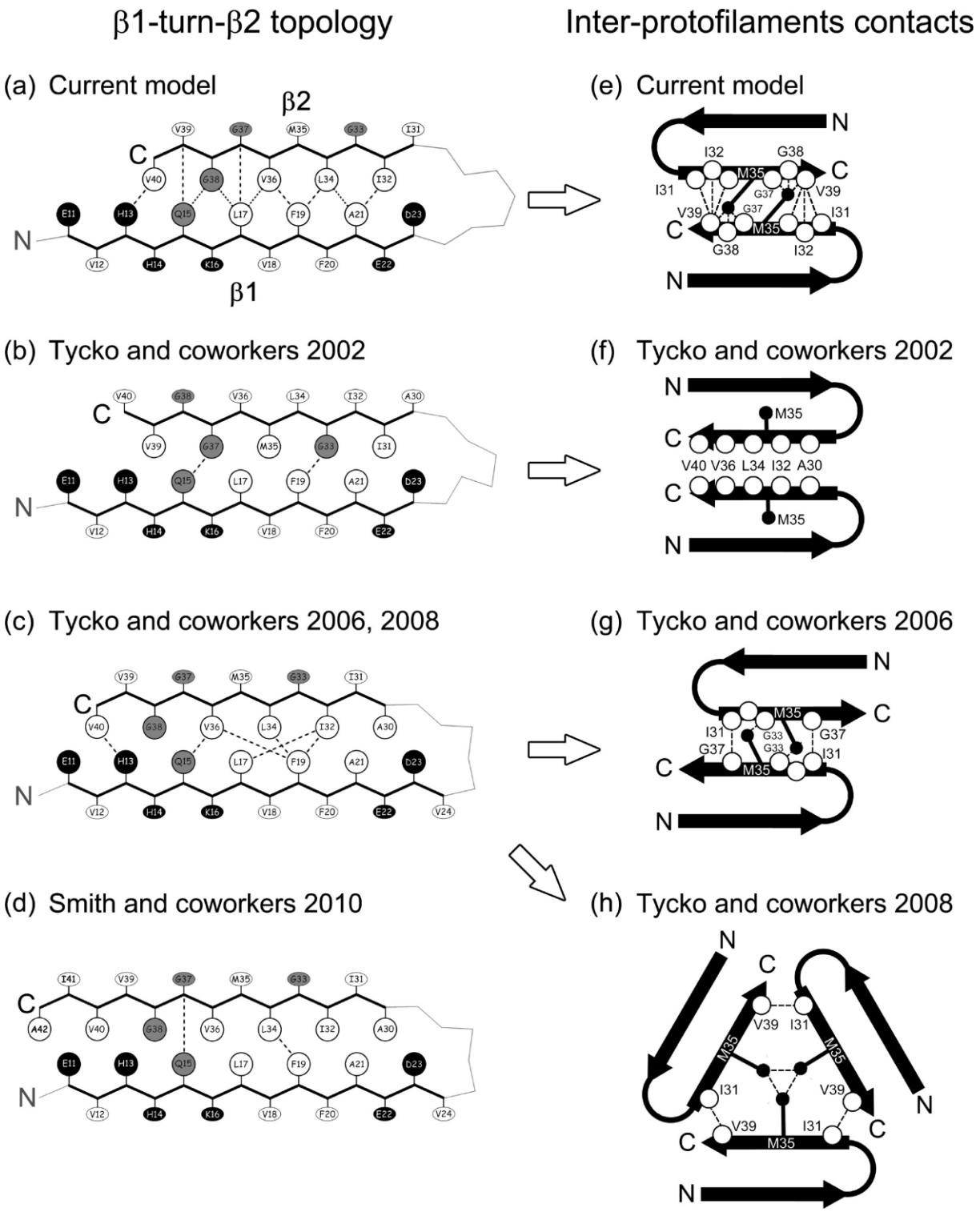

Figure 4. Different topologies of β1-turn-β2 motif (left column) and inter-protofilament contacts (right column) in various SSNMR-derived structural models of Aβ fibrils ((a)Bertini et al. 2011a ; (b) Petkova et al. 2002; (c) Petkova et al. 2006; Paravastu et al. 2008; (d) Ahmed et al. 2010)). Adapted from (Bertini et al. 2011a).

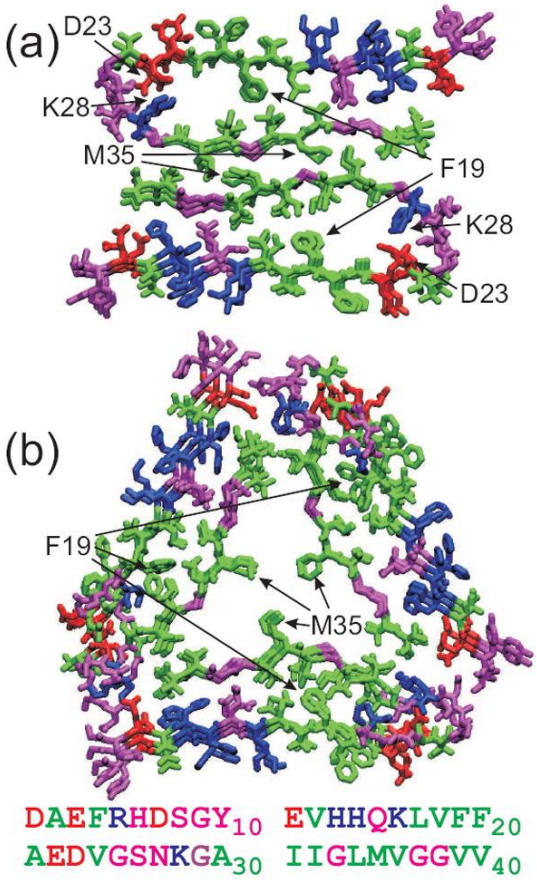

Figure 5. Molecural structural model for a) striated-ribbon and b) twisted pair Aβ40 fibrils. Adapted from (Tycko 2011).

1.2.3 Intermediate amyloidal species

Intermediates amyloidal species e.g. oligomers, protofibrils, Aβ-derived diffusible ligands (ADDLs), as well as Aβ annular assemblies are likely involved in amyloid fibril formation. Various studies had reported that the neurotoxicity of Aβ peptides might be ascribed to these pre-fibrillar assemblies (Benilova et al. 2012; Chimon et al. 2007; Hoshi et al.2003; Kirkitadze et al, 2002; Krafft and Klein, 2010; Lambert et al. 1998; Lesne´ et al. 2006; Noguchi et al. 2009; Selkoe, 2008) as a consequence of their structural flexibility and their hydrophobic exposure. Therefore the high-resolution structural characterization of these soluble species has become an overarching objective for understanding Aβ aggregation pathways, and complex molecular mechanism of AD (Benilova et al. 2012).

Several *in vitro* SSNMR studies established an initial high-resolution insight into certain non-fibrillar (Ahmed et al. 2010; Chimon et al. 2005, 2007; Lopez del Amo et al. 2012) and protofibrillar (Qiang et al. 2012; Scheidt et al. 2011) Aβ aggregates. Several other

experimental and theoretical methods have also been used to obtain residue-specific information on prefibrillar Aβ aggregates and on structural persistence in the monomeric state (Bernstein et al. 2009; Bertini et al. 2013b; Danielsson et al. 2006; Fändrich et al. 2012; Fawzi et al. 2011; Gallion 2012; Haupt et al. 2012; Kheterpal et al. 2006; Pan et al. 2011).

Oligomers and protofibrillar intermediates are likely to be on a pathway to amyloid fibril formation. They might potently impair synapse structure and function, disturb neurotransmission and can cause cell death *in vitro* and *in vivo*. Their biological potency however depend on different polymorphic states. Protofibrils are structurally closest to the mature fibrils and might represent late-stage of the fibrillogenic pathway. They can be distinguished from oligomers by their elongated, linear shape, whereas oligomers are frequently referred as spherical species (fig. 6). Protofibrils usually adapt smooth, curvilinear structures and are thinner (diameters of usually less than 10 nm) and shorter (length usually below 400 nm) comparing to the fibrils. Instead oligomers contain a wide range of species, ranging from low molecular weight (LMW) (comprise dimers, trimers and tetramers) to high molecular weight (HMW) (including spherical, chain-like and annular structure) (Fändrich, 2012; Benilova et al. 2012; Jan et al 2010). All of these intermediate assemblies are rich in β-sheet structure and bind Congo red and Thioflavin-T, although more weakly than mature fibrils (Jan et al. 2010).

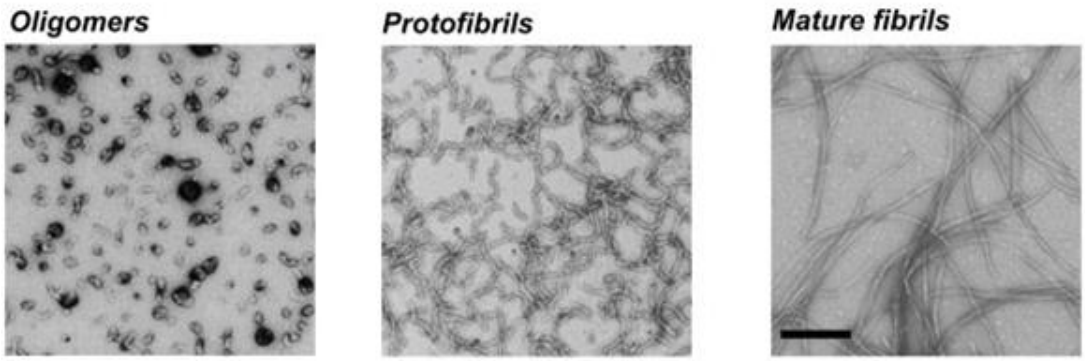

Figure 6. Structure of oligomers, protofibrils and mature fibrils Aβ40. Adapted from (Fändrich, 2012).

However, an investigation of these prefibrillar deposits faces many obstacles. As they are often thermally unstable compared to mature fibrils, in recent years many different methods to immobilize and study these species have been developed and each strategy has its own advantages and disadvantages.

Pioneering work in this direction has been performed by the groups of Smith and Ishii (Ahmed et al. 2010; Chimon et al. 2005, 2007), who focused on Aβ oligomeric form. Taking advantage of the fact that various proteins including Aβ retain their structures after lyophilisation (Benzinger et al. 1998; Petkova et al. 2002; Studelska et al. 1997), many groups trap the thermally labile intermediate by freeze-trapping and subsequent lyophilisation. Different methods of trapping oligomeric and protofibrillar Aβ species as: filtration through low molecular weight cut off filters (Bitan et al. 2005), photo-induced crosslinking of unmodified proteins (Bitan et al. 2003), organic solvent (Haupt et al. 2012), density gradient centrifugation (Ward et al. 2000), size exclusion chromatography (SEC) (Bitan et al. 2003; Hartley et al. 1999; Jan et al. 2010; Walsh et al. 1997) or interaction partners (Bieschke et al. 2012; Lopez del Amo et al. 2012; Scheidt et al. 2011) were used.

In this work we applied a novel method defined as sedimented solutes NMR (SedNMR) to detailed structural characterization of prefibrillar and fibrillar assemblies (Bertini et al. 2013b). In this method, solid-state NMR (SSNMR) experiments are used to observe proteins that are sedimented from solution using an ultracentrifugal field (Bertini et al. 2011b; 2012a; 2012b; 2013a; Polenova, 2011; Ravera et al. 2013). The application of SSNMR is possible, as it has been reported (Ahmed et al. 2010; Bernstein et al. 2009; Fawzi et al. 2011; Kirkitadze et al. 2002; Lee et al. 2011) that Aβ peptides in aqueous solutions spontaneously form soluble aggregates of high molecular weight (50–200 kDa) that are large enough to sediment and thus become visible by SSNMR.

The sedimentation of macromolecules into this type of solid-like phase can be achieved in two different ways. Sedimentation through ultracentrifugation, either by magic angle spinning (*in situ*) or preparative ultracentrifugation (*ex situ*), can be used to immobilize and characterize oligomeric species, measure their formation kinetics, selectively sediment some of these species by their different molecular weights, and reveal the atomic-level structural features of soluble Aβ assemblies.

The collective data obtained from all of these methods demonstrate probable pathway from these fibril precursors to terminal fibrillar states, and also provide evidence that these prefibrillar assemblies already contain β-strand structures (especially most hydrophobic regions), but with different supramolecular organizations and reduced structural order and periodic symmetry, which might define the structures of the multiple conformers in fibrils in amyloid misfolding. However, some authors have suggested that certain oligomers that do not further aggregate to amyloid fibers and that have different secondary structures exist among

the various Aβ intermediate species. Therefore the precise mechanism of the aggregation is still a matter of dispute.

1.2.4 The importance of Aβ40: Aβ42 different ratio for promoting toxicity-associated β-aggregation

Aside from the fact that the neurotoxicity can be induced by the presence of either intermediate assemblies or mature fibrils, recent studies point out the relative ratio of Aβ40 versus Aβ42 as an important determinant of Aβ aggregation, fibrillogenesis, and toxicity. Aβ peptides in specific compositions that balance hydrophilic and hydrophobic interactions might promote the formation of toxic β-aggregates and affect aggregation kinetics (Kuperstein et al. 2010; Pauwels et al. 2012; Yoshiike et al. 2003; Jan et al. 2008). However, the molecular mechanisms by which changes in relative ratio induced and accelerated β-aggregation, fibril formation, and cellular toxicity remain uncertain.

Aβ42 and Aβ40 alloforms co-exist in a molar ratio of 1:9 under normal physiological conditions in the brain. In patients with familial AD this ratio is shifted to a higher level of Aβ42 corresponding to a ratio of 3:7. Investigations of the properties of the Aβ40/Aβ42 mixture by different groups has clearly shown that these two species interact and change each other's dynamic behaviour (Yoshiike et al. 2003; Jan et al. 2008; Kim et al. 2007; Wang et al. 2006). Even minor alterations in the relative amount of the Aβ42/Aβ40 ratio dramatically affect the biophysical and biological properties of the Aβ mixtures reflected in their aggregation kinetics by altering the pattern of oligomer formation. It has been shown that Aβ40 delays Aβ42 aggregation, while Aβ42 has an opposite effect and induces Aβ40 aggregation. This observation was also confirmed by *in vivo* studies, which have shown that a higher percentage of Aβ40 peptides in the brain might be protective (Kim et al. 2007; Wang et al. 2006).

Although it is generally assumed that alterations in the ratios of the Aβ40 and Aβ42 mixture can stabilize distinct intermediate species associated with toxicity, the possibility that neurotoxicity is induced by a number of different conformations should not be neglected. This possibility can be explained by the fact that those toxic intermediate deposits might exist in dynamic equilibrium through theirs assembly and disassembly.

Due to the fact that neurotoxic conformation(s) might be induced by particular ratio of Aβ40 to Aβ42, we focused on the mixture of the fibrils. In this work we will report throught

collective data obtained through SSNMR that a change in the AβM42:AβM40 ratio induces differences in conformational plasticity of the peptide mixtures. The main challenge of this project however is the identification of AβM40:AβM42 reciprocal association in the fibrils, that should broaden our understanding of exacts structural properties, as well as interaction and behavior of these components.

1.3 Superoxide dismutase protein (hSOD1)

Superoxide dismutase 1 (SOD1) is ubiquitously expressed in human cells where it mainly localizes in the cytosol and in the mitochondria intermembrane space (IMS) at micromolar concentrations (Okado-Matsumoto & Fridovich, 2011; Sturtz et al. 2001). At lower levels has been also found in the nucleus and in the peroxisomes. Functionally hSOD1 is responsible for protecting cells from oxidative damage by eliminating superoxide ions through disproportionation (Bertini et al. 1998; Fridovich, 1978).

1.3.1 hSOD1 structural characterization

hSOD1 is a 32 kDa, β-rich, homodimeric protein. Each of the two subunits of SOD1 forms an eight β-stranded Greek key β-barrel and contains several loops (fig. 6), as well as a catalytic copper ion (binding residues: His46, His48, His63 and His120) and a structural zinc ion (binding residues: His63, His71, His80 and Asp83). The protein is stabilized by an intrasubunit disulfide bond formed by Cys-57 and Cys-146 near the active site. In addition there are other two reduced Cys residues, Cys-6 and Cys-111, which are located on β-strand 1 and loop VI respectively (fig. 7). Among the loops connecting the 8 β-strands, 2 have structural and functional roles. The electrostatic loop, namely loop VII (residues 121–144) contains charged residues and plays a role in attraction between negatively-charged superoxide substrate and positive site with copper ion. The long zinc loop, namely IV (residues 49–84) forms the zinc-binding site and is involved in interactions between the two subunits (Banci et al. 2007, 2008, 2009; Chattopadhyay et al. 2008; Fujiwara et al. 2007; Seetharaman et al. 2009; Shaw & Valentine, 2007).

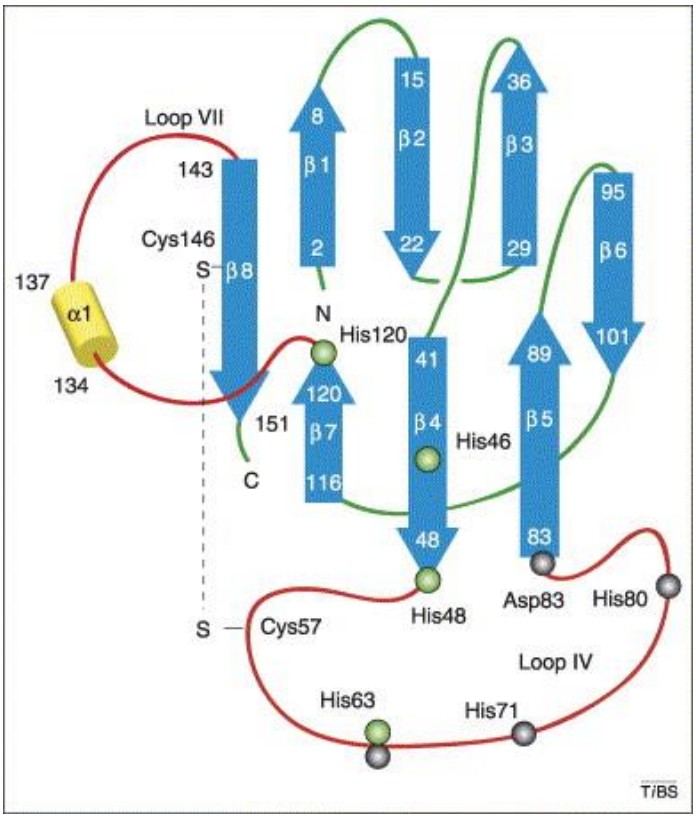

Figure 7. Secondary structural elements of human SOD1 monomer. Adapted from (Shaw & Valentine, 2007).

1.3.2 hSOD1 misfolding and aggregation

The unusually high stability for mature hSOD1, which retains enzymatic activity at high temperatures and in the presence of denaturing agents is ascribed most of all to the presence of metal ions (zinc and copper), dimerization, and an intramolecular disulfide bond. These posttranslational modifications are essential in the maturation of hSOD1. The lack of one or more of these features has a major impact on the properties of hSOD1 and may have relevance in hSOD1 acquisition of toxic properties (Lelie et al. 2011).

Complete removal of the metal ions in hSOD1 could plays a crucial role in aberrant SOD1 oligomerization and aggregation (Teilum, 2009). Proteomic studies indicate that demetallated SOD1 protein is the main and constant component in amyloid deposits widely found in ALS patients and transgenic mice (Lelie et al. 2011), whereas in vitro studies of the aggregation kinetics have implicated the monomeric apo state as the origin for aggregation (Teilum, 2009).

These early species of the maturation process lacking metal ions have been shown to have high tendency to oligomerize *in vitro,* while the mature form of hSOD1 is not prone to aggregation (Banci et al. 2007; Furukawa et al. 2008; Lindberg et al. 2002; Oztug Durer et al. 2009). Previous studies have shown that lack of the metal ions causes dynamic motions and loosen up of the long active-site loops, contributing to the lower stability of the loop conformation, the stability of the β – barrel and whole protein scaffold (Danielsson et al. 2011). Apo hSOD1 acquire high flexibility and can adopt a broad range of conformations, which are highly disordered in some parts and some of which cause the two free cysteines (Cys-6 and Cys-111) to be more exposed, solvent accessible, and less structurally constrained than in the metallated form. Once the free cysteines are solvent-accessible, form intermolecular disulfide bonds which cross-link the molecules into high-molecular-weight oligomers under physiological conditions (37°C, pH 7, and 100 μM protein concentration), which are further stabilized by noncovalent protein–protein interactions between β-sheets (Banci et al. 2007; 2009). These oligomers of high molecular weight (over MDa) are remarkably stable, persisting in the soluble state for months and exhibit positive ThT binding response (Banci et al. 2007; 2009).

Although the stabilizing effects of metal ion binding have been known as significant factor contributing to dimer stability, recent studies have also emphasized the importance of the intrasubunit disulfide bond formed by Cys-57 and Cys-146. Intact disulfide bond shifts monomer-dimer equilibrium towards dimeric species (Arnesano et al. 2004), which is further stabilized by reciprocal interactions of the loop IV and β-strand 8 across the molecular two-fold axis. Reduction of the disulfide bond in the apo protein causes monomerization, as a result of strong destabilization of apo SOD1 scaffold by increase mobility of the disorder loop IV, partial destabilization of the β barrel and weakened interactions across the dimer interface. This could lead to partial misfolding and SOD1 aggregation processes (Chattopadhyay et al. 2008; Seetharaman et al. 2009, Shaw & Valentine, 2007).

Various studies demonstrated that hSOD1 local structural and dynamical properties, as well as the rate of the aggregation process are also changed in different way by diverse mutations. Hitherto, more than 100 ALS-linked mutants on hSOD1 have been found. The presence of a mutation and its location and type might contribute to acquirement by the protein the high flexibility through exposing areas prone to oligomerization, the abolishment of metal binding sites, the reduction of the surface charge, destabilize the dimer and loops (Shaw & Valentine 2007).

These discrepancy in the structural changes caused by disruptions in maturation steps of SOD1 as well as different ALS-linked mutants on hSOD1 resulting in divergence in the structural properties made it very difficult to understand the mechanism of hSOD1 misfolding and aggregation. However it is hypothesized that misfolded hSOD1 monomers might be the intermediate of further aggregation, leading at the final stage to amyloid deposits widely found in ALS patients and transgenic mice.

1.3.3 Aggregation preventing strategy in hSOD1

Many studies have been focused on the searching of therapeutic strategies aimed to prevent SOD1 pathogenic aggregation process that could be relevant with respect to the ALS pathology. Since SOD1 monomers are suspected to be the aggregation intermediates (Rakhit et al. 2004; Khare et al. 2004), these efforts concentrate on the stabilization of SOD1 dimers by the development of small, drug-like molecules. The mechanism of action of these molecules is based on the targeting directly free cysteine residues, which are solvent accessible. These molecules effect in neutralization of the free cysteines, which take part in the formation of intermolecular disulfide bonds, important in SOD1 amyloid formation.

A recent study has shown that cis-diamminedichloroplatinum (II) (cisplatinum) can be selected as potential leading compound for blocking hSOD1 oxidative oligomerization (Banci et al. 2012). Cisplatinum is a small chemotherapeutic drug molecule with very high binding affinity toward thiol groups in proteins (Wang & Lippard, 2005). It has been proved that cisplatinum inhibits the oligomerisation of hSOD1 *in vitro* and *in vivo* by covalently binding to the solvent exposed Cys-111 of the apo-form of the enzyme and leads also to the dissociation of already formed apo hSOD1 oligomers without affecting the normal hSOD1 enzymatic activity (Banci et al. 2012). This effect is relatively specific, since another cysteine reactive, anti-cancer molecule (Imexon) has no significant effect in the inhibition of SOD1 oligomerization, probably because of its larger molecular size. Nevertheless clinical use of this chemotherapeutic agent is severely limited by the development of side effects including nephrotoxicity, emetogenesis, ototoxicity and neurotoxicity (Kelland 2007; Wang &Lippard 2005). The peripheral neuropathy associated with these neurotoxic effects can be prolonged, severe and very often responsible for therapy interruption. Recent data have suggested that cisplatin also induces the formation of reactive oxygen species (ROS) that can trigger cell death (Brozovic et al. 2010; Casaress et al. 2012; Marullo et al. 2013).

It is thus clear that the availability of safe and effective analgesic drugs, able additionally to reverse or counterbalanced the toxic effects of cisplatinum related to the formation of ROS is a target of high interest. In this work we will report that such presumed candidates in suppression of cisplatinum-induced neuropathy are two molecules ADM_09 and ADM_12.

1.4 Aims and topics of the study

The aim of this work was the expression, purification as well as the structural and biophysical characterization of proteins involved in physiological and pathological processes at intra and extracellular level that play a role in a diverse group of neurodegenerative disorders. The first is beta amyloid peptide (Aβ), that is associated to Alzheimer's disease (AD) and the second is superoxide dismutase (SOD1) that is related to amyotrophic lateral sclerosis (ALS). Both Alzheimer's disease (AD) and amyotrophic lateral sclerosis (ALS) are classified as proteopathies and characterized by progressive nervous system dysfunction and so far are relentless and incurable.

Although the direct involvement of Aβ peptides in AD is well-documented, the toxic Aβ species and the precise mechanism of its neurotoxicity remain unclear. Moreover, there is still a significant gap between site-specific structural information and the complex structural diversity of Aβ amyloids. A detailed structural and functional characterization of fibrillar assemblies, as well as the various prefibrillar intermediates is crucial for understanding the role of Aβ formation and aggregation in AD pathogenesis. The recognition of the real culprit for AD onset is fundamental in design of new, effective therapeutic strategies targeted at preventing the formation or impairing the activity of toxic Aβ assemblies involved in AD. In this work a detailed structural characterization of prefibrillar and fibrillar Aβ assemblies has been carried out in order to elucidate the Aβ aggregation pathways, in particular, the structural evolution in different steps, and to identify the toxic Aβ species. We focused on high resolution structural characterization of AβM40 and AβM42 mixture fibrils prepared in different molar ration related to the pathological conditions and demontrated the application of a novel method defined as sedimented solutes NMR (SedNMR) to detailed structural characterization of oligomeric and prefibrillar assemblies. I contributed to the molecular, biological and biophysical part of the project, by preparing double/triple labeled or unlabeled protein samples by heterologous expression of various Aβ peptides in Escherichia coli and purification process. I performed fibrillation experiments under different conditions, as well

as prepared samples for isolation and characterization of Aβ oligomers and protofibrils that facilitated the combined solid state and solution NMR investigation.

The causes of motor neuron death in ALS are poorly understood, however a prominent hypothesis for SOD1-linked familial ALS involves the formation of protein aggregates containing misfolded hSOD1 as the main component in amyloid-like deposits. Therefore many studies have been focused on the investigation of the therapeutic strategies aimed to prevent SOD1 pathogenic aggregation that could be relevant with respect to the ALS pathology. One of the rational drug design was established based on previous knowledge on the chemical mechanism of apo SOD1 aggregation and the chemical reactivity of cisplatin that selectively binds to solvent exposed Cys-111 and strongly inhibits process of oligomerization. However clinical use of this chemotherapeutic agent is severely limited by the development of neurotoxicity and others undesirable effects. Therefor the main objectives of this work was the determination of the propensity of two new molecules, ADM_09 and ADM_12 to revert side effects caused by cisplatinum related to the formation of ROS and cisplatinum-induced neuropathy pain. I contributed to the project by expression, purification of hSOD1 wt protein, preparation of the apo form of SOD1 and monitoring of SOD1 aggregation by ThT fluorescence measurements.

1.5 References:

Ahmed M., Davis J., Aucoin D., Sato T., Ahuja S., Aimoto S., Elliott J. I, Van Nostrand W. E, Smith S. O. 2010. *Nature Structural & Molecular Biology*.17 (5), 561–567.

Aizenstein H. J., Nebes R. D., Saxton J. A., Price J. C., Mathis C. A., Tsopelas N. D., Ziolko S. K., James J. A., Snitz B. E., Houck P. R., Bi W., Cohen A. D., Lopresti B. J., DeKosky S. T.,Halligan E. M., Klunk W. E. 2008. *Arch Neurol.* 65(11):1509-17.

Aksenov M. Y., Aksenova M. V., Butterfield D. A., Hensley K., Vigo-Pelfrey C., Carney J. M. 1996. *Journal of Neurochemistry*. 66: 2050–2056.

Alzheimer A. 1907. *Allgemeine Zeitschrift fur Psychiatrie un Psychish-Gerichtliche Medizin.* 64, 146-148.

Andersen P. M. 2006. *Curr Neurol Neurosci.* 6(1):37-46.

Anoop A., Singh P. K., Jacob R. S., Maji S. K. 2010. *Int J Alzheimers Dis*. pii: 606802. doi: 10.4061/2010/606802.

Arnesano F., Banci L., Bertini I., Martinelli M., Furukawa Y., O'Halloran T. V. 2004. *J Biol Chem.* 279(46): 47998-8003.

Banci, L. I. Bertini, A. Durazo, S. Girotto, E.Butler Gralla, M. Martinelli, J. Selverstone Valentine, M. Vieru, J. P. Whitelegge, 2007. *Biophysics.* 104(27):11263-7.

Banci L., Bertini I., Boca M., Girotto S., Martinelli M., Valentine J. S., Vieru M. 2008. *PLoS One.* 3(2):e1677.

Banci L., Bertini I., Boca M., Calderone V., Cantini F., Girotto S., Vieru M. 2009. *Proc Natl Acad Sci U S A.* 28;106(17).

Banci L., Bertini I., Blaževitš O., Calderone V., Cantini F., Mao J., Trapananti A., Vieru M., Amori I. Cozzolino M., Carrì M. T. 2012. *J Am Chem Soc.* 25;134(16):7009-14.

Barrantes F. J., Borroni V., Vallés S. 2010. *FEBS Lett.* 584(9):1856-63.

Bayer T. A., Cappai R., Masters C. L., Beyreuther K., Multhaup G. 1999. *Molecular psychiatry*. 4(6):524-8.

Bayer T. A. 2013. Eur Neuropsychopharmacol. pii: S0924-977X(13)00110-7.

Benilova I., Karran E., De Strooper B. 2012. *Nature Neuroscience*. 15(3):349-57.

Benzinger T. L. S., Gregory D. M., Burkoth T. S., Miller-Auer H., Lynn D. G., Botto R. E., Meredith S. C.1998. *Proceedings of the National Academy of Sciences USA*. 95 (23), 13407–13412.

Bernstein S. L., Dupuis N. F., Lazo N. D.,Wyttenbach T., Condron M. M., Bitan G., Teplow D. B., Shea J. E., Ruotolo B.T., Robinson C. V., Bowers M. T. 2009. *Nature Chemistry* 1 (4), 326– 331.

Bertini I., Mangani S., Viezzoli M. S., 1998. *Academic Press*. pp 127-250.

Bertini I., Gonnelli L., Luchinat C., Mao J., Nesi A. 2011a. *Journal of the American Chemical Society USA.*133(40): 16013–22.

Bertini I., Luchinat C., Parigi G., Ravera E., Reif B., Turano P. 2011b. *Proceedings of the National Academy of Sciences USA*.108 (26), 10396 –10399.

Bertini I., Engelke F., Luchinat C., Parigi G., Ravera E., Camila R., Paola T. 2012a. *Physical Chemistry Chemical Physics*.14 (2), 439 –447.

Bertini I., Engelke F., Gonnelli L., Knott B., Luchinat C., Osen D., Ravera E. 2012b. *Journal of Biomolecular NMR*.2012, 54 (2), 123 –127.

Bertini I., Luchinat C., Parigi G., Ravera E. 2013a. *Accounts of Chemical Research.* 46(9):2059-69.

Bertini I., Gallo G., Korsak M., Luchinat C., Mao J., Ravera E**.** 2013b. *ChemBioChem.* 14(14):1891-7.

Bieschke J., Herbst M., Wiglenda T., Friedrich R. P., Boeddrich A., Schiele F., Kleckers D., Lopez del Amo J. M., Grüning B. A, Wang Q., Schmidt M R, Lurz R., Anwyl R., Schnoegl S., Fändrich M., Frank R. F., Reif B., Günther S., Walsh D. M., Wanker E. E., 2012. *Nature Chemical Biology.* 8 (1), 93–101.

Bitan G., Kirkitadze M. D., Lomakin A., Vollers S. S., Benedek G. B., Teplow D. B. 2003. *Proceedings of the National Academy of Sciences USA.* 100 (1), 330–335.

Bitan G., Teplow D. B. 2005. *Methods in Molecular Biology.* 299, 3–9.

Brozovic A., Ambriović-Ristov A., Osmak M. 2010. *Crit Rev Toxicol.* 40(4):347-59.

Bruijn L. I., Becher M. W., Lee M. K., Anderson K. L., Jenkins N. A., Copeland N. G., Sisodia S. S., Rothstein J. D., Borchelt D. R., Price D. L., Cleveland D.W. 1997 *Neuron.* 18(2):327-38.

Bruijn L. I., Miller T. M., Cleveland D. W. 2004. *Annu Rev Neurosci.* 27:723-49.

Cameron B., Landreth G. E. 2010. *Neurobiol Dis.*37(3):503-9.

Carrell R. W., Lomas D. A. 1997. *Lancet*. 350(9071):134-8.

Casares C., Ramírez-Camacho R., Trinidad A., Roldán A., Jorge E., García-Berrocal J. R. 2012. *Eur Arch Otorhinolaryngol.* 269(12):2455-9.

Chattopadhyay M., Durazo A., Sohn S. H., Strong C. D., Gralla E. B., Whitelegge J. P., Valentine J. S. 2008. *Proc Natl Acad Sci USA*. 105(48):18663-8.

Chimon S., Ishii Y. 2005. *Journal of the American Chemical Society USA.* 127 (39) :13472–73.

Chimon S., Shaibat M. A., Jones C. R., Calero D. C., Aizezi B., Ishii Y. 2007. *Nature Structural & Molecular Biology.* 14, 1157–1164.

Colletier J. P., Laganowsky A., Landau M., Zhao M., Soriaga A. B., Goldschmidt L., Flot D., Cascio D., Sawaya M. R., Eisenberg D. 2011. Proc Natl Acad Sci U S A. ;108(41):16938-43.

Danielsson J., Andersson A., Jarvet J., Gräslund A. 2006. *Magnetic Resonace in Chemistry* 44, S114– S121.

Danielsson J., Kurnik M., Lang .L, Oliveberg M. 2011. *J Biol Chem.* 286(38):33070-83.

Esch F. S., Keim P. S., Beattie E. C., et al. 1990. *Science* (New York, N.Y.), 248(4959):1122-4.

Fändrich M., Schmidt M. Grigorieff N. 2011. *Trends in Biochemical Sciences.* 36, 338-345.

Fändrich M. 2012. *Journal of Molecular Biology.* 421 (4-5), 427– 440.

Fawzi N. L., Ying J, Ghirlando R., Torchia D. A. Clore M. G. 2011. *Nature*. 480 (7376), 268-272.

Fridovich I. 1978. *Science.* 201: 875-879.

Fujiwara N., Nakano M., Kato S., Yoshihara D., Ookawara T., Eguchi H., Taniguchi N., Suzuki K. 2007. *J Biol Chem.* 282(49):35933-44.

Furukawa Y., Kaneko K., Yamanaka K., O'Halloran T. V., Nukina N. 2008 J Biol Chem. 283(35):24167-76.

Gallion S. L. 2012. *PLoS ONE*. 7(11):e49375.

Glass C. K., Saijo K., Winner B.,Marchetto M. C., Gage F. H. *Cell*. 2010. 40, pp. 918–934.

Glenner G. G., Wong C. W. 1984. *Biochem Biophys Res Commun.* 425(3):534-9.

Grundke-Iqbal I., Iqbal K., Quinlan M., Tung Y. C., Zaidi M. S., Wisniewski H. M. 1986 *J Biol Chem.*261(13):6084-9.

Hardy J. A., Higgins G. A. 1992. *Science.* 256(5054):184-5.

Hardy J. A., Selkoe D. J. 2002. *Science*. 297: 353–356.

Hartley D. M., Walsh D. M., Chian P., Diehl T. S.,Vasquez S., Vassilev P. M., Teplow D. B., Selkoe D. J. 1999. *The Journal of Neuroscience*. 19 (20), 8876–8884.

Haass C., Selkoe D. J. 2007. *Nat Rev Mol Cell Biol*.8(2):101-12.

Haupt C., Leppert J., Ronicke R., Meinhardt J., Yadav J. K., Ramachandran R., Ohlenschoger O., Reymann K. G., Gorlach M., Fandrich M. 2012. *Angewandte Chemie International Edition*. 51 (7), 1576 – 1579.

Herrup K. 2010. *J Neurosci.* 30(50):16755-62.

Hervias I., Beal M. F., Manfredi G. 2006. *Muscle Nerve.* 33(5):598-608.

Hipkiss, A. R. 2009. *Adv. Food Nutr. Res.*57, 87–154.

Hoshi M.,Sato M., Sato M., Matsumoto S., Noguchi A., Yasutake K., Yoshida N., Sato K. 2003. *Proceedings of the National Academy of Sciences USA*.100, 6370–6375 (2003).

Jan A., Gokce O, Luthi-Carter R, Lashuel H. A. 2008. *The Journal of Biological Chemistry*. 283(42):28176-89.

Jan A., Dean M. H., Hilal A. L. 2010. *Nature protocols.* 5(6): 1186–1209.

Johnston J. A., Dalton M. J., Gurney M. E., Kopito R. R. 2000. *Proc Natl Acad Sci USA.* 97(23):12571-6.

Jonsson P. A., Ernhill K., Andersen P. M., Bergemalm D., Brännström T., Gredal O., Nilsson P., Marklund S. L. 2004. *Brain.*127(Pt 1):73-88.

Jucker M., Walker L. C. *Nature.* 2013;501(7465):45-51.

Kelland L. 2007. *Nat Rev Cancer.* 7(8):573-84.

Khare, S. D., Caplow, M., Dokholyan, N. V. 2004. *Proc. Natl Acad. Sci*. USA, 101, 15094–15099.

Kheterpal I., Chen M., Cook K. D., Wetzel R. 2006. *Journal of Molecular Biology*. 361 (4), 785 – 795.

Kim J., Onstead L., Randle S., Price R., Smithson L., Zwizinski C., Dickson D. W., Golde T., McGowan E. 2007. *Journal of Neuroscience.* 27(3):627-33.

Kirkitadze M. D, Bitan G., Teplow D. B. 2002, *Journal of Neuroscience Research.* 69, 567-577.

Krafft G. A., Klein W. L. 2010. *Neuropharmacology*. 59 (4-5), 230–242.

Kumar S., Rezaei-Ghaleh N., Terwel D., Thal D. R., Richard M., Hoch M., Mc Donald J. M, Wüllner U., Glebov K., Heneka M. T., Walsh D. M., Zweckstetter M., Walter J. 2011. *European Molecular Biology Organization Journal*. 30(11):2255-65.

Kuperstein I., Broersen K., Benilova I., Rozenski J., Jonckheere W., Debulpaep M., Vandersteen A., Segers-Nolten I., Van Der Werf K., Subramaniam V., Braeken D., Callewaert G., Bartic C., D'Hooge R., Martins I. C., Rousseau F., Schymkowitz J., De Strooper B. 2010. *European Molecular Biology Organization Journal.* 29(19):3408-20.

Lambert M. P., Barlow A. K., Chromy B. A., Edwards C., Freed R. M., Liosatos M., Morgan T. E., Rozovsky I., Trommer B. L., Viola K., P Wals, Zhang C., Finch C. E., Krafft G. A., Klein W. L. 1998. *Proceedings of the National Academy of Sciences USA.* 95, 6448–6453.

Lansbury P. T., Costa P. R., Griffiths J. M., Simon E. J., Auger M., Halverson K. J., Kocisko D. A., Hendsch Z. S., Ashburn T. T., Spencer R. G. S. 1995. *Nature Structural & Molecular Biology*. 2 (11),990–998.

Lee J., Culyba E. K., Powers E. T., Kelly J. W. 2011. *Nature Chemical Biology*. 7 (9), 602–609.

Lelie H. L., Liba A., Bourassa M. W., Chattopadhyay M., Chan P. K., Gralla E. B., Miller L. M., Borchelt D. R., Valentine J. S., Whitelegge J. P. 2011. *J Biol Chem.* 286(4):2795-806.

Lesne´ S., Koh M. T., Kotilinek L., Kayed R., Glabe C. G., Yang A., Gallagher M., Ashe K. H. 2006. *Nature.* 440 (7082), 352–357.

Lindberg M. J., Tibell L., Oliveberg M. 2002. *Proc. Natl. Acad. Sci. USA.* 99 (26), 16607-16612.

Lopez del Amo J. M., Fink U., Dasari M., Grelle G., Wanker E. E., Bieschke J., Reif B. 2012. *Journal of Molecular Biology.* 421 (4-5), 517–524.

Lorenzo A., Yankner B.A. 1994. *Proceedings of the National Academy of Sciences USA.* 91(25), 12243–12247.

Lu J. X., Qiang W., Yau W. M., Schwieters C. D., Meredith S. C., Tycko R. 2013. *Cell.* 154(6):1257-68.

Lührs T., Ritter C., Adrian M., Riek-Loher D., Bohrmann B., Dobeli H. ,Schubert D., Riek R. 2005. *Proceedings of the National Academy of Sciences USA.* 102(48), 17342–17347.

Martins I. C., Kuperstein I., Wilkinson H., Maes E., Vanbrabant M., Jonckheere W., Van Gelder P., Hartmann D., D'Hooge R., De Strooper B., Schymkowitz J., Rousseau F. 2008. *European Molecular Biology Organization Journal.* 27(1):224-33.

Marullo R., Werner E., Degtyareva N., Moore B., Altavilla G., Ramalingam S. S., Doetsch P. W. 2013. *PLoS One.* 8(11):e81162.

Masters C. L., Multhaup G., Simms G., Pottgiesser J., Martins R. N., Beyreuther K. 1985 *EMBO J.* 4(11):2757-63.

Meinhardt J., Sachse C., Hortschansky P., Grigorieff N., Fändrich M. 2009. *Journal of Molecular Biology.* 386 (3), 869-877.

Merz P. A.,Wisniewski H. M., Somerville R. A., Bobin S. A. , Masters C. L., Iqbal K.1983. *Acta Neuropathologica.* 60(1-2):113-24.

Meyer-Luehmann M., Spires – Jones T. L., Prada C., Garcia – Alloza M., de Calignon Alix, Rozkalne A., Koenigsknecht-Talboo J., Holtzman D. M., Bacskai B. J., Hyman B. T. *Nature.* 2008, 451, 720-7U5.

Mulligan V.K., Chakrabartty A. 2013. *Proteins.* (8):1285-303.

Nativi C., Gualdani R., Dragoni E., Di Cesare Mannelli L., Sostegni S., Norcini M., Gabrielli G., la Marca G., Richichi B., Francesconi O., Moncelli M. R., Ghelardini C., Roelens S. 2013. *Sci Rep.*3:2005.

Noguchi A., Matsumura S., Dezawa M., Tada M., Yanazawa M., Ito A., Akioka M., Kikuchi S., Sato M., Ideno S. 2009. *Journal of Biological Chemistry.* 284 (47), 32895–32905.

Okado-Matsumoto A., Fridovich I. 2001. *J Biol Chem.*,276(42):38388-93.

Oztug Durer Z. A., Cohlberg J. A., Dinh P., Padua S., Ehrenclou K., Downes S., Tan J. K., Nakano Y., Bowman C. J., Hoskins J. L., Kwon C., Mason A. Z., Rodriguez J. A., Doucette P. A., Shaw B. F., Valentine J. S. 2009. *PLoS One.* 4(3):e5004.

Pan J., Han J., Borchers C. H., Konermann L. 2011. *Analytical Chemistry.* 83 (13),5386 – 5393.

Paravastu A. K, Leapman R. D., Yau W. M., Tycko R. 2008. *Proceedings of the National Academy of Sciences USA.* 105 (47), 18349–18354.

Paravastu A. K., Quhwash I., Leapman R. D., Meredith S. C., Tycko R. 2009. *Proceedings of the National Academy of Sciences USA.* 106 (18), 7443-7448.

Parcker, L., Witt, E. H. & Tritschler, H. J. 1995. *Free Radical Biol. Med.* 19, 227–250.

Pauwels K., Williams T.L., Morris K.L., Jonckheere W., Vandersteen A., Kelly G., Schymkowitz J., Rousseau F., Pastore A., Serpell L.C, Broersen K. 2012. *The Journal of Biological Chemistry.* 287(8):5650-60.

Petkova A. T., Ishii Y., Balbach, J. J., Antzutkin O. N., Leapman R. D., Delaglio, F., Tycko R. 2002. *Proceedings of the National Academy of Sciences USA.* 99 (26), 16742–16747.

Petkova A. T., Leapman R. D., Guo Z. H., Yau W. M., Mattson M. P., and Tycko R. 2005. *Science.* 307 (5707):262-5.

Petkova A. T, Yau W. M., Tycko R. 2006. *Biochemistry.* 45 (2),498–512.

Polenova T. 2011. *Nature Chemistry.* 3 (10), 759– 760.

Polymenidou M., Cleveland D. W. 2011. *Cell.* 147(3):498-508.

Qiang W., Yau W. M., Tycko R.. 2011. *Journal of the American Chemical Society.* 133 (11), 4018–4029.

Qiang W., Yau W. M., Luo Y., Mattson M. P., Tycko R. 2012. *Journal of the American Chemical Society USA* 109 (12), 4443–4448.

Qiang W., Kelley K., Tycko R. 2013. *J. Am. Chem. Soc*., 135, pp. 6860–6871.

Rakhit R., Crow J. P., Lepock J. R., Kondejewski L. H., Cashman N. R., Chakrabartty A. 2004. *J Biol Chem*. 279:15499–15504.

Ravera E., Corzilius B., Michaelis V. K., Rosa C., Griffin R. G., Luchinat C., Bertini I. 2013. *Journal of the American Chemical Society USA.* 135 (5), 1641– 1644.

Rosen D. R. 1993. *Nature.* 362:59–62.

Ross C. A., Poirier M. A. 2004. *Nat Med.* 10 Suppl:S10-7.

Sachse C., Fändrich M., Grigorieff N. 2008. *Proceedings of the National Academy of Sciences USA.* 105(21):7462-6.

Sachse C., Grigorieff N., Fändrich M. 2010. *Angewandte Chemie International Edition.* 49(7):1321-3.

Scheidt H. A., Morgado I., Rothemund S., Huster D., Fändrich M. 2011. *Angewandte Chemie International Edition.* 50 (12), 2837–2840.

Seetharaman S. V., Prudencio M., Karch C., Holloway S. P., Borchelt D. R., Hart P. J. 2009. *Exp Biol Med (Maywood).* 234(10):1140-54.

Selkoe D. J. 2004. *Nature Cell Biology.* 6 (11), 1054–1061.

Selkoe D. J. 2008. *Behavioural Brain Research.* 192 (1), 106–113.

Serpell L. C. 2000. *Biochimica et Biophysica Acta.* 1502(1):16-30.

Shankar G. M, Li S., Mehta T. H., Garcia-Munoz A., Shepardson N. E., Smith I., Brett F. M., Farrell M. A., Rowan M. J., Lemere C. A., Regan C. M., Walsh D. M., Sabatini B. L., Selkoe D. J. 2008. *Nat. Med.* 14, 837–842.

Shaw B. F., Valentine J. S. 2007. *Trends Biochem Sci.* 32(2):78-85.

Shibata N., Hirano A., Kobayashi M., Siddique T., Deng H. X., Hung W. Y., Kato T., Asayama K. 1996. *J Neuropathol Exp Neurol.* 55(4):481-90.

Sisodia S. S. 1992. *Proceedings of the National Academy of Sciences of the United States of America*, 89(13):6075-9.

Studelska D. R, McDowell L. M., Espe M. P., Klug C., Schaefer J.1997. *Biochemistry.* 36 (50), 15555–15560.

Sturtz L. A., Diekert K., Jensen L. T., Lill R., Culotta V. C. 2001. *J Biol Chem.* 276(41):38084-9.

Sultana R., Perluigi M., Butterfield D. A. 2009. *Acta Neuropathol.* 118, pp. 131–150.

Teilum K., Smith M. H., Schulz E., Christensen L. C., Solomentsev G., Oliveberg M., Akke M. 2009. *Proc Natl Acad Sci U S A.* (43):18273-8.

Tomic J. L., Pensalfini A., Head E., Glabe C. G. 2009. *Neurobiol. Dis.* 35 (2009), pp. 352–358.

Tortarolo M., Grignaschi G., Calvaresi N., Zennaro E., Spaltro G., Colovic M., Fracasso C., Guiso G., Elger B., Schneider H., Seilheimer B., Caccia S., Bendotti C. 2006. *J Neurosci Res.* 83(1):134-46.

Tõugu V., Tiiman A., Palumaa P.2011. *Metallomics*. 3, pp. 250–261.

Tycko R. 2011. *Annu Rev Phys Chem*. 62:279-99.

Uversky V. N., Dunker A. K. 2010. *Biochim Biophys Acta.*1804(6):1231-64.

Uversky V. N. 2010. *Expert Rev Proteomics.* 7(4):543-64.

Valentine J. S., Doucette P. A., Potter S. Z. 2005. *Annu Rev Biochem.*74:563–593.

Walsh D. M, Lomakin A., Benedek G. B., Condron M. M., Teplow D. B. 1997. *The Journal of biological chemistry*. 272(35): 22364–72.

Walsh D. M., Hartley D. M., Kusumoto Y., Fezoui Y., Condron M. M., Lomakin A., Benedek G. B., Selkoe D. J., Teplow D. B. 1999. *The Journal of Biological Chemistry.* 274 (36), 25945–25952.

Walsh D. M., Thulin E., Minogue A. M., Gustavsson N., Pang E., Teplow D. B., Linse S. 2009. *FEBS Journal.* 276(5): 1266–81.

Wang J., Xu G., Borchelt D.R. 2002. *Neurobiol. Dis.* 9, 139-148.

Wang, D., Lippard, S. J. 2005. *Nat. Rev. Drug Discov.* 4, 307-320.

Wang R., Wang B., He W., Zheng H. 2006. *The Journal of Biological Chemistry.* 281(22):15330-6.

Ward R. V., Jennings K. H., Jepras R., Neville W., Owen D. E., Hawkins J., Christie G., Davis J. B., George A., Karran E. H., Howlett D. R. 2000. *Biochemical Journal*. 348 (Pt 1): 137–144.

Wasco W., Bupp K., Magendantz M., et al. 1992. *Proceedings of the National Academy of Sciences of the United States of America*. 89(22):10758-62.

Wasco W., Gurubhagavatula S., Paradis M. D., et al. 1993. *Nature genetics*. 5(1):95-100.

Watanabe M., Dykes-Hoberg M., Culotta V. C., Price D. L., Wong P. C., Rothstein J. D. 2001. *Neurobiol Dis*. 8(6):933-41.

Yoshiike Y., Chui D. H., Akagi T., Tanaka N., Takashima A. 2003. *J Biol Chem.* 278(26):23648-55.

Zheng H.; Koo E. H. 2011. *Molecular neurodegeneration*. 6(1):27.

Chapter 2 Methodology

In this section the experimental procedures, methods and key materials are described.

2.1 Recombinant protein expression in *E. coli*

The requirement of rapid and economical production of high quality recombinant proteins, has driven the development of a variety of strategies for achieving high level expression of protein. These strategies involve several aspects such as expression vectors design, gene dosage, promoter strength, mRNA stability, translation initiation and termination, host design considerations, codon usage, and fermentation factors. The proper selection and manipulation of the expression conditions is essential in obtaining the high yield of protein at low cost (Jana & Deb, 2005).

Several host systems for protein production, including bacteria, yeast, plants, fungi, insect and mammalian cells have been developed and evaluated (Shatzman 1995). Their choice depends on many factors, including cell growth characteristics, expression levels, intracellular and extracellular expression, posttranslational modifications as well as biological activity of the protein of interest. Extensive knowledge on the genetics and molecular biology of *E. coli*, made this expression system one of the most valuable for the high-level production of recombinant proteins. The important advantages of this host system is that the production of isotope labeled protein for NMR is less complex compared to other organisms. However not every gene can be expressed efficiently in this organism. This limitation may be due to the unique and subtle structural features of the gene sequence, degradation of the protein by host cell proteases, the ease of protein folding, as well as the potential toxicity of the protein to the host. Another drawbacks of *E. coli* as an expression system include the inability to perform many of the posttranslational modifications found in eukaryotic proteins, since *E. coli* is a prokaryote and lacks intracellular organelles, such as the endoplasmic reticulum and the Golgi apparatus, which are responsible for such processes. Moreover *E. coli* is lacking of a secretion mechanism for the efficient release of protein into the culture medium, and has the limited ability to facilitate extensive disulfide bond formation (Jana & Deb, 2005).

Once the expression system is selected, the expression conditions should be tested. It is important to take into consideration such factors as culture media composition, temperature, optical density, isopropyl β-D-1-thiogalactopyranoside (IPTG) inducer concentrations, induction time, as well as different *E. coli* strain possessing various properties that could be

advantageous in the expression of the certain protein. Common examples are Rosetta(DE3) and Codon Plus for genes containing rare codons; Origami(DE3) for proteins containing disulfide bridges, Gold(DE3) for increasing expression yields and BL21(DE3)pLysS, which has a gene for lysozyme. Optical density has significant effects on both the cells and protein production. High cell-density culture systems suffer from several drawbacks, including limited availability of dissolved oxygen at high cell density, carbon dioxide levels which can decrease growth rates and stimulate acetate formation, reduction in the mixing efficiency of the culture, and heat generation. Nutrient composition and fermentation variables such as temperature, pH, and other parameters can differentially affect the translation of different mRNAs proteolytic activity, secretion, and production levels (Jana & Deb, 2005). The composition of the cell growth medium must be carefully formulated dependence of the expression purpose. The cells can be grown in different types of media: rich media, LB, 2xYT, terrific broth, NZY and the minimum media M9. When the labelled protein is necessary, the M9 supplemented with [C^{13}] and [N^{15}] sources is used. In order to increase the expression yield of isotopic labeled protein the good solution is Marley method (Marley et al. 2001). The cells transformed with the expression plasmid are grown initially in rich medium until high optical densities, then are centrifuged and exchanged into an isotopically defined minimal media enriched with ($^{15}NH_4)_2SO_4$(1 g/L) and (^{13}C) glucose (4 g/L). There are also commercially available and isotopically enriched rich media e.g. Silantes., which are particularly advantageous for the expression of deuterated labeled protein in terms of simplified cells adaptation process.

The best approach to verify simultaneously all these parameters is preliminary test expression performed in a small – volume scale. This tactic allows for the rapid identification of the optimal conditions to be reproduced in scale up downstream process of a soluble recombinant protein. Sometimes, however main fraction of the protein is produced in the insoluble fraction, as inclusion bodies. Although inclusion bodies are usually unwanted, cause of the problem with the refolding of the protein, they are good alternative in the case of intrinsically disordered proteins, as their separation from the cell lysate is easy and efficient way of protein purification. In case of ordered proteins this limitation can be overcome by refolding process. Nevertheless it is a challenging task, cause of the fact that each protein is unique and require specific approach for the refolding process. When all the refolding trails are unsuccessful, the last choices are to redesign the expressed domain or to use another expression system.

2.2 Protein purification

High protein purity is essential for the characterization of the function, structure and interactions of the protein of interest. The number of applied purification steps will always depend upon the purity requirements and purpose for which the protein is needed. However, the best protein purification strategy is one in which the highest level of purification is reached in the fewest steps, since each protein purification step usually results in some degree of product loss.

The preliminary step in protein purification is cell lysis, where the cells are disrupted and relevant protein fraction is extracted. The method of choice of protein extraction depends on how fragile the protein is and how sturdy the cells are. Its suitable selection is crucial, because inadequate chosen method can affect the target protein's integrity and activity, or expose it to degradative conditions. Among many various mechanical, physical or chemical techniques, more frequently used are sonication, repeated freeze-thaw lysis, detergent lysis, enzymatic lysis and osmotic lysis. The extraction process also release proteolytic enzymes which might degrade or artificially modify the extracted protein, that lower the overall yield. To prevent these effects it is usually desirable to add directly in the cell suspension a cocktail of protease inhibitors, proceed quickly, and keep the extract cooled, to slow down proteolysis.

The subsequent steps of purification procedure involve several chromatographic methods. Their choice depends mainly on the biophysical and biochemical properties of specific protein and exploit differences in protein size, charge, as well as binding affinity. Among many different chromatography techniques, the three most used techniques in this work were: ion exchange chromatography (IEX), size exclusion chromatography (SEC) and immobilized metal ion affinity chromatography (IMAC).

Ion exchange chromatography (IEX) separates proteins with differences in charge. The separation is based on the reversible interaction between a charged protein and an oppositely charged chromatographic medium. The sample is loaded onto a column in conditions favoring specific binding, such as calibrated pH and low ionic strength salt concentration, in order to enhance the interaction between target protein and column matrix. The net surface charge of a protein varies according to the surrounding pH. Typically, when the pH is above its isoelectric point (pI), a protein will bind to a positively charged anion exchanger. Below its pI, a protein will bind to a negatively charged cation exchanger. Elution is usually performed by changing

the pH or the ionic strength of the elution buffer in a gradient, or stepwise. Most commonly, samples are eluted with salt (NaCl), using a gradient elution.

Size-exclusion chromatography (SEC) is a chromatographic technique in which molecules are separated by their size, ideal for the final step purification for the preparation high purity samples. The column matrix is composed of a range of beads with slightly different pore sizes. When the dissolved molecules of various sizes flow into the column, large molecules migrate quickly through the column, because they do not penetrate the pores. On the other hand, small molecules enter deep into the pores and consequently flow more slowly through the column. SEC can be used to separate protein by size and shape, to exchange the buffer and isolate protein mixtures, as well as separate monomers from aggregates. High resolution fractionation can be used to determine the molecular mass performing a molecular weight distribution analysis using available standards.

Immobilized metal ion affinity chromatography (IMAC) is the most used affinity technique in case of peptide with fusion tags. IMAC separates proteins on the basis of reversible interaction between side-chains of specific amino acids (usually histidine) and a specific ligand attached to a chromatographic matrix (mainly chelated transition metal ions e.g. Zn^{2+} or Ni^{2+}). The target protein is usually washed from the impurities and then, eluted using increasing concentration of imidazole, which acts like a competitive agent. Desorption might be also performed nonspecifically by changing pH, which decrease the affinity of the tag for the resin, changing ionic strength or polarity. To remove the fusion partner from the target protein, enzymatic digestion using a specific protease such as TEV, Thrombin etc. is necessary. In order to separate the fusion tag from the target native protein a second IMAC is usually performed.

2.3 Biotechnological production of Aβ peptides.

I described the biotechnological methods of samples preparation of different kinds of Aβ peptides.

The AβM40, Iowa (D24N) and Flemish (A22G) mutants of AβM40 and AβM42 peptides without any fusion tags, as well as Aβ40 and Aβ42 without starting methionine fused with N-terminal hexahistidine affinity tag, were expressed as inclusion bodies in *E. coli.*

2.3.1 Aβ peptides with Met

The complementary DNA of AβM40/AβM42 was cloned in the pET3a vector using the *Nde*I and *Bam*HI restriction enzymes.

In order to obtain Iowa (D24N) and Flemish (A22G) mutants of AβM40, site directed mutagenesis was performed.

The peptides were expressed in the BL21 (DE3)pLys *E. coli* strain. The expressed peptides contain exogenous N-terminal methionine due to the translation of start codon. However, as it is reported in the literature (Walsh et al. 2009), the presence of an N-terminal methionine, does not affect the fibrillation kinetics or morphology of the fibrils formed by AβM40 or AβM42. In order to increase the proteins yield, the growth was performed using the Marley method (Marley et al., 2001). The cells transformed with the AβM40/AβM42 expression plasmid were predominately grown in rich medium at 37°C until OD600 reached 0,6, centrifuged and exchanged into an isotopically defined minimal media enriched with $(^{15}NH_4)_2SO_4$(1 g/L) and [^{13}C] glucose (4 g/L). The peptides expression was induced with 1.2 mM isopropyl β-D-1-thiogalactopyranoside and cells were harvested after 4 hours incubation at 39°C.

The peptides were purified as reported (Bertini et al. 2011a; Hellstrand et al. 2010; Jan et al. 2010; Walsh et al. 2009) with some modifications using a combination of anion-exchange and size exclusion chromatography. All the manipulations were performed at slightly alkaline pH in order to avoid the formation of structural contaminants produced by isoelectric precipitation. The inclusion bodies were first solubilized with 8M urea and then purified by ion exchange chromatography performed in batch. The use of free resin in the batch mode versus prepacked column (DEAE-cellulose column) prevent the possible aggregation and allows to obtain high yield of monomeric peptide (Walsh et al. 2009). For this purpose resin DE52 on Büchner funnel with filter paper on a vacuum glass bottle was used. Elution was done using different concentration of buffer of NaCl. Protein was eluted with 125 mM concentration of the salt. In the case of AβM42, protein was also presented in fraction 20 mM, 150 mM, 200 mM and 1M, probably cause of progressive aggregation of the sample. Guanidinium chloride was then added to the solution to reach the final concentration of 6 M. All obtained fraction of diluted protein was concentrated to final volume using Amicon device. A number of methods to concentrate the Aβ solution was examined. Although several different methods, within the 3 kDa molecular mass cut-off centrifugal

devices, proved useful, Amicon device resulted as the best solution for highly concentrated proteins. The next step of purification was gel filtration, which was performed using the preparative column Sephadex 75 HiLoad 26/60 with the 50 mM (NH_4)OAc pH 8.5 as a buffer. The obtained fractions were collected together and concentrated. During all purification protein purity was analysed using SDS-PAGE electrophoresis, whereas the protein concentration was estimated using spectrophotometer.

This two-step purification allow to obtain a highly pure products with the yield in the range 10 mg of AβM40 and 5-10 mg AβM42 per liter of culture.

2.3.2 Aβ peptides without Met

Aβ40 and Aβ42 was produced in the *E. coli* cytoplasm as fusion protein with N-terminal hexahistidine affinity tag. The fusion construct consists of a soluble polypeptide segment comprising 19 repeats of the tetrapeptide sequence NANP, a TEV protease cleavage site (sequence ENLYFQ), dipeptide linker sequences and the Aβ sequence.

Aβ40 and Aβ42 without methionine were expressed in the BL21 (DE3) *E. coli* strain. Cells were grown in rich medium (LB or Terrific broth) till high OD values. The peptide expression was induced with 1-1.2mM IPTG and cells were harvested after 4 hours incubation at 39°C. After the removal of the soluble proteins the inclusion bodies were solubilized with 20mM TRIS pH 8.0, 8M and purified by affinity chromatography using a nickel chelating (His-Trap) column under the denaturating conditions, followed by digestion with AcTEV protease. To avoid protein aggregation and improve the separation of cutted/uncutted protein 8M urea or 6M guanidine hydrochloride was introduced in second affinity column steps. As a final step of purification a gel filtration in 50mM ammonium acetate pH 8.5 using a Sephadex 75 26/60 column was used. Obtained protein was dialyzed in water and liofilized.

In order to improve the tag digestion in case of Aβ42 peptides, different purification procedure, introducing organic solvents were adopted. The inclusion bodies were solubilized by 6M guanidinium chloride, and the protein was purified by metal chelating affinity chromatography on Ni^{2+}-nitrilotriacetic acid agarose in the presence of 6M guanidinium chloride lowering the pH. The fusion proteins were further purified via reversed phase high-performance liquid chromatography (RP-HPLC) using semi-preparative Zorbax SB300 C8 column (Agilent), lyophilized from aqueous acetonitrile and directly used for TEV protease

cleavage. A cleavage efficiency of about 70% was achieved after incubation at pH 8.0 and 4°C for 16 h at a protein concentration of 100 μM in the presence of 5 μM TEV protease. The cleavage mixture was subsequently applied to RP-HPLC which allowed quantitative separation of the hydrophobic Aβ42 peptide from the other, more hydrophilic components in the cleavage reaction. The final yield of purified Aβ42 was 20 mg/l of culture. However this approach encounter problem with solubilization of liofilized protein in water. To disaggregate the Aβ and generate monomeric random coil structure different procedures were proposed: predissolution of the peptide in dilute base solution, predissolution in TFA and 1,1,1,3,3,3-hexafluoro-2-propanol solvents (HFIP) (Jao et al. 1997). Finally already reported protocol (Broersen et al. 2011) for the solubilization of Aβ peptide, that involves sequential solubilization using structure-breaking organic solvents hexafluoroisopropanol and DMSO followed by column purification and results in standardized aggregate-free Aβ peptide was applied. As it was reported in pure DMSO, Aβ appears to be monomeric and lacks any β -sheet character (Shen and Murphy 1995).

2.4 Preparation of Aβ fibrils for solid state NMR (SSNMR) studies

A general overview

Highly ordered and homogeneous samples is crucial for high-resolution studies by SSNMR. However, in amyloid systems it is rather common that several differently shaped aggregates coexist in a mixture, making preparation of the proper samples very difficult. They usually increase the complexity of spectra and impede further data analysis at site-specific level. These limitations can be overcome by programmed isotopic labelling schemes or sequence truncation, but each of these methods hampers complete structural analysis by SSNMR. Another strategy to overcome this restraint is the seeding procedure, which leads not only to an improvement in the homogeneity of Aβ fibrils, but also permits insights into the molecular structures of amyloid fibrils developing in human tissue. This tactic is feasible after reconstruction of isotope enriched *in vivo* fibrils using brain tissues as seeds from patients with AD (Paravastu et al. 2009). This approach is made possible by the fact that *in vitro* studies have shown that seeding procedure allows for obtaining fibrils that retain exactly the same molecular structures, corresponding to the seeds from the brain of patients with AD (Petkova et al. 2005). This strategy also has many drawbacks, because the sample obtained in this way might contain significant contamination from many tissue components such as lipids.

However it permits to restore pathological samples from AD patients and get high resolution structural characterization of these assemblies.

As heterogeneity also depends significantly upon different aggregation conditions, several different factors must be taken into consideration. One important key factor is the purity of the starting materials. The presence of pre-existing aggregates can result in a lack of reproducibility, as well as in a meaningful discrepancy in fibrillogenesis kinetics. Several different protocols have been developed in order to solve this issue, resulting in standardized aggregate-free Aβ peptide samples (Broersen et al. 2011, Jao et al. 1997, Fezoui et al. 2000). Disaggregation of the Aβ assemblies involved the use of the structure-breaking organic solvents hexafluoroisopropanol (HFIP) and DMSO, trifluoroacetic acid (TFA) pre-treatment, and pre-dissolution of the peptide in a dilute base solution (e.g. NaOH). Aggregates might be also removed by less drastic methods as filtration, using a syringe filter (0,20 μM) or centrifugation. Each of these approaches allows aggregate-free material to be obtained. Another significant aspect is represented by the conditions of the fibrillation protocols such as concentration, pH, ionic strength, temperatures. The incubation of the sample in quiescent condition leads to fibrils with the morphology of "twisted pairs" (Paravastu et al. 2008), instead gentle agitation results in striated ribbons (Petkova et al. 2006) or "flat" striated bundles (Bertini et al. 2011a). The appropriate selection of fibrillation strategy is essential for obtaining high quality samples for high resolution SSNMR.

Protocol for generation of Aβ fibrils

In this work, fibril mixture samples of double labeled AβM40 and unlabeled AβM42 in molar ratio (7:3), double labeled AβM40 and unlabeled AβM42 in molar ratio (1:1) and double labeled AβM42 and unlabeled AβM40 in the molar ratio of (1:1) were prepared.

Samples of Aβ fibrils for the SSNMR studies were prepared according to previously published, validated and optimized protocol (Bertini et al. 2011a), which provides the high reproducibility of the samples. Uniformly (^{13}C,^{15}N) – enriched protein samples at 100 μM concentration in 50 mM ammonium acetate (pH 8.5) were filtered through a 0,20 μM syringe filter and subsequently incubated at 37 °C under shaking (950 rpm) for 4 weeks. Fibrils were collected by the overnight ultracentrifugation at 60000 rpm (ca. 2.65 × 105 g) and 4 °C for 24 h. The pellet was washed with fresh and cold ultrapure water (Millipore) for three times (1 mL per time), and then wet material was packed into a 3.2 mm ZrO_2 MAS rotor under 4 °C. The fibril samples were kept fully hydrated during all the steps.

2.5 Biotechnological production of hSOD1 apo protein

I described the method of samples preparation of wild type (wt) superoxide dismutase (SOD1) protein and its mutant C57A/C146A for spectroscopic characterization.

Superoxide dismutase (SOD1) wild type (wt) and SOD mutant C57A/C146A were overexpressed in the BL21 DE3 Origami plys *E. coli* strain. The fusion proteins were obtained by growing the cells in minimal medium in shaking flasks at 37°C until OD600 reached 1 and then induced with 0.5 mM IPTG for 12 h at 25°C. Proteins were isolated by sonication in 5 mM imidazole buffer at pH 8 and centrifuged at 40 000 RPM for 20 min. Purification was performed by affinity chromatography using a nickel chelating (His-Trap) column and digestion with AcTEV protease. Next step of purification was gel filtration, which was performed using the preparative column Sephadex 75 HiLoad 26/60. The metal-free proteins was prepared by the dialysis according to previously published protocols (McCord & Fridovich, 1969).

2.6 Biophysical characterization

Biophysical techniques provide low-resolution structural characterization of biological macromolecules. However they require small amounts of biological material, and what is more important they don’t demand labeling, what make them excellent complementation of NMR study.

2.6.1 UV-visible spectroscpy (UV-vis)

UV-visible spectroscopy (UV-vis) is a technique that measure the absorption of electromagnetic radiation by molecules in the ultrviolet-visible region. In this region of the electromagnetic spectrum, molecules undergo electronic transition.

UV-vis spectroscopy allows for following ligand-binding interactions, enzyme catalysis, conformation transitions and is commonly used as a tool to quantify the concentration of proteins and nucleic acids. Potein concentration can be determined by the absorption around 280 nm (most of the proteins contain aromatic acid residues - tryptophan, tyrosine and phenylalanine), using the protein extinction coefficient and the Beer-Lambert law.

2.6.2 Fluorescence spectroscopy

Fluorescence spectroscopy is a common technique used in studies of the structure and dynamics of macromolecules, which allows a real-time observation of the dynamics of intact biological systems with an unprecedented resolution. In fluorescence spectroscopy, the molecule is first excited, by absorbing a photon, from its ground electronic state to one of the various vibrational states in the excited electronic state. This higher energy state is unstable, and when the molecule returns to the ground state again a photon with a different wavelength is emitted and can be measure (Lakowicz 1983).

Fluorescent studies provide a number of information about physical and physicochemical properties of proteins, as well as theirs intermolecular interactions and conformational changes. In addition, fluorescence spectroscopy can be used to study those structural and dynamic properties of proteins which are directly related to such biological functions as specific binding (recognition), biocatalysis, membrane transport, and muscular motility.

However, the use of fluorescence spectroscopy is only possible when the biologically active compounds contain in their structure a fluorophore. Fluorescent proteins contain three aromatic amino acid residues (tryptophan, tyrosine, phenylalanine) which may contribute to their intrinsic fluorescence when are excited by ultraviolet light. The most important is the presence of tryptophan, which has much stronger fluorescence and higher quantum yield than the other two aromatic amino acids.

In this work fluorescence spectroscopy was used to monitor the formation of oligomeric species by hSOD1 wt in the presence of cisplatinum and in the presence of cisplatinum together with small molecules (MNO1106 and MNO1109) according to previously described procedure (Banci et al. 2007 ; Banci et al. 2008). The solution fluorescence emission was measured, over time of incubation, with a Cary 50 Eclipse spectrophotometer supplied with a single-cell Peltier thermostated cell holder regulated at 37˚C. Fluorescence was followed with ThT, a dye that binds to extended β-sheets, which is typical structural feature of amyloids (Biancalana & Shohei 2010; Naiki et al.1989). Free ThT has excitation and emission maxima at 350 and 450 nm, respectively. However, upon binding to amyloid-oligomers, the excitation and emission wavelengths change to 450 and 485 nm, respectively. Fifty-four microliter aliquots of sample were added to 646 µl of a 215 µM Tht solution in a 20 mM phosphate buffer at pH 7.0. The background fluorescence spectrum of

the buffer was subtracted. The excitation wavelength was 446 nm (bandwidth, 10nm), and the emission was recorded at 480 nm (bandwidth, 10 nm). Fluorescence intensity at 483 nm was plotted against the time of incubation.

2.6.3 Transmission electron spectroscopy (TEM)

Transmission electron microscopy (TEM) is a microscopy technique in which a beam of electrons is transmitted through an ultra-thin specimen of interest, interacting with the specimen as it passes through. An image is formed from the interaction of the electrons transmitted through the specimen. Once the electrons pass the anode, they are focused by condenser lens onto the sample grid. The sample grid is usually a copper mesh grid with a support film. Before TEM analysis, specimen of interest is adsorbed to this film and typically stained using a heavy metal salt which have high atomic number capable of scattering electrons.

The TEM reveals levels of detail and complexity inaccessible by light microscopy, because it uses a focused beam of high energy electrons and allows detailed micro-structural examination through high-resolution. It is used to investigate the morphology, examine the structure, composition, and properties of specimens in submicron detail.

Here transmission electron microscope was used to characterized the morphology and molecular architecture of Aβ fibrils and prefibrillar aggregates. For TEM tests, a solution of Aβ fibrils was dropped and dried on a Cu grid covered by carbon film. The fibrils were then stained in freshly prepared aqueous uranyl acetate solution for 20 min. After that the grid was rinsed gently using ultrapure water for 1 min and dried again. The bright-field TEM images were collected on a Philips CM12 microscope operating at 80 kV.

2.7 SSNMR spectroscopy

NMR spectroscopy is a technique based on the interaction of the nuclear spin with the electromagnetic radiation, in the presence of an external magnetic field. Nowadyas solution and solid state NMR (SSNMR) are powerful tools to characterize the structure, dynamics, and interactions of biomolecules. Solution NMR is the most common tool for structure determination, but SSNMR is becoming important technique as a consequence of developments in sample preparation and in theoretical background.

SSNMR is one of the best techniques for obtaining atomic resolution structures of amyloid fribrils sufficient for the development of complete molecular models (Tycko 2010). Since application of X-ray crystallography is limited to small amyloidogenic peptides and cryo-electron microscopy (cryo-EM) is hindered by its relatively low spatial resolution, SSNMR allows for substantial advancement in understanding the structure of amyloid fibrils.

In this work SSNMR was applied to detailed structural characterization of prefibrillar and fibrillar assemblies. To investigate prefibrillar deposits a method termed sedimented solutes NMR (SedNMR) was used. To immobilize macromolecules and make them amenable for SedNMR studies, sedimentation through ultracentrifugation, either by magic angle spinning (in situ) (Bertini et al. 2011b) or preparative ultracentrifuge (ex situ) (Bertini et al. 2012) was introduced. In situ SedNMR allows to control the kinetics of formation of soluble Aβ assemblies. Ex situ sedimentation by common ultracentrifuge with the help of devices previously designed to pack NMR rotors with precipitates or microcrystals (Böckmann et al. 2009) effectively increase the amount of solid-state NMR sensitive material in the rotor improving this way the sensitivity of the experiments. This approach allows for sedimentation of even smaller solutes and allows to obtain species of different molecular weights by changing the experimental conditions.

2.8 References:

Banci L., Bertini I., Durazo A., Girotto S., Butler Gralla E., Martinelli M., Selverstone Valentine J., Vieru M., Whitelegge J. P., 2007. *Biophysics.* 104(27):11263-7.

Banci L., Bertini I., Boca M., Girotto S., Martinelli M., Valentine J. S., Vieru M. 2008. *PLoS One.* 3(2):e1677.

Bertini I., Gonnelli L., Luchinat C., Mao J., Nesi A. 2011a. *Journal of the American Chemical Society USA.* 133(40): 16013–22.

Bertini I.; Luchinat C.; Parigi G.; Ravera E.; Reif B.; Turano P. 2011b. *Proc. Natl. Acad. Sci. USA,* 108, 10396-10399.

Bertini I.; Engelke F.; Luchinat C.; Parigi G.; Ravera E.; Rosa C.; Turano P. 2012. *Phys. Chem. Chem. Phys.* 14, 439-447.

Biancalana M. & Shohei Koide S. 2010. *Biochim Biophys Acta*.1804(7):1405-12.

Böckmann A., Gardiennet C., Verel R., Hunkeler A., Loquet A., Pintacuda G., Emsley L., Meier B. H., Lesage A. 2009. *Journal of Biomolecular NMR*. 45 (3), 319 –327.

Broersen, K., Wim J., Rozenski J., Vandersteen A., Pauwels K., Pastore A., Frederic Rousseau, J. Schymkowitz. 2011. *Protein engineering, design &selection: PEDS* 24(9): 743–50.

Fezoui Y., Hartley D. M., Harper J. D., Khurana R., Walsh D. M., Condron M. M., Fink A. L., Teplow D. B. 2000. *Amyloid.* 7(3):166-78.

Hellstrand E., Boland B., Walsh D. M., Linse S. 2010. *ACS chemical neuroscience.* 1(1): 13-18.

Jan A., Hartley D. M., Lashuel H. A. 2010. *Nature protocols.* 5(6): 1186–1209.

Jana S. & Deb J. K. 2005. *Appl. Microbiol. Biotechnol.* 67, 289-298.

Jao S. C., Kan M., Talafous J., Orlando R., Zagorski M. G. 1997. *International Journal of Experimental & Clinical Investigation.* 4(4): 240–52.

Lakowicz J. R. 1983. *Principles of fluorescence spectroscopy.* Plenum Press, New York.

Marley J., Lu M., Bracken C. 2001. *Journal of biomolecular NMR.* 20(1): 71–75.

McCord J. M. , Fridovich I. 1969. *J Biol Chem*. 244:6049-6055.

Naiki H., Higuchi K., Hosokawa M., Takeda T. 1989. *Anal Biochem.* 177(2):244-9.

Paravastu A. K, Leapman R. D., Yau W. M., Tycko R. 2008. *Proceedings of the National Academy of Sciences USA.* 105 (47), 18349–18354.

Paravastu A. K., Quhwash I., Leapman R. D., Meredith S. C., Tycko R. 2009. *Proceedings of the National Academy of Sciences USA.* 106 (18), 7443-7448.

Petkova A. T., Leapman R. D., Guo Z. H., Yau W. M., Mattson M. P., and Tycko R. 2005. *Science.* 307(5707):262-5.

Petkova A. T., YauWai-Ming, Tycko R. 2006. *Biochemistry*. 45 (2),498–512.

Shatzman A. R. 1995. *Current Opinion in Biotechnology*. 6, 491-493.

Shen C. L., Murphy R. M. 1995. *Biophysical journal*. 69(2): 640–51.

Tycko R. 2010. *Annual Review of Physical Chemistry*. 62:279-99.

Walsh D. M., Thulin E., Minogue A. M., Gustavsson N., Pang E., Teplow D. B., Linse S. 2009. *FEBS Journal*. 276(5): 1266–81.

Chapter 3 Results

3.1 Formation kinetics and structural features of Beta-amyloid aggregates by sedimented solute NMR

I performed protein expression, purification and electrophoresis tests together with Gianluca Gallo and supported preparation the ultracentrifugation samples for SSNMR. I participated in data analysis and interpretation, and wrote with Gianluca Gallo part of matherials and methods for the manuscript and contribuited in paper revision.

3.2 Structural characterization of AβM40/AβM42 fibril mixture

I contributed to the molecular, biological and biophysical part of the project, performing expression, purification and fibrillation experiments (including optimization) together with Gianluca Gallo. I participated in data analysis and interpretation, as well as in writing of the draft.

3.3 Lipoic derivatives in synergistic treatment of human superoxide dismutase with cisplatin

I expressed and purified hSOD1 wt protein and prepared apo form of SOD1. I also carried out monitoring SOD1 aggregation by ThT fluorescence measurements and wrote part of the draft.

3.4 From IDP to Alzheimer's disease. Brief review

I proposed the content of the chapter, wrote together with Tatiana Kozyreva first draft and contributed in the chapter revision.

3.5 Recombinant IDPs for NMR. Tips and tricks

I contributed to the content of the chapter and participated in the chapter revision.

“Formation kinetics and structural features of Beta-amyloid aggregates by sedimented solute NMR.”

Ivano Bertini [a,b,c], *Gianluca Gallo* [a,d], *Magdalena Korsak* [a,b], *Claudio Luchinat* [a,c,d], *Jiafei Mao* [a,c,e], *Enrico Ravera* [a,d]

[a]Magnetic resonance Center (CERM), University of Florence, Via L. Sacconi 6, 50019 Sesto Fiorentino, Italy

[b]Giotto Biotech, Via Madonna del Piano 6, 50019 Sesto Fiorentino, Italy

[c]Fondazione Farmacogenomica FiorGen onlus, Via L. Sacconi 6, 50019 Sesto Fiorentino, Italy

[d]Department of Chemistry “Ugo Schiff”, University of Florence, Via della Lastruccia 3, 50019 Sesto Fiorentino, Italy

[e]Current address: Goethe Universität
Max-von-Laue-Strasse 9, Biozentrum N202
60438 Frankfurt am Main (Germany)

ChemBioChem 2013, 14, 1891-1897

ChemPubSoc Europe

DOI: 10.1002/cbic.201300141

Formation Kinetics and Structural Features of Beta-Amyloid Aggregates by Sedimented Solute NMR

Ivano Bertini†,[a, b, c] Gianluca Gallo,[a, d] Magdalena Korsak,[a, b] Claudio Luchinat,*[a, c, d] Jiafei Mao,[a, c, e] and Enrico Ravera[a, d]

Dedicated to Prof. Dr. Ivano Bertini (1940–2012): his brilliant mind and motivating spirit shine in this work and will continue to inspire us for many years to come.

The accumulation of soluble toxic beta-amyloid (Aβ) aggregates is an attractive hypothesis for the role of this peptide in the pathology of Alzheimer's disease. We have introduced sedimentation through ultracentrifugation, either by magic angle spinning (in situ) or preparative ultracentrifuge (ex situ), to immobilize biomolecules and make them amenable for solid-state NMR studies (SedNMR). In situ SedNMR is used here to address the kinetics of formation of soluble Aβ assemblies by monitoring the disappearance of the monomer and the appearance of the oligomers simultaneously. Ex situ SedNMR allows us to select different oligomeric species and to reveal atomic-level structural features of soluble Aβ assemblies.

Introduction

We have developed a method, termed sedimented solutes NMR (SedNMR), in which solid-state NMR (SSNMR) experiments are used to observe proteins that are sedimented from solution using an ultracentrifugal field.[1–7] In concentrated protein solutions, rotational diffusion is restricted by self-crowding.[8] SedNMR relies on the extreme concentration of the sediment[3,9,10] to make the protein appear solid on the MAS timescale and observable through SSNMR. Sedimentation of macromolecules into this type of solid-like phase can be achieved in two ways: 1) direct in situ sedimentation by magic angle spinning (MAS) of the NMR rotor that acts as an ultracentrifuge[1] (MAS-induced sedimentation;[3] Figure 1 A), or 2) ex situ sedimentation by common ultracentrifuge[3–5] with the help of devices previously designed to pack NMR rotors with precipitates or microcrystals[11] (UC-induced sedimentation;[3] Figure 1 B).

[a] Prof. Dr. I. Bertini, G. Gallo, M. Korsak, Prof. C. Luchinat, Dr. J. Mao, Dr. E. Ravera
Magnetic Resonance Center (CERM), University of Florence
Via L. Sacconi 6, 50019 Sesto Fiorentino (Italy)
E-mail: claudioluchinat@cerm.unifi.it

[b] Prof. Dr. I. Bertini, M. Korsak
Giotto Biotech
Via Madonna del Piano 6, 50019 Sesto Fiorentino (Italy)

[c] Prof. Dr. I. Bertini, Prof. C. Luchinat, Dr. J. Mao
Fondazione Farmacogenomica FiorGen onlus
Via L. Sacconi 6, 50019 Sesto Fiorentino (Italy)

[d] G. Gallo, Prof. C. Luchinat, Dr. E. Ravera
Department of Chemistry "Ugo Schiff", University of Florence
Via della Lastruccia 3, 50019 Sesto Fiorentino (Italy)

[e] Dr. J. Mao
Current address: Goethe Universität
Max-von-Laue-Strasse 9, Biozentrum N202
60438 Frankfurt am Main (Germany)

[†] Prof. Dr. I. Bertini passed away on July 7th 2012

Supporting information for this article is available on the WWW under http://dx.doi.org/10.1002/cbic.201300141.

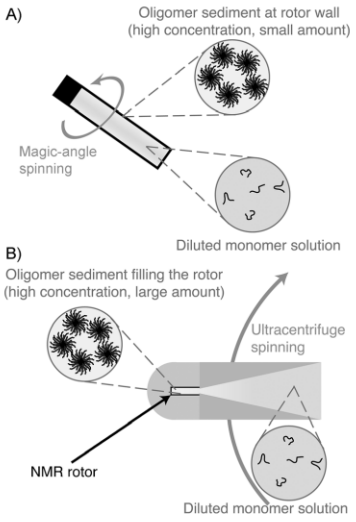

Figure 1. Pictorial representation of the process of sedimentation. In MAS-induced sedimentation (top), the sediment is created in a thin layer at the rotor walls (width of the sediment layer is greatly exaggerated). UC-induced sedimentation (bottom) can be used to effectively fill the rotor with sediment.

Previous theoretical calculations, as well as experimental evidence, have shown that proteins or protein complexes with molecular weights above 30 kDa could be efficiently sedimented.[1,3] In situ SedNMR has been demonstrated for ferritin,[1] bovine serum albumin, and carbonic anhydrase,[3] and has already been applied to the study of αB-crystallin dynamics[12]

and reactivity.[13] Ex situ SedNMR has been applied to ferritin[3] and to a dodecameric helicase.[5]

Aβ aggregates show marked synaptotoxicity and neurotoxicity in both isolated neuronal cells and animal models and are therefore believed to be pathologically relevant in Alzheimer's disease (AD).[14–16] From the recent literature, these species show significant morphological and structural diversities and exert varied toxic effects.[17–20] Therefore, high-resolution structural characterization of Aβ aggregates is of primary importance to understand the complex molecular mechanisms of AD.[16] We propose that in situ or ex situ SedNMR can be used to characterize oligomeric species, measure their formation kinetics, and even selectively sediment some of these species by their different molecular weights.

Different structural models of mature Aβ fibrils have been proposed in several recent solid-state NMR (SSNMR) works.[21–24] Residue-specific information on prefibrillar Aβ aggregates (e.g., oligomers and protofibrils) and on structural persistence in the monomer has also been obtained through various experimental and theoretical methods.[15,17,20,25–32] However, prefibrillar assemblies are often unstable compared to mature fibrils and, therefore, cannot be trapped easily unless dehydration,[28] organic solvents,[32] or interaction partners[15,33,34] are introduced during sample preparation. To date, characterization of prefibrillar Aβ aggregates in purely aqueous environments remains a significant challenge.[35] In pioneering works by the groups of Smith and Ishii, SSNMR characterization of Aβ oligomeric states in the lyophilized state were obtained and showed that the arrangement of the peptide was mainly β-sheet.[25,28]

It has been reported[20,28,29,36,37] that in aqueous solutions, Aβ peptides spontaneously form soluble aggregates of high molecular weight (50–200 kDa). These species should be large enough to sediment and thus become visible by SSNMR. Here we show that this is indeed the case, and that aggregates of different molecular weights can be selectively obtained by changing the experimental conditions.

Results and Discussion

Kinetics determination through in situ SedNMR

Freshly prepared solutions of Met-0 Aβ40 peptide (AβM40; 160 μmol dm^{-3}) were analyzed by solution NMR at 280 K. The free, intrinsically disordered Aβ monomer (4.6 kDa) was always the only component in NMR spectra of the fresh samples. The disappearence of the sofastHMQC[38] signal was used to monitor aggregation. Consistent with what was observed in ref. [39], the signal of the monomer persisted for a long time in the un-agitated solution. After scratching the sample with a glass rod, the signal of the monomer began to decrease, with a time dependence that appeared as an exponential decay after the induction time (Figure S1).

For in situ SedNMR experiments, the ^{13}C signals of free monomers and of AβM40 sedimented aggregates can be monitored using different ^{1}H–^{13}C polarization transfer methods: the solution portion (i.e., having a τ_c of the order of tenths of ns, containing the monomer and possibly aggregates with MW < 60 kDa) can be excited through the J-coupling-based insensitive nuclei enhancement by polarization transfer (INEPT[40]) and detected under low power ^{1}H decoupling (2.5 kHz) or no decoupling at all;[41,42] dipolar-based cross-polarization (CP[43]) can be used to excite the solid portion with results that are immobilized on the MAS timescale (i.e., having τ_c longer than the MAS period).[1,44] When freshly prepared and concentrated AβM40 solutions are introduced in the SSNMR rotor, only the INEPT signal is visible (Figure S2). After applying MAS for a period of time, the intensity of the INEPT signal decreases in favor of the growth of the CP signal (Figure 2).

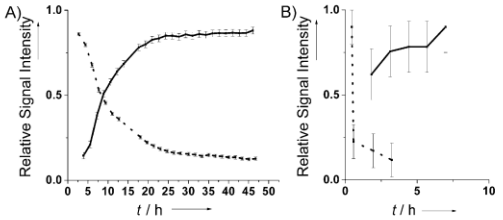

Figure 2. Relative signal intensity of INEPT (dashed) and CP (solid) signals for AβM40 (left) and AβM42 (right) as a function of time, spinning at 12 kHz and 277 K.

We have quantified the relative contribution of the solution and the solid portions as a function of time. An 8 mmol dm^{-3} AβM40 solution was sealed in a 4.0 mm solid state NMR rotor (internal radius 1.5 mm) and spun at 12 kHz over three days, during which periodically interwoven INEPT and CP spectra were recorded. The intensities of the solution and solid signals are plotted in Figure 2 (left) as dashed and solid lines, respectively. Data processing is described in the Supporting Information. By using Equation (3) in ref. [3], it is possible to calculate that the sediment observed under these conditions contains species with molecular weights above 70 kDa, as calculated from a MAS rate of 12 kHz (see the Supporting Information). Aggregates of this molecular weight would be expected to sediment completely in about 3 h (see the Supporting Information), whereas Figure 2 (left) shows that the formation process is not completed until about 30 h. Therefore, the rate of formation of these aggregates is significantly slower than that of their sedimentation. Aggregates formed slowly, thereby enabling us to obtain clean information about the kinetics. This physical picture is summarized in Figure 3. It is also important to note that the 1D ^{13}C CP spectra do not change significantly with time (Figure S3).

On the basis of these data, kinetic information was obtained for oligomer formation; due to the use of ultracentrifugation, these species were trapped and were prevented from changing. The kinetic behavior of this sample is consistent with what previously reported in ref. [37], given the differences in construct, temperature, and initial monomer concentration. To obtain an independent validation of our approach, the same experiment was performed on an AβM42 sample at

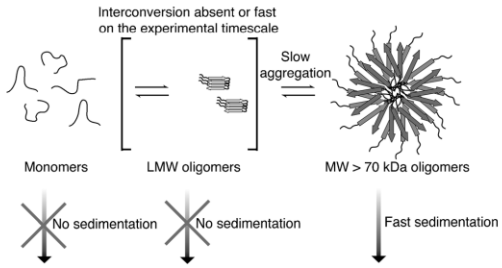

Figure 3. The physical picture underlying the kinetic determination: monomers and low-molecular-weight oligomers are too small to sediment. Their conversion into larger oligomers is slow on the experimental timescale; thus, they are the only contribution to the solution NMR signal. Larger oligomers are sedimented as soon as they are formed; thus, they are the only contribution to the solid state NMR signal. The quaternary structures shown only reflect morphologies reported in the literature.

0.8 mmol dm^{-3} concentration. In this case, the aggregation rate is significantly faster (half-time of less than 1 h, Figure 2 (right)), consistent with the known behavior of the Aβ42 isoform.[39,45,46] This observation confirms that the much slower kinetics observed in the case of the AβM40 species is not due to the sedimentation of the oligomers but truly reflects their formation (Figure 3). By the same token, we can conclude that for AβM42, detailed analysis is prevented by formation and sedimentation possibly occurring on similar timescales. Data are plotted in Figure 2 (right) as solid (CP) and dashed (INEPT) lines.

In summary, species above 70 kDa can be observed by CP, whereas those below this molecular weight can be observed through INEPT. The fact that the relative intensities of the two signals sum to about 1 throughout the time course of the experiment shows that intermediate species that are invisible both by solution-state NMR and by SSNMR are not formed to an appreciable extent. Further discussion is given in the Supporting Information.

Sedimentation is much more efficient on large Aβ aggregates than on small Aβ monomers; in the experimental conditions applied here for MAS-induced sedimentation, the monomer does not form an appreciable concentration gradient. Therefore, sedimentation has the ability to separate the soluble aggregates from the bulk solution and drive the equilibrium towards the oligomeric species.[7,47] Obviously, if a small amount of large aggregates is already present, it will sediment along with the small species that are forming. However, in this case, the presence of significant amounts of large aggregates can be excluded, given that no solid-state NMR signal is observed at the beginning of the experiment.

It should be noted that formation of fibrils is a highly anisotropic phenomenon, mainly requiring aggregation in only one dimension. Although this is easily attained in classical fibrillation approaches,[23,24,48,49] we expect that this process can be hindered by the strongly impaired rotation of the oligomeric species once they are sedimented. Minton and Ellis have predicted, using scaled particle theory, that aggregation is made faster by macromolecular crowding,[50] and experimental verification was provided in ref. [51]. Our hypothesis is in line with coarse-grained calculations in ref. [52], suggesting that crowding will increase the oligomerization kinetics, simultaneously preventing the formation of fibrils. This means that a sedimented sample could be rendered inert, and prefibrillar Aβ aggregates could be stabilized in such a phase.

The impact of self-crowding on aggregation kinetics might not be trivial: the oligomers increase in concentration; thus, they can extend by binding the free monomers. The aggregation kinetics will therefore be accelerated by the increase in the concentration of one reagent. Overall, three major aspects must be considered:

1) the tight packing of the oligomers at the rotor walls will prevent diffusion of the species; thus, at some point in the process, the solution will be devoid of free monomers, and successive aggregation will be hindered;
2) the concentration of the oligomers is increased within a limited amount of space; thus, the bulk monomer will not sense any increase in oligomer content;
3) The oligomers are subtracted from the bulk and therefore cannot function as seeds[53] for further aggregation.

The overall effect on the measured kinetics is the following (shown in Figure S1): aggregation is made faster with respect to the unagitated solution (half time is reduced by approximately a factor of 4) and the kinetics appears more monoexponential, consistent with point 3 above). It is possible to monitor disappearance of the monomer by normal solution experiments (see Figure S1), but it is important to notice that only the comparison with the cross-polarization signal is able to reveal in full the kinetic properties of the system. In summary, MAS-induced sedimentation can be a simple but useful tool to monitor the kinetics of formation of the prefibrillar Aβ aggregates, especially by comparing different preparations, reducing the possible bias arising from MAS.

Structural features through ex situ SedNMR

A 2D ^{13}C–^{13}C correlation spectrum was recorded on the MAS-induced sediment. The appearance in the spectrum of the oligomers in the MAS-induced sediment suggests that elements of β-sheet structure are present (Figure S5). In the following section, we wish to demonstrate that structural information can be extracted from the SSNMR spectra of sedimented samples. In the above-described MAS-induced sedimentation experiment, all prefibrillar aggregates with molecular weights greater than 70 kDa that might be present in the solution are collected into sediment and cannot be distinguished. In contrast, in UC-induced sedimentation,[3–5] selection on the basis of the ultracentrifugation time is possible, and fractional centrifugation (a classical ultracentrifuge preparation) can be also used to differentiate fractions by molecular weight. An approach based on fractional centrifugation was successfully applied to soluble oligomers of α-synuclein, and SSNMR spectra were acquired in the frozen state.[54] In line with this, we applied UC-induced

Table 1. Condition for preparation of UC-induced samples.

Sample	Initial AβM40 concentration [mmol dm^{-3}]	Ultracentrifugation frequency[a] [rpm] centrifugation time [h]	Ultra-	Calculated lower limit of MW to sediment- [kDa]
UC-1	1.4	32000	24	70
UC-2	10.0	32000	24	70
UC-3	1.4	15000	72	150

[a] In a Beckman Coulter Optima L80K floor preparative ultracentrifuge using an SW32 rotor.

sedimentation to AβM40 preparations under different conditions. Conditions and samples are listed in Table 1.

Taking into account the time during which sedimentation was performed, the molecular weight limit was determined by the integrated Svedberg equation[55] to be about 70 kDa in samples UC-1 and UC-2, and 140 kDa for sample UC-3 (see the Supporting Information).

A priori control over the observed species in a MAS-induced sedimentation experiment on prefibrillar aggregates is not possible: to achieve sufficient averaging of anisotropic interactions, MAS should be operated at a frequency that provides centrifugal accelerations higher than what are normally done in an ultracentrifuge. This reduces the possibility of differentiating between high-molecular-weight components, and fractional centrifugation is unpractical in the closed rotor.

For the sample manipulations reported in Table 1, by numerical integration of Equation (3) of ref. [3] the lowest molecular weight of the sedimenting material should be of the order of 20 kDa,[4,29] (see the Supporting Information). The value of 70 kDa for sample UC-1 is in agreement with the value observed in its native gel, as shown in Figure 4. Bands of oligomeric AβM40 with molecular weights of 69 kDa (15-mer), 138 kDa (30-mer), and 207 kDa (45-mer) were observed. Oligomer bands were not found in the native gel of the UC-2 sample, but the bands of monomers as well as SDS-stable dimers and tetramers were detected from SDS-PAGE analysis of this sample, suggesting that larger assemblies can form at high initial monomer concentration.[56]

Sample UC-1 was analyzed through dipolar-coupling-based ^{13}C–^{13}C 2D SHANGHAI[57] spectra and ^{15}N–^{13}C correlation spectra (NCA/NCO,[58] Figure S4). Spectra have lines of the order of 80 Hz at 850 MHz and 100 Hz at 700 MHz for the Ile31 Cγ1 signal (Figure 5). As expected, samples UC-2 and UC-3, likely to contain a larger distribution of species and larger species, respectively, yielded less-resolved spectra, as reported in Figure S5. In the case of UC-2, this could be due to the large inhomogeneity of the oligomer sizes at high concentration; as seen by gel electrophoresis (Figure 4), larger species might be formed at high initial concentrations. In the case of UC-3, the lower resolution is probably due to a wider range of oligomer sizes at the high end, given the longer time during which the sample is allowed to aggregate.

Notably, the mixing times required for obtaining connectivities in sample UC-1 are rather long as compared, for instance, to the mature fibrils,[23] suggesting that fairly high mobility is present in the aggregates. One explanation for this would be that disordered oligomers[59] are subjected to compaction due to the self-crowding induced by sedimentation, but only an incompletely compact state is achieved. For the larger species expected in samples UC-2 and UC-3, the supramolecular organization is expected to be more stable, converging to what is observed in the mature fibrils, and the same mixing times yield richer patterns. The sharp lines and relative paucity of the peaks in sample UC-1 suggest a significant degree of order. For samples UC-2 and UC-3, which likely contain a larger range of molecular weights, the order progressively decreases, and the spectra become progressively broader.

It is also important to note that, in the SSNMR rotor, formation of the sediment is reversible for concentrations as high as 5 mmol dm^{-3}, whereas it becomes irreversible at higher concentrations. In the case of the UC-induced sediment, the reversibility, also in the absence of further aggregation, is intrinsically limited by the ratio of the surface exposed to the solvent and the volume of the sediment.[3]

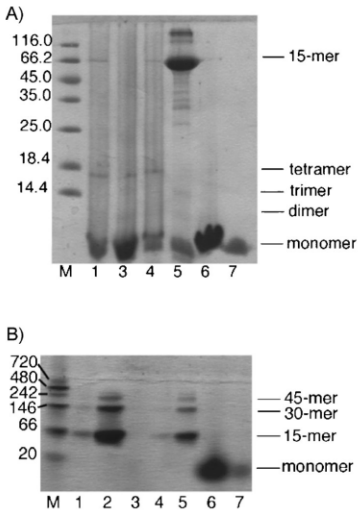

Figure 4. A) SDS-PAGE showing the apparent mass of SDS-resistant species; samples are in the following order: M, marker; 1, UC-induced at 1.4 mmol dm^{-3}; 3, UC-induced sediment at 10 mmol dm^{-3}; 4, MAS-induced sediment at 8 mmol dm^{-3}; 5, MAS-induced sediment at 2 mmol dm^{-3}; 6, supernatant from the preparation of samples 1–2; 7, monomer. The tetramer band (18 kDa) is evident in samples 1, 3, and 4, whereas sample 5 shows the marked presence of heavier species at 68 kDa and approximately 146 kDa. B) Native gel electrophoresis showing the apparent mass of oligomers; samples are in the following order: M, marker; 1 and 2, UC-induced at 1.4 mmol dm^{-3}; 3, UC-induced sediment at 10 mmol dm^{-3}; 4, MAS-induced sediment at 8 mmol dm^{-3}; 5, MAS-induced sediment at 2 mmol dm^{-3}; 6, supernatant from the preparation of samples 1–2; 7, monomer. The most abundant species in samples 1, 2 and 4, 5 is the 68 kDa oligomer (15-mer), in agreement with theoretical predictions, with two other major bands at about 146 and 207, consistent with the 30-mer and 45-mer, respectively. In sample 3, no soluble species is observed.

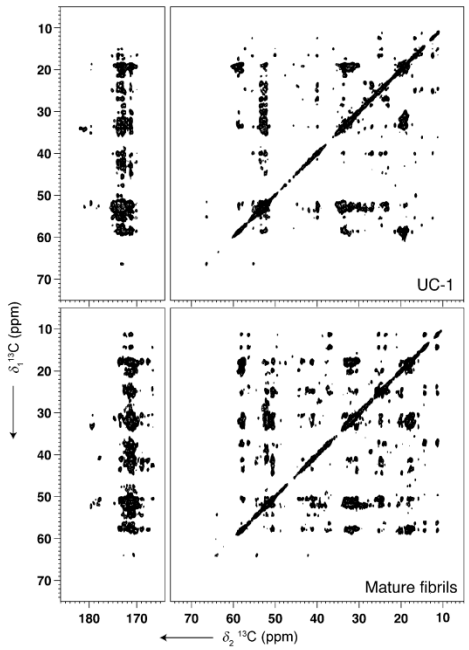

Figure 5. Comparison of the 300 ms ^{13}C–^{13}C SHANGHAI spectrum of the UC-1 sample (top) and the mature fibrils[23] (bottom).

All of the peaks appearing in the ^{13}C,^{13}C 2D SHANGHAI spectrum of the MAS-induced sediment (red in Figure S6) are maintained in the corresponding spectrum recorded for the UC-1 sample (green in Figure S6). This suggests that similar species are formed and observed in the two experiments. In the latter case, the higher signal-to-noise ratio, probably combined with greater compaction, allowed the detection of a larger number of weaker crosspeaks, without compromising the resolution. On the other hand, as shown in Figure 5, the ^{13}C–^{13}C 2D SHANGHAI spectrum of UC-1 is not superimposable on the corresponding spectrum of mature Aβ fibrils prepared in the same solution conditions.[23] The UC-1 sample was stable throughout the full spectroscopic characterization.

A partial sequential assignment was obtained, taking advantage of the high resolution and adequate sensitivity of the 2D spectra on the UC-1 samples, as well as of the short and simple sequence pattern of the Aβ peptide. The intensity and resolution of the peaks in the Cα region (see Figure 5) allowed for recognition of Cα–Cα and Cα–CX crosspeaks between neighboring residues in the 2D ^{13}C–^{13}C SHANGHAI spectra, and these connectivities were followed in order to achieve a sequential walk passing from Lys16 to Gly38, as exemplified in Figure S7, comparing the shifts with the expected amino acid-specific values. We have found that only one set of chemical shifts, as reported in Table S1, can explain all of these sequential/short range contacts, and no signal doubling was observed

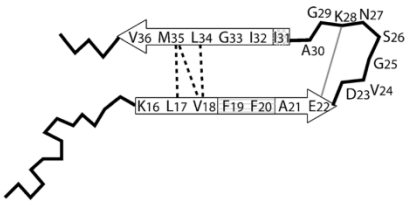

Figure 6. Schematics of the structural information obtained for Aβ oligomers. The preformed secondary structure elements, based on the PREDITOR prediction, are reported as red arrows. Phe19 and Phe20 are line-hatched because the side chain resonances cannot be distinguished. Ile31 is cross-hatched to highlight its structural heterogeneity. The unambiguous contact between Glu22 and Lys28 is shown as a solid line, whereas the ambiguous contacts Leu17,Val18–Leu34,Met35 are reported as dashed lines.

with the exception of Ile31. For this residue (cross-hatched in Figure 6), more than one set of resonances were observed. This indicates conformational heterogeneity in the turn region near the β2 element. No sequential connectivity was found for residues 1–15, consistent with an increased mobility in this region, as already observed in many fibrillar preparations.

Based on these backbone chemical shifts, some structural features of these aggregates can be obtained for the UC-1 sample. Such observations, described below, are summarized in Figures 6 and 7. We recall that this sample is in a fully hydrated and free state, without the addition of interacting molecules, and that no structural information has been made available so far for such a sample.

The secondary chemical shifts indicate that the most hydrophobic regions (mostly residues 16–22 and, to a minor extent, residues 30–38) of the AβM40 peptide already form β-strands in the present oligomeric species. This observation is consistent with that proposed on the basis of recent DEST studies of

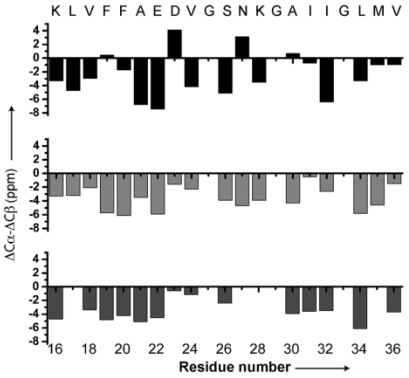

Figure 7. NMR observations as predictors for secondary structure content for the oligomers (top panel): β structure of regions 16–22 and 32–36 can be inferred. Comparison is made to the mature fibrils[23] (middle panel) and to oligomers stabilized in the presence of HFIP[32] (lower panel). Glycines are not shown.

Aβ prefibrillar aggregates.[29] Figure S9 reports the PREDITOR[60] and TALOS[61] predictions of the backbone dihedral angles calculated through the WeNMR web interfaces.[62] Both programs predict extended beta secondary structures, and PREDITOR also pinpoints a break in the beta-stretch between residues 23 and 30.These stretches are within the longer β1- and β2-regions in mature fibrils (10–22 and 26–38), indicating that expansion of these two "nascent" β-strands is possibly one of the main events during Aβ fibril maturation. This is also consistent with what was previously proposed by other groups based on the observation of samples trapped in the oligomeric states by different approaches.[15,25,28,63] The signals of residues 39 and 40 are not found. This is consistent with the increased mobility of these residues, previously reported for antibody-stabilized protofibrils.[15] Moreover, the β-propensities of these two residues are slightly decreased compared to the central region of the β2 strand in mature fibrils.[23] This suggests that such structural differences within mature fibrils originate from the prefibrillar stage. Ser26 was also found to have a high chemical shift perturbation, and we were able to assign crosspeaks consistent with the presence of a salt bridge between Glu22 and Lys28 (solid line in Figure 6, spectrum in Figure S8). Such an interaction would decrease the mobility of the loop and justify the large chemical shift perturbation of Ser26. Crosspeaks in the crowded surrounding region (δ_1, $\delta_2 = 20$ ppm, 55 ppm) that can be ambiguously attributed to contacts Leu17,Val18–Leu34,Met35 (dashed lines, Figure 6) were also observed. These contacts might be consistent with arrangements typical of mature fibrils (in a form of mature fibrils, a similar register was observed by Tycko and co-workers[49,64]), or with a β-hairpin arrangement. The latter has been observed in ref. [59], in complex with an affibody binding protein.

Conclusions

In conclusion, we have shown that SedNMR allows for collecting and trapping of AβM40 aggregates in a fully hydrated environment without adding cosolvents or interaction partners, and therefore provides a unique way to access the formation kinetics and structural features of these species with reduced perturbations. With minimal sample preparation, we probed the kinetics of aggregation of the AβM40 peptide. This information was validated by comparison with the faster aggregating AβM42. A similar form of the prefibrillar AβM40 aggregates, obtained by sedimentation in a preparative ultracentrifuge, was analyzed to obtain a qualitative picture of its structural features. This approach can be easily applied to other amyloid systems and, more generally, to the study of many supramolecular assembly processes.

Acknowledgements

Discussions with Gary J. Pielak on crowding effects and with Yoshitaka Ishii on Aβ reactivity during the Chianti/Instruct Workshop on BioNMR 2012 are acknowledged. We thank Marco Fragai for careful reading of the manuscript and for providing insightful suggestions. This work was supported by the EC contracts East-NMR no. 228461 and Bio-NMR no. 261863, Ente Cassa Risparmio Firenze, and INSTRUCT, part of the European Strategy Forum on Research Infrastructures (ESFRI) and supported by national member subscriptions. Specifically, we thank the EU ESFRI Instruct Core Centre, CERM, Italy. M.K. acknowledges EC MC ITN IDPbyNMR Contract no. 264257 for financial support.

Keywords: centrifugation · kinetics · oligomerization · sedimentation · solid-state NMR spectroscopy

[1] I. Bertini, C. Luchinat, G. Parigi, E. Ravera, B. Reif, P. Turano, *Proc. Natl. Acad. Sci. USA* **2011**, *108*, 10396–10399.
[2] T. Polenova, *Nat. Chem.* **2011**, *3*, 759–760.
[3] I. Bertini, F. Engelke, C. Luchinat, G. Parigi, E. Ravera, C. Rosa, P. Turano, *Phys. Chem. Chem. Phys.* **2012**, *14*, 439–447.
[4] I. Bertini, F. Engelke, L. Gonnelli, B. Knott, C. Luchinat, D. Osen, E. Ravera, *J. Biomol. NMR* **2012**, *54*, 123–127.
[5] C. Gardiennet, A. K. Schütz, A. Hunkeler, B. Kunert, L. Terradot, A. Böckmann, B. H. Meier, *Angew. Chem.* **2012**, *124*, 7977–7980; *Angew. Chem. Int. Ed.* **2012**, *51*, 7855–7858.
[6] E. Ravera, B. Corzilius, V. K. Michaelis, C. Rosa, R. G. Griffin, C. Luchinat, I. Bertini, *J. Am. Chem. Soc.* **2013**, *135*, 1641–1644.
[7] I. Bertini, C. Luchinat, G. Parigi, E. Ravera, *Acc. Chem. Res.* **2013**; DOI: 10.1021/ar300342f.
[8] Y. Wang, C. Li, G. J. Pielak, *J. Am. Chem. Soc.* **2010**, *132*, 9392–9397.
[9] S. Lundh, *Arch. Biochem. Biophys.* **1985**, *241*, 265–274.
[10] S. Lundh, *J. Polym. Sci. Polym. Phys. Ed.* **1980**, *18*, 1963–1978.
[11] A. Böckmann, C. Gardiennet, R. Verel, A. Hunkeler, A. Loquet, G. Pintacuda, L. Emsley, B. H. Meier, A. Lesage, *J. Biomol. NMR* **2009**, *45*, 319–327.
[12] A. J. Baldwin, P. Walsh, D. F. Hansen, G. R. Hilton, J. L. P. Benesch, S. Sharpe, L. E. Kay, *J. Am. Chem. Soc.* **2012**, *134*, 15343–15350.
[13] A. Mainz, B. Bardiaux, F. Kuppler, G. Multhaup, I. C. Felli, R. Pierattelli, B. Reif, *J. Biol. Chem.* **2012**, *287*, 1128–1138.
[14] N. Carulla, M. Zhou, E. Giralt, C. V. Robinson, C. M. Dobson, *Acc. Chem. Res.* **2010**, *43*, 1072–1079.
[15] H. A. Scheidt, I. Morgado, S. Rothemund, D. Huster, M. Fändrich, *Angew. Chem.* **2011**, *123*, 2889–2892; *Angew. Chem. Int. Ed.* **2011**, *50*, 2837–2840.
[16] I. Benilova, E. Karran, B. De Strooper, *Nat. Neurosci.* **2012**, *15*, 349–357.
[17] S. L. Gallion, *PLoS One* **2012**, *7*, e49375.
[18] R. Roychaudhuri, M. Yang, M. M. Hoshi, D. B. Teplow, *J. Biol. Chem.* **2009**, *284*, 4749–4753.
[19] G. Bitan, S. S. Vollers, D. B. Teplow, *J. Biol. Chem.* **2003**, *278*, 34882–34889.
[20] S. L. Bernstein, N. F. Dupuis, N. D. Lazo, T. Wyttenbach, M. M. Condron, G. Bitan, D. B. Teplow, J. E. Shea, B. T. Ruotolo, C. V. Robinson, M. T. Bowers, *Nat. Chem.* **2009**, *1*, 326–331.
[21] M. Fändrich, M. Schmidt, N. Grigorieff, *Trends Biochem. Sci.* **2011**, *36*, 338–345.
[22] R. Tycko, *Annu. Rev. Phys. Chem.* **2011**, *62*, 279–299.
[23] I. Bertini, L. Gonnelli, C. Luchinat, J. Mao, A. Nesi, *J. Am. Chem. Soc.* **2011**, *133*, 16013–16022.
[24] J. M. Lopez del Amo, M. Schmidt, U. Fink, M. Dasari, M. Fändrich, B. Reif, *Angew. Chem.* **2012**, *124*, 6240–6243; *Angew. Chem. Int. Ed.* **2012**, *51*, 6136–6139.
[25] S. Chimon, Y. Ishii, *J. Am. Chem. Soc.* **2005**, *127*, 13472–13473.
[26] J. Danielsson, A. Andersson, J. Jarvet, A. Gräslund, *Magn. Reson. Chem.* **2006**, *44*, S114–S121.
[27] I. Kheterpal, M. Chen, K. D. Cook, R. Wetzel, *J. Mol. Biol.* **2006**, *361*, 785–795.
[28] M. Ahmed, J. Davis, D. Aucoin, T. Sato, S. Ahuja, S. Aimoto, J. I. Elliott, W. E. Van Nostrand, S. O. Smith, *Nat. Struct. Mol. Biol.* **2010**, *17*, 561–567.
[29] N. L. Fawzi, J. Ying, R. Ghirlando, D. A. Torchia, G. M. Clore, *Nature* **2011**, *480*, 268–272.
[30] J. Pan, J. Han, C. H. Borchers, L. Konermann, *Anal. Chem.* **2011**, *83*, 5386–5393.

[31] M. Fändrich, *J. Mol. Biol.* **2012**, *421*, 427 – 440.
[32] C. Haupt, J. Leppert, R. Rönicke, J. Meinhardt, J. K. Yadav, R. Ramachandran, O. Ohlenschläger, K. G. Reymann, M. Görlach, M. Fändrich, *Angew. Chem.* **2012**, *124*, 1608 – 1611; *Angew. Chem. Int. Ed.* **2012**, *51*, 1576 – 1579.
[33] J. Bieschke, M. Herbst, T. Wiglenda, R. P. Friedrich, A. Boeddrich, F. Schiele, D. Kleckers, J. M. Lopez del Amo, B. A. Grüning, Q. Wang, M. R. Schmidt, R. Lurz, R. Anwyl, S. Schnoegl, M. Fändrich, R. F. Frank, B. Reif, S. Günther, D. M. Walsh, E. E. Wanker, *Nat. Chem. Biol.* **2012**, *8*, 93 – 101.
[34] J. M. Lopez del Amo, U. Fink, M. Dasari, G. Grelle, E. E. Wanker, J. Bieschke, B. Reif, *J. Mol. Biol.* **2012**, *421*, 517 – 524.
[35] J. C. Stroud, L. Cong, P. K. Teng, D. Eisenberg, *Proc. Natl. Acad. Sci. USA* **2012**, *109*, 7717 – 7722.
[36] M. D. Kirkitadze, G. Bitan, D. B. Teplow, *J. Neurosci. Res.* **2002**, *69*, 567 – 577.
[37] J. Lee, E. K. Culyba, E. T. Powers, J. W. Kelly, *Nat. Chem. Biol.* **2011**, *7*, 602 – 609.
[38] P. Schanda, E. Kupce, B. Brutscher, *J. Biomol. NMR* **2005**, *33*, 199 – 211.
[39] K. Pauwels, T. L. Williams, K. L. Morris, W. Jonkheere, A. Vandersteen, G. Kelly, J. Schymkowitz, F. Rousseau, A. Pastore, L. C. Serpell, K. Broersen, *J. Biol. Chem.* **2012**, *287*, 5650 – 5660.
[40] G. A. Morris, R. Freeman, *J. Am. Chem. Soc.* **1979**, *101*, 760 – 762.
[41] W. Bermel, I. Bertini, I. C. Felli, M. Piccioli, R. Pierattelli, *Prog. Nucl. Magn. Reson. Spectrosc.* **2006**, *48*, 25 – 45.
[42] R. Riek, G. Wider, K. Pervushin, K. Wüthrich, *Proc. Natl. Acad. Sci. USA* **1999**, *96*, 4918 – 4923.
[43] A. Pines, M. G. Gibby, J. S. Waugh, *J. Chem. Phys.* **1972**, *56*, 1776 – 1777.
[44] A. Mainz, S. Jehle, B. J. van Rossum, H. Oschkinat, B. Reif, *J. Am. Chem. Soc.* **2009**, *131*, 15968 – 15969.
[45] W. B. Stine, Jr., K. N. Dahlgren, G. A. Krafft, M. J. LaDu, *J. Biol. Chem.* **2003**, *278*, 11612 – 11622.
[46] I. Kuperstein, K. Broersen, I. Benilova, J. Rozenski, W. Jonekheere, M. Debulpaep, A. Vandersteen, I. Segers-Nolten, K. Van der Werf, V. Subramaniam, D. Braeken, G. Callewaert, C. Bartic, R. D'Hooge, I. C. Martins, F. Rousseau, J. Schymkowitz, B. De Strooper, *EMBO J.* **2010**, *29*, 3408 – 3420.
[47] R. C. Chatelier, A. P. Minton, *Biopolymers* **1987**, *26*, 507 – 524.
[48] A. T. Petkova, R. D. Leapman, Z. H. Guo, W. M. Yau, M. P. Mattson, R. Tycko, *Science* **2005**, *307*, 262 – 265.
[49] A. K. Paravastu, R. D. Leapman, W. M. Yau, R. Tycko, *Proc. Natl. Acad. Sci. USA* **2008**, *105*, 18349 – 18354.
[50] R. J. Ellis, A. P. Minton, *Biol. Chem.* **2006**, *387*, 485 – 497.
[51] D. A. White, A. K. Buell, T. P. J. Knowles, M. E. Welland, C. M. Dobson, *J. Am. Chem. Soc.* **2010**, *132*, 5170 – 5175.
[52] A. Magno, A. Caflisch, R. Pellarin, *J. Phys. Chem. Lett.* **2010**, *1*, 3027 – 3032.
[53] T. P. J. Knowles, C. A. Waudby, G. L. Devlin, S. I. A. Cohen, A. Aguzzi, M. Vendruscolo, E. M. Terentjev, M. E. Welland, C. M. Dobson, *Science* **2009**, *326*, 1533 – 1537.
[54] H.-Y. Kim, M.-K. Cho, A. Kumar, E. Maier, C. Siebenhaar, S. Becker, C. O. Fernandez, H. A. Lashuel, R. Benz, A. Lange, M. Zweckstetter, *J. Am. Chem. Soc.* **2009**, *131*, 17482 – 17489.
[55] Y. F. Mok, G. J. Howlett, *Methods Enzymol.* **2006**, *413*, 199 – 217.
[56] D. Kashchiev, R. Cabriolu, S. Auer, *J. Am. Chem. Soc.* **2013**, *135*, 1531 – 1539.
[57] B. Hu, O. T. J. Lafon, Q. Chen, J.-P. Amoureux, *J. Magn. Reson.* **2011**, *212*, 320 – 329.
[58] N. M. Loening, M. Bjerring, N. C. Nielsen, H. Oschkinat, *J. Magn. Reson.* **2012**, *214*, 81 – 90.
[59] A. Sandberg, L. M. Luheshi, S. Sollvander, T. P. de Barros, B. Macao, T. P. J. Knowles, H. Biverstal, C. Lendel, F. Ekholm-Petterson, A. Dubnovitsky, L. Lannfelt, C. M. Dobson, T. Hard, *Proc. Natl. Acad. Sci. USA* **2010**, *107*, 15595 – 15600.
[60] M. V. Berjanskii, S. Neal, D. S. Wishart, *Nucleic Acids Res.* **2006**, *34*, W63 – W69.
[61] Y. Shen, F. Delaglio, G. Cornilescu, A. Bax, *J. Biomol. NMR* **2009**, *44*, 213 – 223.
[62] T. A. Wassenaar, M. van Dijk, N. Loureiro-Ferreira, G. van der Schot, S. J. de Vries, C. Schmitz, J. van der Zwan, R. Boelens, A. Giachetti, L. Ferella, A. Rosato, I. Bertini, T. Herrmann, H. R. A. Jonker, A. Bagaria, V. Jaravine, P. Guntert, H. Schwalbe, W. F. Vranken, J. F. Doreleijers, G. Vriend, G. W. Vuister, D. Franke, A. Kikhney, D. I. Svergun, R. H. Fogh, J. Ionides, E. D. Laue, C. Spronk, S. Jurksa, M. Verlato, S. Badoer, S. Dal Pra, M. Mazzucato, E. Frizziero, A. M. J. J. Bonvin, *J. Grid Comput.* **2012**, *10*, 743 – 767.
[63] S. Chimon, M. A. Shaibat, C. R. Jones, D. C. Calero, B. Aizezi, Y. Ishii, *Nat. Struct. Mol. Biol.* **2007**, *14*, 1157 – 1164.
[64] A. T. Petkova, W. M. Yau, R. Tycko, *Biochemistry* **2006**, *45*, 498 – 512.

Received: March 11, 2013
Published online on July 2, 2013

CHEMBIOCHEM

Supporting Information

Formation Kinetics and Structural Features of Beta-Amyloid Aggregates by Sedimented Solute NMR

Ivano Bertini†,[a, b, c] Gianluca Gallo,[a, d] Magdalena Korsak,[a, b] Claudio Luchinat,*[a, c, d] Jiafei Mao,[a, c, e] and Enrico Ravera[a, d]

cbic_201300141_sm_miscellaneous_information.pdf

Protein expression and purification

The sample preparation was performed as previously reported[23]. The DNA encoding for beta amyloid peptide with methionine as first amino acid (AβM40) was cloned into a pET3a vector using *Nde*I and *Bam*HI restriction enzymes. BL21 (DE3) *Escherichia coli* cells were used for peptide expression. Cells were grown in LB rich medium at 37 °C until OD_{600} reached 0.8. The cells were then centrifuged and resuspended in minimal medium enriched with $(^{15}NH_4)_2SO_4$ (1 g/L) and [U-^{13}C]glucose (4 g/L). After 1 h 1mmol dm^{-3} isopropyl β-D-1-thiogalactopyranoside (IPTG) was added in order to induce the peptide expression. Cells were harvested after 4 h incubation at 39 °C, sonicated and ultracentifuged. Inclusion bodies were resuspended in 8 mol dm^{-3} urea and the peptide was purified by an anion exchange chromatography and a size-exclusion chromatography in 50 m mol dm^{-3} ammonium acetate (pH 8.5). In order to keep AβM40 in the monomeric form guanidinium chloride was added to a final concentration of 6 mol dm^{-3} before the last step of purification.

Ex situ sedimentation and estimation of the amount of sedimented material

Ex situ sedimentation was performed at 4 °C in a Beckman Coulter Optima L80K floor preparative ultracentrifuge using a SW32 swinging bucket rotor using an ultracentrifuge (University of Florence).[4] These preparations resulted in approximately 2.6 mg, 3.2 mg and 7.8 mg of sediment in the rotor respectively. Since the rotor contains also solution, the amount of protein in the rotor was not estimated by weighing but from the CP intensity with respect to the mature fibrils[23] (same CP conditions were used for this quantification).

Solid state NMR spectroscopy

Spectra were acquired on Bruker Avance II spectrometers operating either at 850 MHz or 700 MHz ^{1}H larmor frequency equipped with a 3.2 mm triple resonance probe (850) and 3.2 mm or 4 mm triple resonance probes (700).

The temperature was kept at 274 K (at sample) for the experiments acquired in the 3.2 mm rotors and at 277 K for the experiments acquired in the 4 mm rotors. ^{1}H excitation and decoupling nutation frequencies were 92.6 kHz in all cases. ^{13}C and ^{15}N 90° pulse lengths were 4.5 μs and 7.1 μs respectively, the ^{1}H, ^{13}C and ^{15}N carrier frequencies were set to 3.5 ppm, 90 ppm and 118 ppm, respectively.

The acquisition times in the SHANGHAI[57] experiment conducted at the 850 MHz spectrometer were 18 ms in the direct dimension and 3 ms in the indirect dimension. The acquisition times in the SHANGHAI

experiment conducted at the 700 MHz spectrometer were 19 ms in the direct dimension and 7 ms in the indirect dimension.

Interscan delay of 3.0 s was used and a different number of scans (from 160 to 256) in different experiments were accumulated for each t1 point.

The spectra were acquired using the States-TPPI mode. The spectra were processed with a 1024×4096 points matrix using squared cosine and Gaussian window functions for the indirect and direct dimensions, respectively. Linear prediction with 12 coefficients was applied.

In the NCA and NCO conducted at the 700 MHz instrument, the ^{13}C carrier frequency was set to 54 ppm (NCA) or 172 ppm (NCO), and moved back to 90 ppm after the DCP. Optimal control pulses derived from Loening et al. were used[58]. Spectra were recorded with 544 scans (NCA) and 704 scans (NCO) per t1 increment. Acquisition times were 12 ms and 6 ms for the direct and indirect dimension respectively for NCA and 17 ms and 14 ms for the direct and indirect dimension respectively for NCO.

The spectra were acquired using the States-TPPI mode. The spectra were processed with a 256×4096 points matrix using squared cosine and Gaussian window functions for the indirect and direct dimensions, respectively. Linear prediction with 8 coefficients was applied.

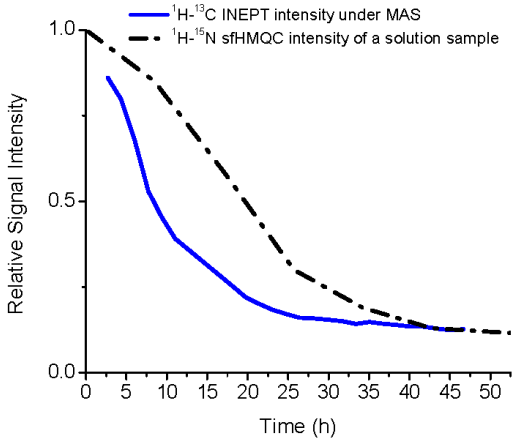

Figure S1. Kinetics of disappearance of Aβ monomer from solution. The diagram shows the signal intensity of the solution component of two AβM40 samples. Blue, solid line: the ^{1}H-^{13}C INEPT signal intensity observed for a 1.6 mM solution at 275 K, sealed in a 4 mm MAS rotor and spun at 12 kHz. Frictional heating can be estimated to be around 10 K. Black, dashed line: ^{1}H-^{15}N sfHMQC signal intensity (observed as a trace in the sidechains region in the 2D spectrum) for a 0.16 mM sample at 298 K after scratching with a glass rod. Despite a 10 times higher concentration, the disappearance kinetics under MAS is only 4 times faster.

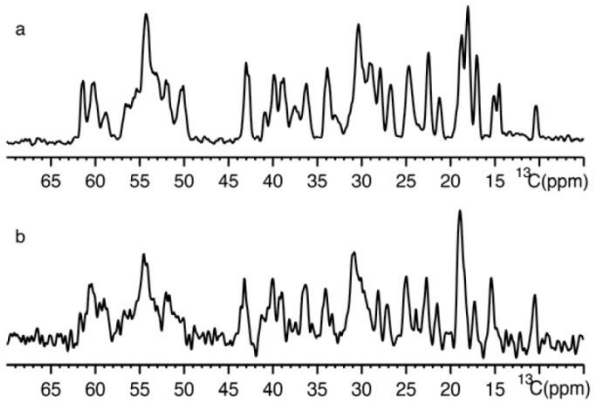

Figure S2. Refocused INEPT spectra at the beginning of the MAS-induced sedimentation. $^{1}H,^{13}C$ refocused INEPT spectra of the AβM40 (a) and of the sample of AβM42 (b) at the beginning of the MAS induced sedimentation experiment

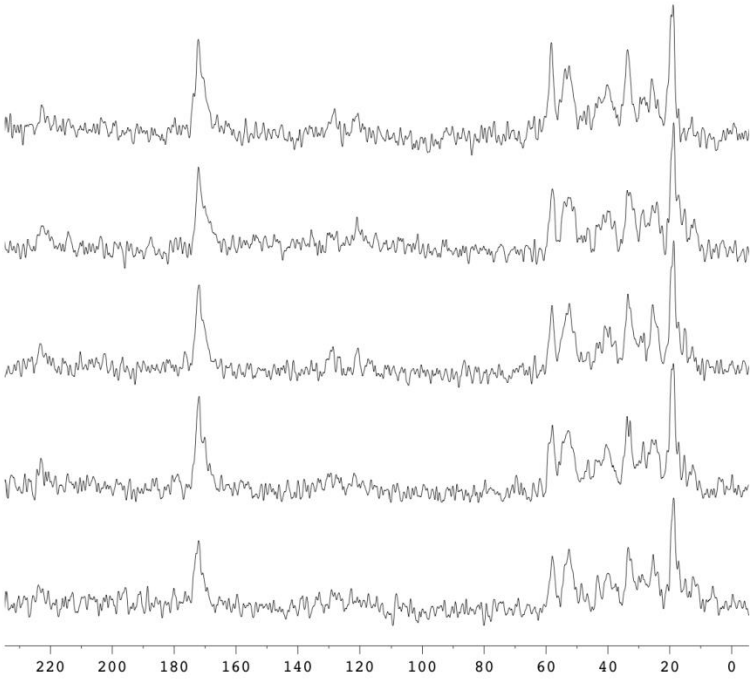

Figure S3. CP spectra of the AβM42 sample over the course of kinetics determination. $^{1}H,^{13}C$ CP spectra of the sample of AβM42 during the course of the kinetics determination *via* MAS induced sedimentation. From bottom to top experiments recorded at increasing time (1 h 49', 3 h 7', 4 h 25', 5 h 40', 7 h)

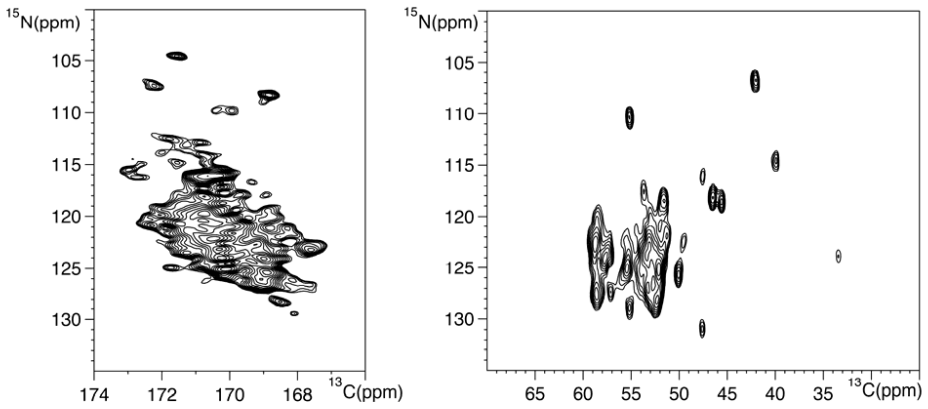

Figure S4. NCO and NCA spectra of UC-1 sample. NCO (left) and NCA (right) spectra of UC-1 sample acquired at 700 MHz, 14 kHz spinning rate.

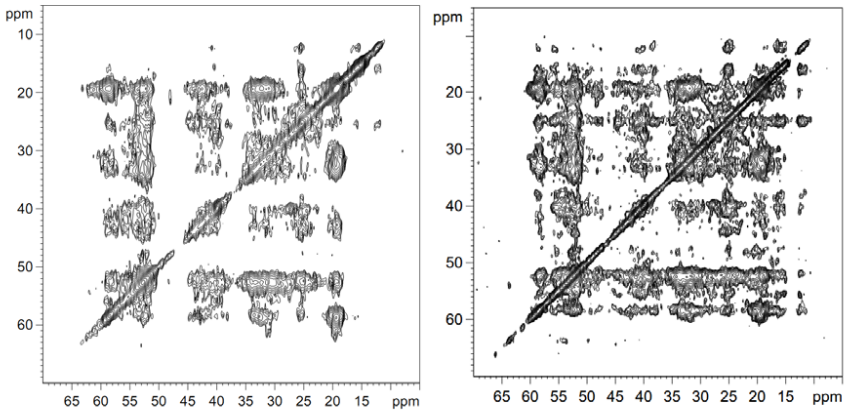

Figure S5. Spectra of UC-2 and UC-3 samples. Representative 300 ms $^{13}C,^{13}C$ SHANGHAI spectra of the preparations UC-2 and UC-3. UC-2 sample has higher initial concentration and the spectra suggest higher heterogeneity in the preparation. UC-3 should contain particles at higher molecular weight; the spectrum is more resolved than that of UC-2 but less resolved than that of UC-1, suggesting that longer time allows for formation of different species. It is noteworthy that and the number of crosspeaks in the spectrum of UC-3 is much larger than the corresponding spectrum of UC-1, suggesting that increased weight is accompanied by more compaction.

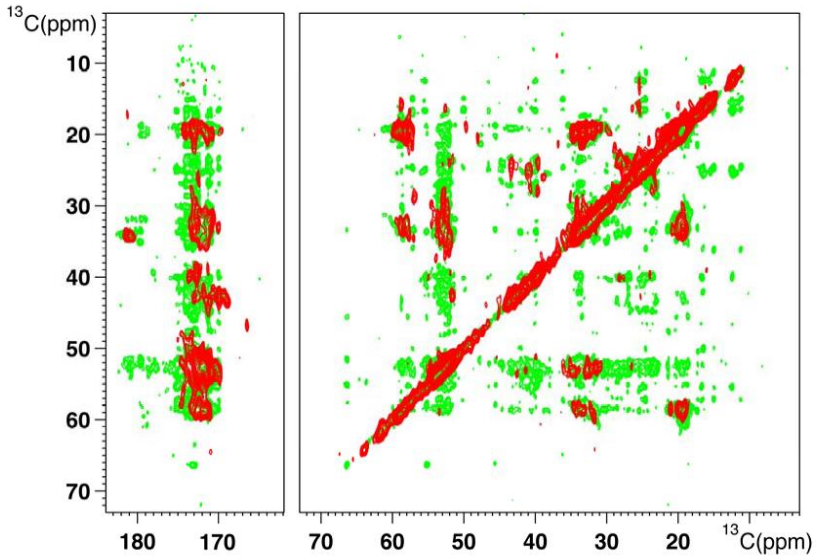

Figure S6. Comparison of UC-1 and MAS-induced sediment spectra. Overlay of 300 ms ^{13}C,^{13}C SHANGHAI spectra of UC-1 sample (black) and MAS-induced sediment (red).

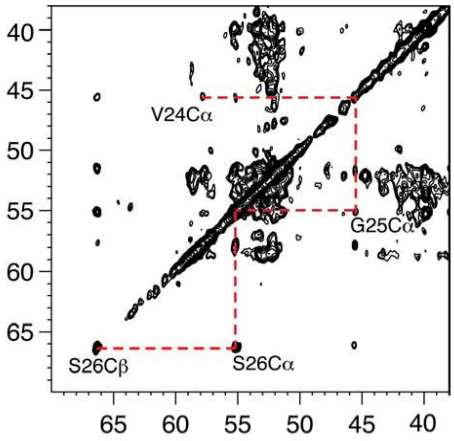

Figure S7. Exemplification of the assignment strategy. The figure indicates the approach that was followed to track sequential connectivity.

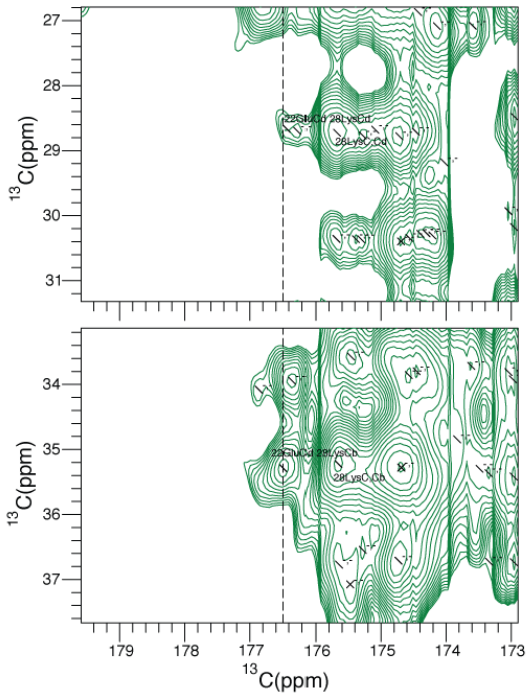

Figure S8. Crosspeaks between E22 and K28. Enlargement of the carbonyl region in the 300 ms $^{13}C,^{13}C$ SHANGHAI spectrum of the UC1 sample, highlighting the crosspeaks between E22Cδ and carbon atoms from K28.

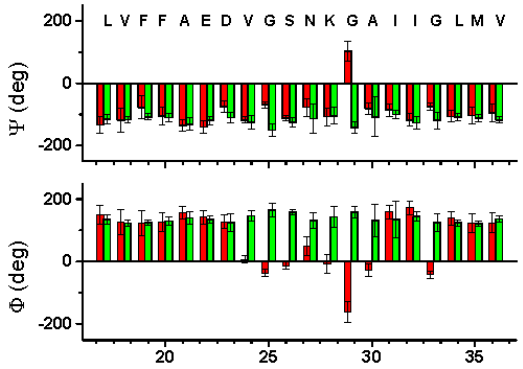

Figure S9. TALOS and PREDITOR secondary structure prediction. The figure reports the TALOS+ (green) and PREDITOR (red) estimates of the backbone dihedral angles.

Sedimentation in solid-state NMR rotors

The concentration profile of a single species in the centrifugal field induced by the magic angle spinning of the solid state NMR rotor (i.e.: a cylinder spinning about its symmetry axis) is described by the following equation[3]:

$$c(r) = \frac{c_{\text{limit}}}{A\exp\left[-\frac{M(1-\bar{v}\rho)\omega_r^2 r^2}{2RT}\right]+1} \qquad (1)$$

where A is analytically evaluated as:

$$A = \frac{\exp\left[\frac{M(1-\bar{v}\rho)\omega_r^2 b^2}{2RT}\left(1-\frac{c_0}{c_{\text{limit}}}\right)\right]-1}{1-\exp\left[-\frac{M(1-\bar{v}\rho)\omega_r^2 b^2}{2RT}\frac{c_0}{c_{\text{limit}}}\right]} \qquad (2)$$

and the limiting concentration c_{limit} is experimentally found to be around 700 mg/mL.[9;10]

From the results obtained for bullfrog apoferritin, we can estimate that the protein becomes rotationally immobilized at approximately 85% of this threshold value. The lowest MW for which enough material is sedimented is 69 kDa.

Data analysis and further considerations in kinetics determination via MAS induced sedimentation

Signal intensities of INEPT and CP of the AβM40 sample in figure 2 are obtained as normalized to the most intense signal of the respective series by Bruker Topspin 2.1. Successively they were multiplied by a factor 0.87, so that the sum of the last two points was 1, as obtained solving the following system:

$$\begin{cases} k'S(t_0) = x \\ k'S(t_{fin}) = 1-y \\ kL(t_0) = 1-x \\ kL(t_{fin}) = y \end{cases}$$

Where S is the solid-state CP signal and L is the liquid state INEPT signal (the same factor 0.87 was used for the AβM42 sample) at times t_0 and t_{fin}. This corresponds to the assumption that only two species are present in the sample at times t_0 and t_{fin}. As the two normalized curves sum to approximately 1 also at all intermediate times, no appreciable amounts of invisible intermediate species can be present (unless the invisible species is formed with the same kinetics of the visible one and is indefinitely stable). In addition to this, soluble oligomers up to >70 kDa should still be visible by INEPT, thus overlapping with the estimated MW of the sedimented species. This further excludes that invisible species may be present. This is

not necessarily true for more diluted solutions or lower MAS rates, that would cause sedimentation starting from higher MW species that, when still in solution, may already have become invisible by INEPT. This could be the case for the AβM42 sample.

Clearing factor of a 4 mm solid-state NMR rotor

The clearing factor (K) with this kind of geometry cannot be evaluated according to the integrated Svedberg equation

$$t = \frac{K}{s} = \frac{\ln(r_{max}/r_{min})}{s\omega^2}\frac{10^{13}}{3600} \qquad (3)$$

since no "extra" gravity exists for the molecules in solution exactly at the axis of rotation (r_{min}=0), thus the required time would turn out to be infinite.

Anyway, even a minor movement of the center of mass out of the rotation axis will bring the protein into the centrifugal field, and the time required for the sediment NMR signal to appear can be used to estimate the clearing factor.

The time required for sedimenting a solution of bullfrog M apoferritin (17 S) at 12 kHz was measured to be 1.5 h.

By its definition the clearing factor was calculated to be

$$K(12) = t(12)\cdot s = 1.5\cdot 17 \approx 26 \qquad (4)$$

and verified at 9 kHz

$$K(9) = K(12)\frac{12^2}{9^2} = 26\cdot 1.78 \approx 46 \qquad (5)$$

which corresponds to a sedimentation time at 9 kHz of

$$t(9) \approx \frac{46}{17} \approx 2.7h \qquad (6)$$

consistently with what experimentally determined.

Sedimentation in ultracentrifugal device and calculation of the sedimentation coefficients

The concentration profile of a single species in the ultracentrifugal device is described by equation 1, although in this case A cannot be obtained analytically[4] and must be evaluated by numerical integration of the equation:

$$\int_{r_{min}}^{r_{max}} S(r)c(r)\mathrm{d}r = c_0 V_{device} \qquad (7)$$

where $S(r)$ is the area of the device at position r. In our experimental conditions (f = 32000 rpm, T = 4 °C) the minimum molecular weight for which sedimentation is obtained is about 20 kDa.

So, in this case, the smallest sedimentation coefficient of the species that sediment at the rotor can be estimated by equation 3, or, more conveniently, by the following equation:

$$s = \frac{K}{t} = \frac{\ln(r_{max}/r_{min})}{tf^2} 2.533 \cdot 10^{11} = \frac{\ln(134.7/89.50) \cdot 2.533 \cdot 10^{11}}{24 \cdot 1.024 \cdot 10^9} \approx 4.2S$$

From this value, according to the analysis performed by Fawzi et al.[29], a molecular mass of about 70 kDa can be calculated.

Table S1. ^{13}C chemical shifts of the assigned residues

Residue number	Residue type	CO	Cα	Cβ	Cγ	Cδ	Cε	N
16	Lys	172.7	53.9	33.8	26.5	28.6	41.2	128.9
17	Leu	173.9	53.57	46.29	28.41	25.58,19.00	-	124.9
18	Val	171.91	60.43	34.77	19.04,23.06	-	-	123.8
19	Phe	172.99	56.84	39.4	-	-	-	128.89
20	Phe	172.7	56.89	41.6	-	-	-	129.11
21	Ala	172.7	48.98	22.96	-	-	-	125.6
22	Glu	172.5	52.5	33.94	36.73	176.49	-	117.8
23	Asp	174.54	53.79	37.07	181.24	-	-	124.4
24	Val	174.6	59.35	34.92	20.39,21.90	-	-	123.1
25	Gly	172.86	47.22	-	-	-	-	110.4
26	Ser	174.61	56.79	67.9	-	-	-	110.55
27	Asn	172.8	53.05	35.82	182.59	-	-	116.4
28	Lys	175.54	55.24	35.35	25.24	28.55	41.61	128.2
29	Gly	171.7	43.54	-	-	-	-	105.4
30	Ala	175.57	51.66	18.18	-	-	-	122.3
31	Ile	174.83	58.8	37.83	16.73,26.23	12.93	-	120.6
32	Ile	176.85	57.01	41.7	18.39,26.73	14.19	-	124.4
33	Gly	171.6	48.13	-	-	-	-	115.5
34	Leu	172.93	53.84	45.14	30.28	28.69,24.82	-	127.6

35	Met	172.72	54.66	33.95	31.93	-	20.53	125
36	Val	176.71	60.04	32.4	20.41,21.97	-	-	125.7
37	Gly	170.62	40	-	-	-	-	
38	Gly	169	42.9	-	-	-	-	

[1.] I. Bertini, C. Luchinat, G. Parigi, E. Ravera, B. Reif, P. Turano, *Proc. Natl. Acad. Sci. USA* **2011,** *108* 10396-10399.

[2.] T. Polenova, *Nature Chemistry* **2011,** 759-760.

[3.] I. Bertini, F. Engelke, C. Luchinat, G. Parigi, E. Ravera, C. Rosa, P. Turano, *Phys. Chem. Chem. Phys.* **2012,** *14* 439-447.

[4.] I. Bertini, F. Engelke, L. Gonnelli, B. Knott, C. Luchinat, D. Osen, E. Ravera, *J. Biomol. NMR* **2012,** *54* 123-127.

[5.] C. Gardiennet, A. K. Schütz, A. Hunkeler, B. Kunert, L. Terradot, A. Böckmann, B. H. Meier, *Angew. Chem. Int. Ed* **2012,** *51* 7855-7858.

[6.] E. Ravera, B. Corzilius, V. K. Michaelis, C. Rosa, R. G. Griffin, C. Luchinat, I. Bertini, *J. Am. Chem. Soc.* **2013,** *135* 1641-1644.

[7.] I. Bertini, C. Luchinat, G. Parigi, E. Ravera, *Acc. Chem. Res.* **2013,** *Epub ahead of print* .

[8.] Y. Wang, C. Li, G. J. Pielak, *JACS* **2010,** *132* 9392-9397.

[9.] S. Lundh, *Arch. Biochem. Biophys.* **1985,** *241* 265-274.

[10.] S. Lundh, *J. Polym. Sci. Polymer Physics Edition* **1980,** *18* 1963-1978.

[11.] A. Böckmann, C. Gardiennet, R. Verel, A. Hunkeler, A. Loquet, G. Pintacuda, L. Emsley, B. H. Meier, A. Lesage, *J. Biomol. NMR* **2009,** *45* 319-327.

[12.] A. J. Baldwin, P. Walsh, D. F. Hansen, G. R. Hilton, J. L. P. Benesch, S. Sharpe, L. E. Kay, *J. Am. Chem. Soc.* **2012,** *134* 15343-15350.

[13.] A. Mainz, B. Bardiaux, F. Kuppler, G. Multhaup, I. C. Felli, R. Pierattelli, B. Reif, *J. Biol. Chem.* **2012,** *287* 1128-1138.

[14.] N. Carulla, M. Zhou, E. Giralt, C. V. Robinson, C. M. Dobson, *Acc. Chem. Res.* **2010,** *43* 1072-1079.

[15.] H. A. Scheidt, I. Morgado, S. Rothemund, D. Huster, M. Fandrich, *Angew. Chem. Int. Ed.* **2011,** *50* 2837-2840.

[16.] I. Benilova, E. Karran, B. De Strooper, *Nat. Neurosci.* **2012,** *15* 1-9.

[17.] S. L. Gallion, *Plos ONE* **2012,** *7* e49375.

[18.] R. Roychaudhuri, M. Yang, M. M. Hoshi, D. B. Teplow, *J. Biol. Chem.* **2009,** *284* 4749-4753.

[19.] G. Bitan, S. S. Vollers, D. B. Teplow, *J. Biol. Chem.* **2003,** *278* 34882-34889.

[20.] S. L. Bernstein, N. F. Dupuis, N. D. Lazo, T. Wyttenbach, M. M. Condron, G. Bitan, D. B. Teplow, J. E. Shea, B. T. Ruotolo, C. V. Robinson, M. T. Bowers, *Nat. Chem.* **2009,** *1* 326-331.

[21.] M. Fandrich, M. Schmidt, N. Grigorieff, *Trends Biochem. Sci.* **2011,** *36* 338-345.

[22.] R. Tycko, *Annu. Rev. Phys. Chem.* **2011,** *62* x-xx.

[23.] I. Bertini, L. Gonnelli, C. Luchinat, J. Mao, A. Nesi, *J. Am. Chem. Soc.* **2011,** *133* 16013-16022.

[24.] J. M. Lopez del Amo, M. Schmidt, U. Fink, M. Dasari, M. Fändrich, B. Reif, *Angew. Chem Int. Ed. Engl.* **2012,** *51* 6136-6139.

[25.] S. Chimon, Y. Ishii, *J. Am. Chem. Soc.* **2005,** *127* 13472-13473.

[26.] J. Danielsson, A. Andersson, J. Jarvet, A. Gräslund, *Magn Reson. Chem.* **2006,** *44* S114-S121.

[27.] I. Kheterpal, M. Chen, K. D. Cook, R. Wetzel, *J. Mol. Biol.* **2006,** *361* 785-795.

[28.] M. Ahmed, J. Davis, D. Aucoin, T. Sato, S. Ahuja, S. Aimoto, J. I. Elliott, W. E. Van Nostrand, S. O. Smith, *Nat. Struct. Mol. Biol.* **2010,** *17* 561-567.

[29.] N. L. Fawzi, J. Ying, R. Ghirlando, D. A. Torchia, G. M. Clore, *Nature* **2011,** *480* 268-272.

[30.] J. Pan, J. Han, C. H. Borchers, L. Konermann, *Anal. Chem.* **2011,** *83* 5386-5393.

[31.] M. Fandrich, *J Mol. Biol.* **2012,** *421* 440.

[32.] C. Haupt, J. Leppert, R. Rönicke, J. Meinhardt, J. K. Yadav, R. Ramachandran, O. Ohlenschläger, K. G. Reymann, M. Görlach, M. Fandrich, *Angew. Chem. Int. Ed Engl.* **2012,** *51* 1576-1579.

[33.] J. Bieschke, M. Herbst, T. Wiglenda, R. P. Friedrich, A. Boeddrich, F. Schiele, D. Kleckers, J. M. Lopez del Amo, B. A. Grüning, Q. Wang, M. R. Schmidt, R. Lurz, R. Anwyl, S. Schnoegl, M. Fandrich, R. F. Frank, B. Reif, S. Günther, D. M. Walsh, E. E. Wanker, *Nat. Chem. Biol.* **2012,** *8* 93-101.

[34.] J. M. Lopez del Amo, U. Fink, M. Dasari, G. Grelle, E. E. Wanker, J. Bieschke, B. Reif, *J. Mol. Biol.* **2012,** *421* 517-524.

[35.] J. C. Stroud, L. Cong, P. K. Teng, D. Eisenberg, *Proc. Natl. Acad. Sci. USA* **2012,** *109* 7717-7722.

[36.] M. D. Kirkitadze, G. Bitan, D. B. Teplow, *J. of Neurosci. Res.* **2002,** *69* 567-577.

[37.] J. Lee, E. K. Culyba, E. T. Powers, J. W. Kelly, *Nat. Chem. Biol.* **2011,** *7* 602-609.

[38.] P. Schanda, E. Kupce, B. Brutscher, *J. Biomol. NMR* **2005,** *33* 199-211.

[39.] K. Pauwels, T. L. Williams, K. L. Morris, W. Jonkheere, A. Vandersteen, G. Kelly, J. Schymkowitz, F. Rousseau, A. Pastore, L. C. Serpell, K. Broersen, *J. Biol. Chem.* **2012,** *287* 5650-5660.

[40.] G. A. Morris, R. Freeman, *J. Am. Chem. Soc.* **1979,** *101* 760-762.

[41.] W. Bermel, I. Bertini, I. C. Felli, M. Piccioli, R. Pierattelli, *Progr. NMR Spectrosc.* **2006,** *48* 25-45.

[42.] R. Riek, G. Wider, K. Pervushin, K. Wüthrich, *Proc. Natl. Acad. Sci. USA* **1999,** *96* 4918-4923.

[43.] A. Pines, M. G. Gibby, J. S. Waugh, *J. Chem. Phys.* **1972,** *56* 1776-1777.

[44.] A. Mainz, S. Jehle, B. J. van Rossum, H. Oschkinat, B. Reif, *J. Am. Chem. Soc.* **2009,** *131* 15968-15969.

[45.] W. B. Jr. Stine, K. N. Dahlgren, G. A. Krafft, LaDu M.J., *J Biol. Chem.* **2003,** *278* 11612-11622.

[46.] I. Kuperstein, K. Broersen, I. Benilova, J. Rozenski, W. Jonekheere, M. Debulpaep, A. Vandersteen, I. Segers-Nolten, K. Van der Werf, V. Subramaniam, D. Braeken, G. Callewaert, C. Bartic, R. D'Hooge, I. C. Martins, F. Rousseau, J. Schymkowitz, B. De Strooper, *EMBO J.* **2010,** *29* 3408-3420.

[47.] R. C. Chatelier, A. P. Minton, *Biopolymers* **1987,** *26* 507-524.

[48.] A. T. Petkova, R. D. Leapman, Z. H. Guo, W. M. Yau, M. P. Mattson, R. Tycko, *Science* **2005,** *307* 262-265.

[49.] A. K. Paravastu, R. D. Leapman, W. M. Yau, R. Tycko, *Proc. Natl. Acad. Sci. USA* **2008,** *105* 18349-18354.

[50.] R. J. Ellis, A. P. Minton, *Biol. Chem.* **2006,** *387* 485-497.

[51.] D. A. White, A. K. Buell, T. P. J. Knowles, M. E. Welland, C. M. Dobson, *J. Am. Chem. Soc.* **2010,** *132* 5170-5175.

[52.] A. Magno, A. Caflisch, R. Pellarin, *J. Phys. Chem. Lett.* **2010,** *1* 3027-3032.

[53.] T. P. J. Knowles, C. A. Waudby, G. L. Devlin, S. I. A. Cohen, A. Aguzzi, M. Vendruscolo, E. M. Terentjev, M. E. Welland, C. M. Dobson, *Science* **2009,** *326* 1533-1537.

[54.] H.-Y. Kim, M.-K. Cho, A. Kumar, E. Maier, C. Siebenhaar, S. Becker, C. O. Fernandez, H. A. Lashuel, R. Benz, A. Lange, M. Zweckstetter, *J. Am. Chem. Soc.* **2009,** *131* 17482-17489.

[55.] Y. F. Mok, G. J. Howlett, *Methods Enzymol.* **2006,** *413* 199-217.

[56.] D. Kashchiev, R. Cabriolu, S. Auer, *J. Am. Chem. Soc.* **2013,** *135* 1531-1539.

[57.] B. Hu, O. T. J. Lafon, Q. Chen, J.-P. Amoureux, *J. Magn. Reson.* **2011,** *212* 320-329.

[58.] N. M. Loening, M. Bjerring, N. C. Nielsen, H. Oschkinat, *J. Magn. Reson.* **2012,** *214* 81-90.

[59.] A. Sandberg, L. M. Luheshi, S. Sollvander, T. P. de Barros, B. Macao, T. P. J. Knowles, H. Biverstal, C. Lendel, F. Ekholm-Petterson, A. Dubnovitsky, L. Lannfelt, C. M. Dobson, T. Hard, *Proc. Natl. Acad. Sci. USA* **2010,** *107* 15595-15600.

[60.] M. V. Berjanskii, S. Neal, D. S. Wishart, *Nucleic Acids Res.* **2006,** *34* W63-W69.

[61.] Y. Shen, F. Delaglio, G. Cornilescu, A. Bax, *J.Biomol. NMR* **2009,** *44* 213-223.

[62.] T. A. Wassenaar, M. van Dijk, N. Loureiro-Ferreira, G. van der Schot, S. J. de Vries, C. Schmitz, J. van der Zwan, R. Boelens, A. Giachetti, L. Ferella, A. Rosato, I. Bertini, T. Herrmann, H. R. A. Jonker, A. Bagaria, V. Jaravine, P. Guntert, H. Schwalbe, W. F. Vranken, J. F. Doreleijers, G. Vriend, G. W. Vuister, D. Franke, A. Kikhney, D. I. Svergun, R. H. Fogh, J. Ionides, E. D. Laue, C. Spronk, S. Jurksa, M. Verlato, S. Badoer, S. Dal Pra, M. Mazzucato, E. Frizziero, A. M. J. J. Bonvin, *J. Grid Comput.* **2012,** *10* 743-767.

[63.] S. Chimon, M. A. Shaibat, C. R. Jones, D. C. Calero, B. Aizezi, Y. Ishii, *Nat. Struct. Mol. Biol.* **2007,** *14* 1157-1164.

[64.] A. T. Petkova, W. M. Yau, R. Tycko, *Biochemistry* **2006,** *45* 498-512.

“Structural characterization of AβM40/AβM42 fibril mixture”

Ivano Bertini [a,b,c], Linda Cerofolini [b], Marco Fragai [a,d], Gianluca Gallo [a,d], Magdalena Korsak [a,b], Claudio Luchinat [a,c,d], Enrico Ravera [a,d]

[a]Magnetic resonance Center (CERM), University of Florence, Via L. Sacconi 6, 50019 Sesto Fiorentino, Italy

[b]Giotto Biotech, Via Madonna del Piano 6, 50019 Sesto Fiorentino, Italy

[c]Fondazione Farmacogenomica FiorGen onlus, Via L. Sacconi 6, 50019 Sesto Fiorentino, Italy

[d]Department of Chemistry “Ugo Schiff”, University of Florence, Via della Lastruccia 3, 50019 Sesto Fiorentino, Italy

(Manuscript in preparation)

Introduction

Amyloid β (Aβ) peptides have been widely considered responsible for the onset of the neurodegenerative process in the Alzheimer's disease (AD) (Annaert and De Strooper 2002). One of the principal hallmark of AD are, indeed, amyloidic senile plaques, constituted by amyloid fibrils, formed from the aggregation process of Aβ peptides. Aβ peptides are generated from the amyloid precursor protein (APP) by β- and γ-secretases-combined cleavage, that produces a heterogeneous mixture of peptides varying in length at their carboxy-termini (from 37 to 43 amino acids). The two major Aβ species are constituted by 40 and 42 amino acids, respectively. Although neurotoxicity can be induced by deposits of Aβ fibrils, recent studies have established close link between the reciprocal ratio of Aβ40 and Aβ42 and the stability of intermediate neurotoxic species. Moreover, Aβ40 and Aβ42 have been found to affect each other's aggregation kinetics (Kuperstein et al 2010; Pauwels et al 2012). According to these studies, neurotoxicity might be explained by the dynamic nature of the ongoing Aβ aggregation process, rather than by the prevailing view that Aβ toxicity is associated with a distinct assembly. A change in the Aβ42:Aβ40 ratio induces differences in the conformational plasticity of the oligomeric peptide mixtures and in the pattern of the detectable oligomeric species (Yoshiike et al 2003; Jan et al 2008a; Jan et al 2010; Kuperstein et al 2010; Pauwels et al 2012). Investigation of the properties of the mixture of Aβ40 and Aβ42, by different groups, clearly show that this two species interact, as well as one changes the dynamic behavior of the other. It was proved that Aβ40 delays Aβ42 aggregation, whereas Aβ42 has an opposite effect and induces Aβ40 aggregation. This observation was also confirmed by in vivo studies, which have showed that higher percentage of Aβ40 peptides in the brain might have a protective effect (Wang et al 2006; Kim et al 2007).

Under normal physiological conditions in the brain, Aβ40 and Aβ42 alloforms co-exist in molar ratio 9:1. Conversely, in patients with familial AD this ratio is shifted to a higher level of Aβ42 and correspond to 7:3. At this point, a detailed structural characterization of Aβ40:Aβ42 mixed fibrils is needed. In the present paper, the structure of Aβ40:Aβ42 mixed fibrils in different molar ratios has been investigated, in order to shed light on the processes related to the onset of the disease and on their correlation with Aβ peptides reciprocal ratios. Mixed fibrils of AβM40 and AβM42 peptides in the molar ratios of (7:3) and (1:1) have been prepared and analyzed through transmission electron microscopy (TEM) and solid state NMR (ssNMR). The conformation acquired by the two peptides in the fibrils and their reciprocal organization along the fibril axis has been investigated.

Materials and Methods

Expression, Purification, and sample preparation of Aβ40: Aβ42 mixed fibrils

The cDNA of AβM40/AβM42 was cloned in the pET3a vector using the NdeI and BamHI restriction enzymes. The peptides were expressed in the BL21 (DE3)pLys *E. coli* strain. Both polypeptides contain an exogenous N-terminal methionine residue (Met0), due to the translation start codon, that has been shown not to play a significant role in aggregation, nor in toxicity, as reported in the literature (Walsh et al 2009). The growth of AβM40 and AβM42 peptides was performed using the Marley method (Marley et al 2001). The cells transformed with the AβM40/AβM42 expression plasmid were predominately grown in rich medium at 310 K until OD_{600} reached 0.6, centrifuged and exchanged into an isotopically defined minimal media enriched with $(^{15}NH_4)_2SO_4$ (1 g/L) and [^{13}C] glucose (4 g/L). The peptide expression was induced with 1.2 mM IPTG and cells were harvested after 4 hours incubation at 312 K. The peptides were purified as reported in literature (Walsh et al 1999; Jan et al 2008b; Walsh et al 2009; Hellstrand et al 2009; Bertini et al 2011) with some modifications using a combination of anion-exchange and size exclusion chromatography. All the manipulations were performed at slightly alkaline pH in order to avoid the formation of structural contaminants produced by isoelectric precipitation. The inclusion bodies were first solubilized with 8M urea and then purified by ion exchange chromatography performed in batch. For this purpose resin DE52 on Büchner funnel with filter paper on a vacuum glass bottle was used. Elution was done using different concentration of buffer of NaCl. The protein was eluted with 125 mM concentration of the salt. In the case of AβM42, the protein was also present in fraction 20 mM, 150 mM, 200 mM and 1M, probably because of progressive aggregation of the sample. All obtained fractions of diluted protein were concentrated to final volume using Amicon device. The next step of purification was gel filtration, which was performed using the preparative column Sephadex 75 HiLoad 26/60 with the 50 mM (NH_4)OAc pH 8.5 as buffer. The obtained fractions were collected together and concentrated. During all the purification steps, the protein purity was analysed using SDS-PAGE electrophoresis, whereas the protein concentration was estimated using the spectrophotometer. These two-steps of purification allow to obtain highly pure products with the yield in the range of 10 mg for AβM40 and 5-10 mg for AβM42 per liter of culture.

The mixed fibrils for ssNMR studies were produced according to the protocol described in Bertini et al. 2011. The samples were obtained by mixing batches of ^{13}C, ^{15}N-

uniformly enriched AβM40 polypeptide with aliquots of the AβM42 polypeptide in natural isotopic abundance. The mixtures of 70μM AβM40 and 30μM AβM42 and of 50 μM AβM40 and 50 μM AβM42 in 50 mM ammonium acetate (pH 8.5) were incubated at 310 K under shaking (950 rpm) for 5 weeks. Fibrils were collected by the overnight ultracentrifugation at 60000 rpm and 277 K for 24 h. The pellet was washed with fresh and cold ultrapure water (Millipore) for three times (1 mL per time), and then ~14 mg of the wet material were packed into a 3.2 mm ZrO_2 magic angle spinning (MAS) rotor at 277 K. The fibril samples were kept fully hydrated during all steps. The mixture of ^{13}C, ^{15}N-uniformly enriched AβM42 polypeptide and AβM40 polypeptide in natural isotopic abundance was prepared using the same protocol.

For transmission electron microscopy (TEM) tests, a suspension of Aβ40:Aβ42 mixed fibrils was dropped and dried on a Cu grid covered by carbon film. The fibrils were then stained in freshly prepared aqueous uranyl acetate solution for 20 min. After that, the grid was rinsed gently using ultrapure water for 1 min and dried again. Bright-field TEM images were collected on a Philips CM12 microscope operating at 80 kV.

NMR measurements

NCA, NCO, NCACX (3D), NCOCX (3D), NCACB (3D), N(CO)CACB(3D) and CANCO (3D) experiments were performed on a Bruker Avance III 850 MHz wide-bore spectrometer (20.0 T, 213.7 MHz ^{13}C Larmor frequency) equipped with a 3.2 mm DVT MAS probe head in triple-resonance mode. The MAS frequency ($\omega r/2\pi$) was 14.0 kHz (± 2 Hz) during most of these experiments. The NCA, NCO, NCACX (3D), NCOCX (3D), NCACB (3D), N(CO)CACB (3D) and CANCO (3D) experiments were carried out using the standard pulse sequences as reported in the literature.

2D ^{13}C-^{13}C proton-driven spin diffusion (PDSD)/DARR correlation spectra and 2D ^{13}C-^{13}C SHANGHAI with different mixing times (15, 25, 50, 75, 100, 200, 300, 400, 800 ms) were recorded on a Bruker Avance 700 MHz wide-bore instrument (16.4 T, 176.0 MHz ^{13}C Larmor frequency) equipped with a 3.2 mm DVT probe head in the double-resonance mode. During the 2D ^{13}C-^{13}C DARR mixing time, a radio frequency (RF) pulse of constant strength equal to $\omega r/2\pi$ was applied on the ^{1}H channel. For these experiments, the MAS frequency was stabilized at 12 kHz (± 2 Hz). During the experiments carried out using the 3.2 mm probe heads, the sample was cooled by a dry, cold air flow (> 935 L/h) generated by a BCU unit

(BCUXtreme or BCU-05), and the effective sample temperature during the experiments was estimated to be ~283 K.

All spectra were processed with the Bruker TOPSPIN software packages and analyzed by the program CARA (Computer Aided Resonance Assignment, ETH Zurich) (Keller 2003).

ssNMR data analysis and structural modeling.

The sequential assignment of the new species present in the AβM40:AβM42 mixed fibrils was performed starting from the identification of the unique 31Ile-32Ile couple and following the same procedure reported in Bertini et al. 2011. The secondary structural probability was calculated by the TALOS+ program using the chemical shifts of the N, C, Cα, Cβ atoms.

For model building, the length of β1 and β2 strands was based on the secondary structure predicted by the TALOS+ program. The β1- and β2-strands were then docked to one another by the HADDOCK program (Dominguez et al 2003; de Vries et al 2010) using the experimental long-range β1-β2 restraints. HADDOCK calculations were performed on the WeNMR GRID (http://www.wenmr.eu/) through the HADDOCK webserver Guru interface. All observed long-range contacts were implemented in the calculation. The lower distance cutoff in the HADDOCK calculations was set to 3.0 Å, and the upper distance cutoff was set to 6.0 Å for the shorter mixing contacts (100 and 200 ms) and to 7.5-8.0 Å for the long mixing contacts (300 and 400 ms). The charges on the N- and C-termini of the β1-strands and on the N-termini of the β2-strands were not included in the calculations in order to prevent electrostatic interactions, which do not exist when the two β-strands are linked by a turn region. The histidine protonation states were automatically determined by the WHATIF program which is embedded in the HADDOCK server on the WeNMR GRID. During the rigid docking calculations, 1000 structures were generated, then the best 200 structures were selected for the semi-rigid simulated annealing in torsion angle space, and finally refined in Cartesian space with explicit solvent.

The β-sheets were then constructed by duplicating the β1 and β2 strands along the direction of the backbone N-H and C=O bonds with PYMOL, using a typical inter-strand distance of 4.8 Å (Kirschner et al 1986), according to the parallel registry (see Results). Eight β-strands for each β1 and β2 sheets were built, considering for the β2-sheet an alternation of the Aβ40 and Aβ42 sequences.

The turn regions were randomly generated using the program MODELLER (Sali and Blundell 1993; Fiser and Šali 2003) and the final one was selected from the resulted pool of 50 structures.

Similar to the procedure used to define the monomer folding, the inter-protofilament structural model was calculated by docking two β2-sheets from two different protofilaments through the HADDOCK WeNMR GRID webserver. The Guru interface was used for job submission so that non-crystallographic symmetry restraints between the two β2-sheets could be defined in the calculation. All observed intermolecular long-range contacts and inter-strand distance restraints were implemented in the calculations. All the restraints were duplicated symmetrically between the two β2-sheets using the same protocol used for structural calculations of symmetric dimers. Since these long range distance restraints could be identified only using long mixing times, the upper distance cutoffs in the HADDOCK calculation was set to 8.0 Å. Semi-flexible refinement was enabled on both β2-sheets.

Results and Discussion

TEM Characterization, High-Resolution SSNMR Spectra, and Sequential Assignment.

The mature fibrils of AβM40:AβM42 in the ratio of 7:3 were analyzed through Transmission Electron Microscopy (TEM) and Solid State NMR (SSNMR). TEM micrographs revealed that the morphology of the fibrils is consistent with the results previously presented by Kuperstein et al. 2010 and by Pauwels et al. 2012. TEM micrographs of the mixtures of these fibrils (Figure 1) showed that the sample is mainly composed by short (100 μm) and highly entangled fibrillar material. The average section across is about 8±1 x 18±4 nm. The samples contain mainly "striated" bundles composed by laterally associated filaments, as it occurred for the previous sample of AβM40 alone. The morphology of "twisted pairs", which were observed in the Aβ40 fibrils prepared under quiescent conditions, is not observed in our samples.

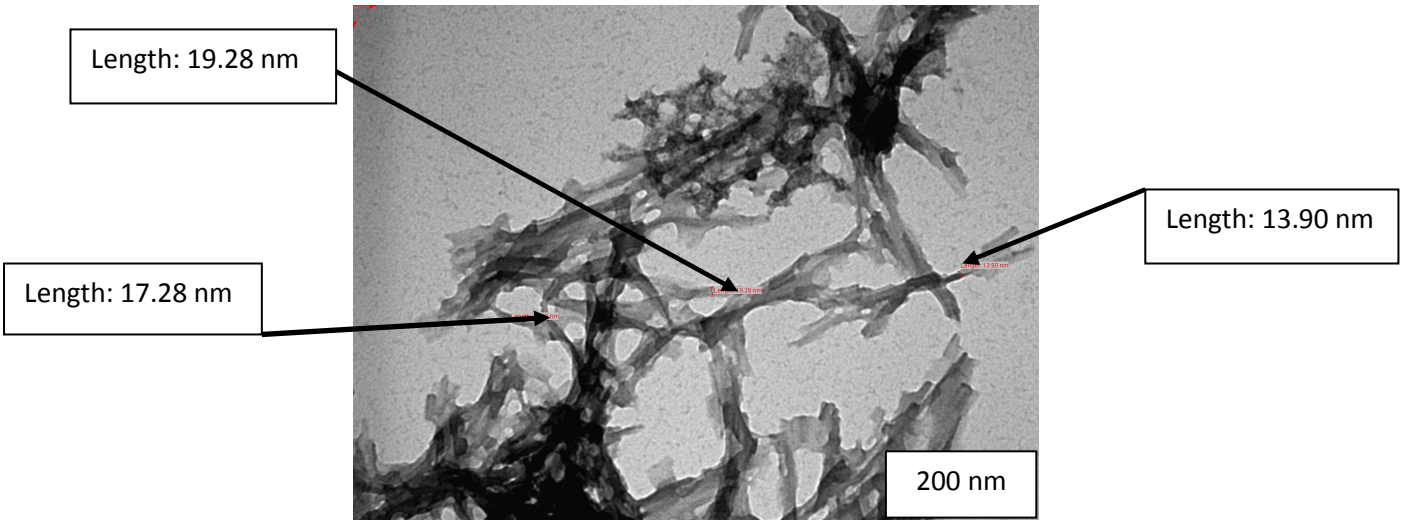

Figure 1. Transmission electron microscopy (TEM) micrographs of fibrils mixtures of double labeled AβM40 and unlabeled AβM42 in molar ratio (7:3).

Although TEM micrograph seems to suggest a large heterogeneity in the fibrils, the quality of the obtained SSNMR spectra is comparable with that of the spectra obtained from samples containing fibrils formed by the AβM40 polypeptide alone (Bertini et al 2011).

Protein sample was analyzed through dipolar-coupling based 2D ^{13}C-^{13}C SHANGHAI spectra and 2D ^{15}N-^{13}C correlation spectra (NCA/NCO). 2D ^{13}C-^{13}C-SHANGHAI spectrum of the fibril mixtures was overlaid with to the 2D ^{13}C-^{13}C-DARR spectra of fibrils AβM40 prepared in the same solution condition and 2D ^{15}N-^{13}C NCA spectrum of the fibril mixtures was overlaid with to the 2D ^{15}N-^{13}C NCA spectra of fibrils AβM40 (Figure 2). The registered spectra resemble those of the fibrils formed by the AβM40 polypeptide alone, with several additional signals. This suggests the presence of two specie, one corresponding to the AβM40 polypeptide with the same conformation and contacts previously characterized by Bertini et al. 2011, and a second species with a different conformation and/or contacts. The ratio between the two species has been estimated from 2D ^{13}C-^{13}C DARR and 2D ^{13}C-^{13}C SHANGHAI spectra to be of the order of 30%, not consistent with an asymmetric dimer as basic subunit (Lopez del Amo et al 2012). Another extremely important clue is provided by the fact that no cross-peaks between the two different forms of AβM40 can be observed.

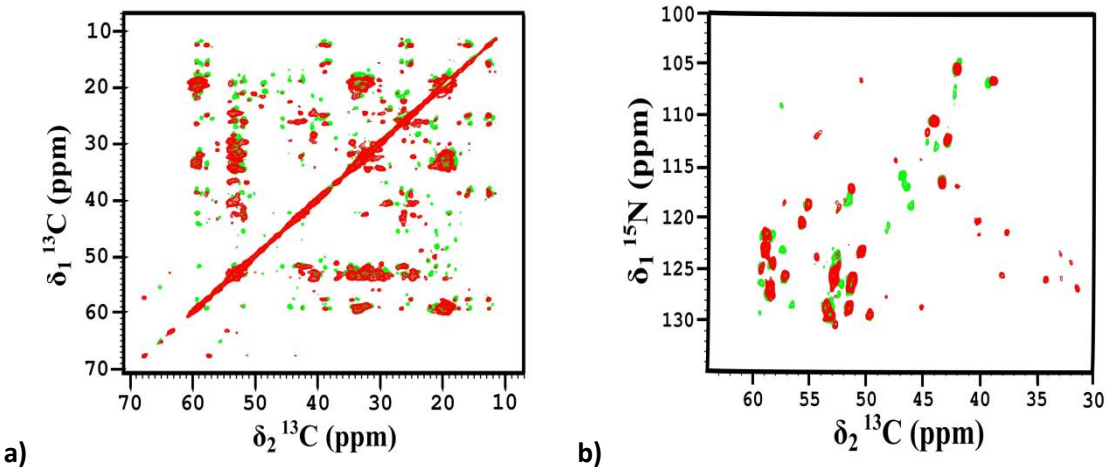

Figure 2. a) 2D ^{13}C-^{13}C-SHANGHAI spectrum of the fibril mixtures in molar ratio 7:3 (green) overlaid with to the 2D ^{13}C-^{13}C-DARR spectra of fibrils AβM40 (red). Magnetic field: 700 MHz (16.4 T), dimension of rotor: 3.2 mm (~14 mg of fibrils), 12 kHz spinning, 100 kHz ^{1}H decoupling, **b)** 2D ^{15}N-^{13}C NCA spectrum of the fibril mixtures in molar ratio 7:3 (green) overlaid with to the 2D ^{15}N-^{13}C NCA spectra of fibrils AβM40 (red). Magnetic field: 700 MHz (16.4 T), dimension of rotor: 3.2 mm (~14 mg of fibrils), 14 kHz spinning, 100 kHz ^{1}H decoupling.

However high resolution structural analysis of this sample by SSNMR was hampered due to its high heterogeneity. In order to shed light on the structural features of the mixed fibrils, a new samples of double labeled AβM40 and unlabeled AβM42 fibrils in a ratio 1:1 were prepared. The figure below shows the comparison of the 2D NCA spectra of the 1:1 AβM40:AβM42 mixture (green) with respect to the Aβ40 fibrils. The spectra obtained from the 1:1 mixed fibrils are simplified with respect to those of the 7:3 mixed fibrils, with only the cross-peaks corresponding to the new species detectable (Figure 3).

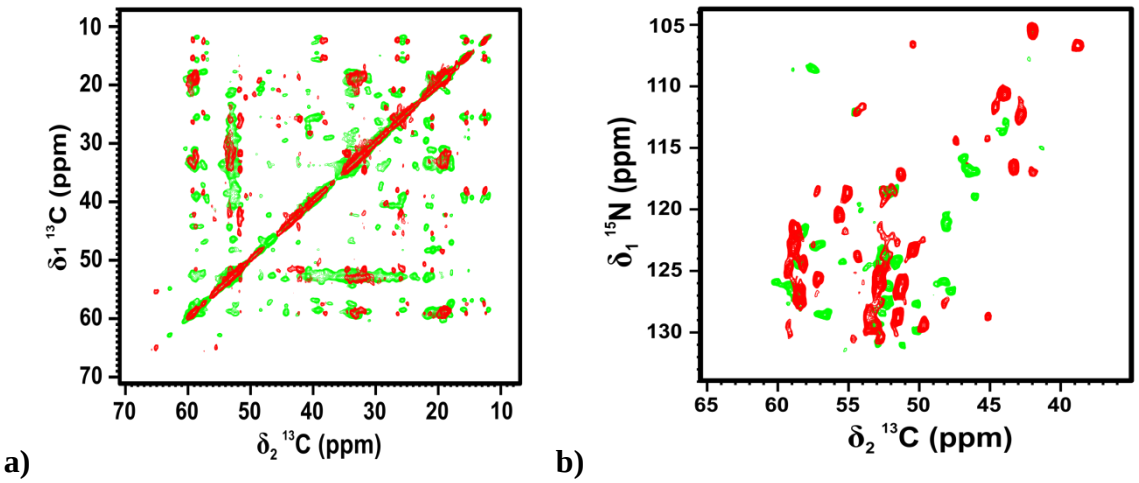

Figure 3. a) ^{13}C-^{13}C-SHANGHAI spectrum of the fibril mixtures in molar ratio 1:1 (green) overlaid with to the ^{13}C-^{13}C-DARR spectra of fibrils AβM40 (red). Magnetic field:700 MHz (16.4 T), dimension of rotor: 3.2 mm (~14 mg of fibrils), 12 kHz spinning, 100 kHz ^{1}H decoupling, **b)** ^{15}N-^{13}C NCA spectrum of the fibril mixtures in molar ratio 1:1 (green) overlaid with to the ^{15}N-^{13}C NCA spectra of fibrils AβM40 (red). Magnetic field: 700 MHz (16.4 T), dimension of rotor: 3.2 mm (~14 mg of fibrils), 14 kHz spinning, 100 kHz ^{1}H decoupling.

In order to perform the full assignment of the resonances of the new species, a toolbox of SSNMR experiments (2D NCA, 2D NCO, 3D NCACX, 3D NCOCX, 3D CANCO, 3D NCACB and 3D N(CO)CACB) were acquired. The sequential assignment of the backbone and side-chains of AβM40 forming the new species was successfully obtained (fig. 4).

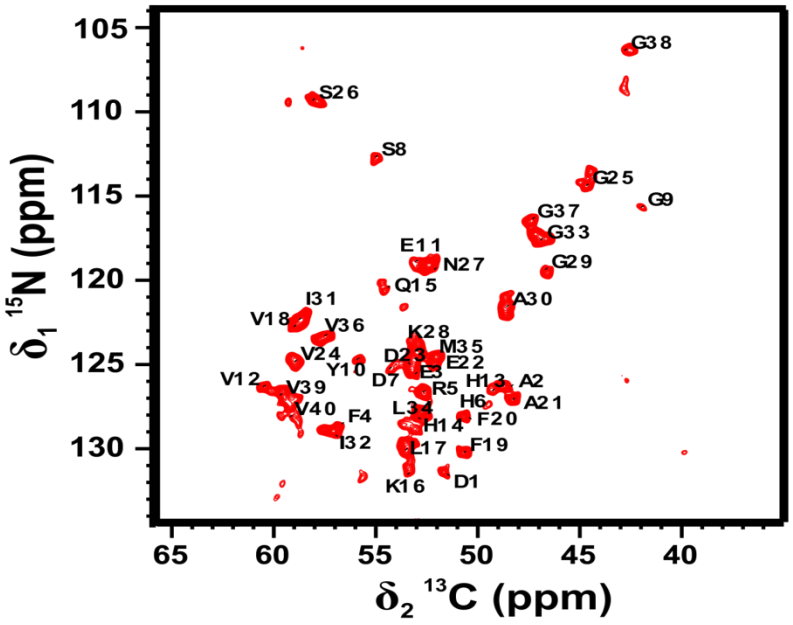

Figure 4. ^{15}N-^{13}C NCA spectra of the fibril mixtures in molar ratio 1:1: the full assignment of the spectrum is displayed.

The strategy used for the assignment is illustrated in (Figure 5).

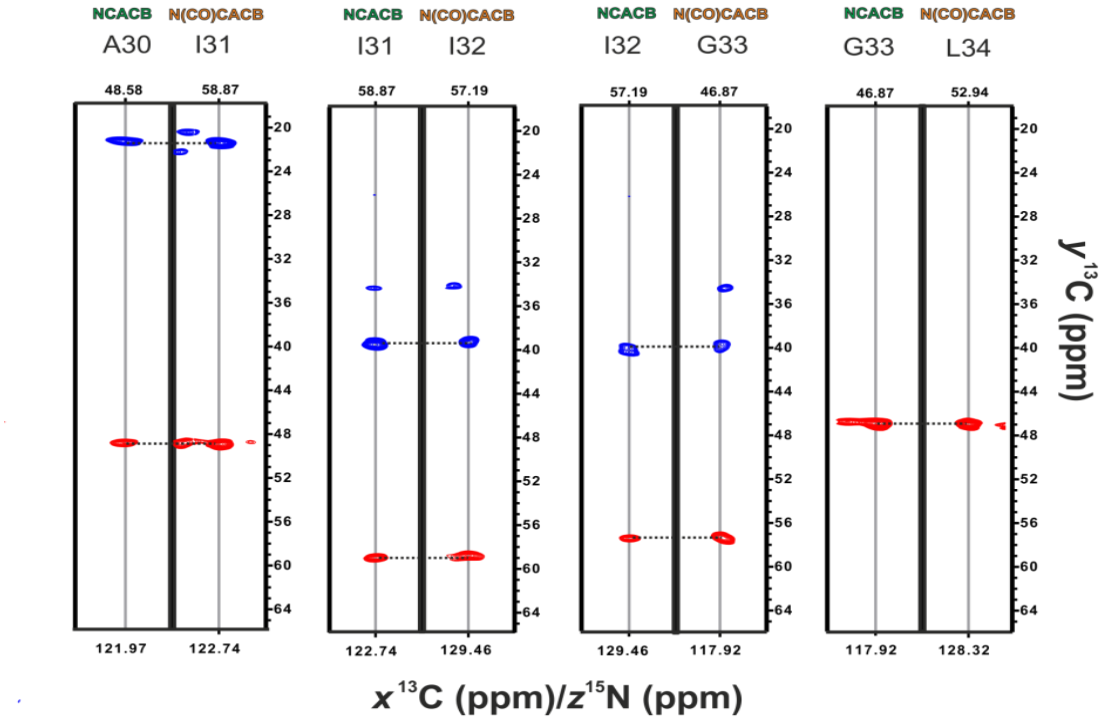

Figure 5 . Assignment strategy used for the sample of AβM40:AβM42 (1:1) mixture. Four correlated strips (planes NCB) of the 3D spectra NCACB and N(CO)CACB are displayed. The combination of these 3D spectra, together with 3D NCOCX and NCACX, allowed for the sequential assignment of the AβM40.

β-Strand-Turn-β-Strand Motif of Aβ40 in Aβ40:Aβ42 Protofilaments

The secondary structures of AβM40 polypeptide, predicted by TALOS+, in the mixture of the fibrils, contains a β-strand-turn-β-strand motif as found in other Aβ40 fibrils, with N-terminal region showing some propensity to form β-strand (Figure 6).

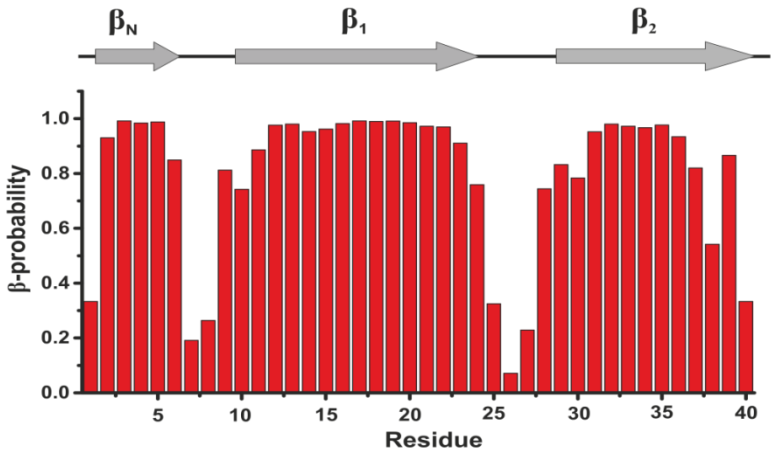

Figure 6. Secondary structure prediction of AβM42:AβM40 (1:1) fibrils obtained with Talos+.

The organization of the β-strand-turn-β-strand motif has been investigated in detail. Signals correlating the side chains of Leu17 with Leu34/Val36, Phe19 with Gly33/Leu34, and Ala21with Ile32 were detected and assigned unambiguously on the ^{13}C-^{13}C SHANGHAI spectra with 100-400 ms mixing times. These long-range unambiguous restraints are only consistent with the conformation of the U-shaped motif. The folding of the monomer, called also β –arch, was calculated with the same protocol reported in Bertini et al. 2011, using HADDOCK (Dominguez et al 2003; de Vries et al 2010). In the current conformation of the β –arch, as indicated by the contacts, a different reciprocal packing of the two beta-strands (β1 and β2), with respect to the model obtained for the fibrils of AβM40 alone (Bertini et al. 2011), is observed (Figure 7). The conformation assumed by AβM40 in the presence of AβM42 resemble the most that reported in literature for fibrils of AβM42 alone (Ahmed et al 2010) with respect to that of fibrils of AβM40 alone (Bertini et al 2011). Interestingly, AβM42 seems to force AβM40 to assume its own conformation in order to better maximize the hydrophobic contacts and minimize the steric hindrance due to the addition of two further residues at the C-termini.

Aβ40 Current Model

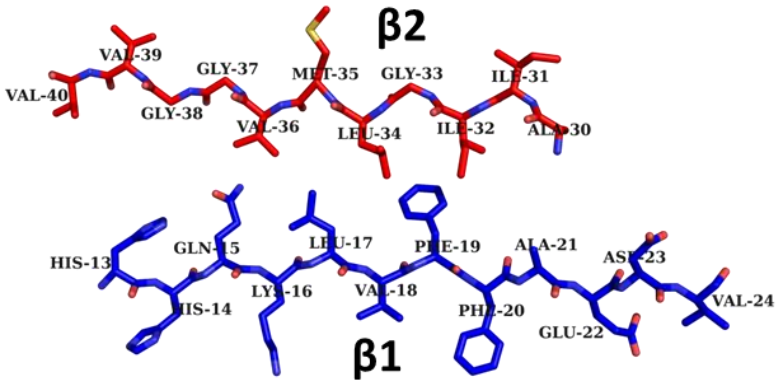

Aβ40 Bertini et al. 2011

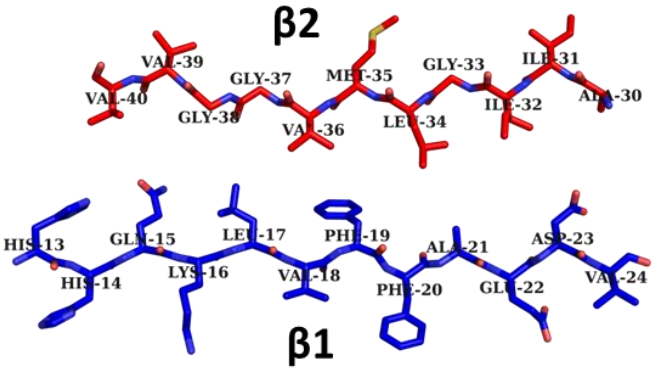

Figure 7. Folding of monomeric Aβ40 peptide **a)** in the model of Aβ42:Aβ40 (1:1) fibrils and **b)** in the model obtained for the fibrils of AβM40 alone (Bertini et al. 2011). The linker between β1 and β2 was generated using Modeller.

This result further supports the idea that the polymorphism of Aβ40 fibrils is not only due to different inter-protofilaments lateral association, but can also derive from the structural differences in the β-strand-turn-β-strand motif, since these are the building blocks of the mature fibrils.

The analysis of the cross-peaks in the various spectra (SHANGHAI, DARR/PDSD) supports a parallel packing of the protein molecules in the proto-filament. In particular, no cross peaks correlating the beginning and ending parts of β1 or β2 segments can be assigned in an unambiguous and consistent manner. Therefore, the β-strand-turn-β-strand motifs must be organized in parallel cross-β sheets as reported in literature for mature fibrils of Aβ40 (Petkova et al 2002; Petkova et al 2006; Paravastu et al 2008; Ahmed et al 2010; Qiang et al 2011; Bertini et al 2011).

Moreover, the presence of a single pattern of signals for each residue in the ssNMR spectra only agrees, for symmetric considerations, with the presence of a parallel in-registry β-spine (Nielsen et al 2009).

Inter-protofilament Interactions in Mature Aβ40:Aβ42 mixed fibrils.

The lateral association among different proto-filaments in the fibrils has been also calculated implementing long-range distance restraints in HADDOCK. Contacts among the C-terminus and the N-terminus of β2-strand have been found from the ssNMR spectra analysis, indicating the presence of an head to tail antiparallel association of two β2-strands of different monomers. In particular, contacts between the side chains of Ile31 with Val39/Val40 and Met35 with Gly38/Val39 have been assigned from ^{13}C-^{13}C SHANGHAI and DARR/PDSD spectra. These experimental restraints are in agreement with two-fold rotational symmetry (or a so-called co-aligned homo-zipper (Nielsen et al 2009)) and with the parallel registry of the protofilament.

Folding of Aβ42 in Aβ40:Aβ42 mixed fibrils.

A sample containing a mixture of double labeled ($^{13}C^{15}N$) AβM42 and unlabeled AβM40 in the molar ratio of (1:1) has been further prepared with the purpose to characterize the conformation of AβM42 in the fibrils..

The spectra of AβM42 appear almost completely superimposable to those of AβM40, indicating that the conformations acquired by the two peptides are mostly the same (figure 8). The two C-terminal residues of AβM42 could be also identified and assigned in the NCA spectrum.

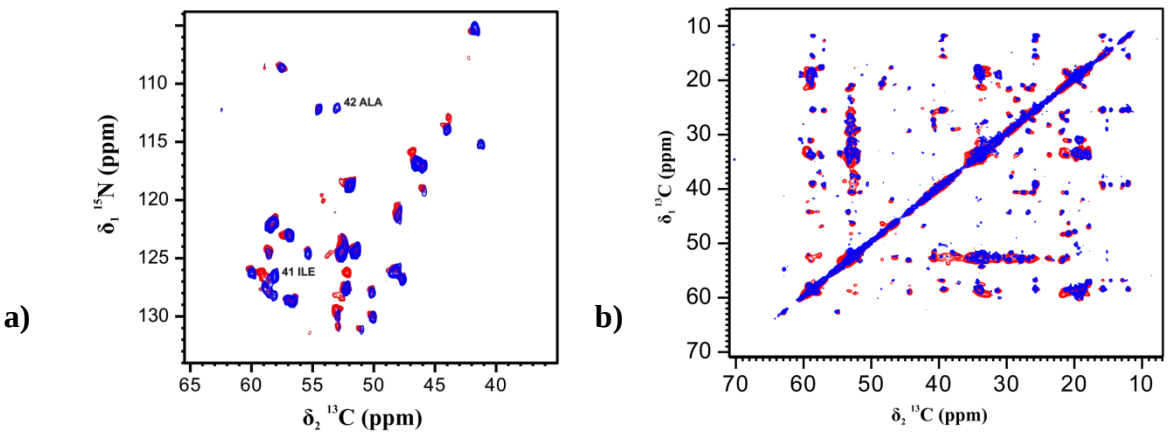

Figure 8. a) 2D ^{15}N-^{13}C NCA spectrum of AβM42 ^{13}C:^{15}N/AβM40 unlabelled (1:1) (blue) overlaid with to the 2D ^{15}N-^{13}C NCA spectrum of AβM40 ^{13}C:^{15}N/ AβM42 unlabelled (1:1) (red). Magnetic field: 700 MHz (16.4 T), dimension of rotor: 3.2 mm (~14 mg of fibrils), 12 kHz spinning, 100 kHz ^{1}H decoupling, T = 265 K. **b)** 2D ^{13}C-^{13}C- DARR spectrum of AβM42 ^{13}C:^{15}N/AβM40 unlabelled (1:1) (blue) overlaid with to the 2D 15N-13C NCA spectra of AβM40 ^{13}C:^{15}N/ AβM42 unlabelled (1:1) (red). Mixing time = 100 ms. Magnetic field: 700 MHz (16.4 T), dimension of rotor: 3.2 mm (~14 mg of fibrils), 12 kHz spinning, 100 kHz ^{1}H decoupling, T = 265K.

Aβ40/Aβ42 reciprocal association in the mixed fibrils

In order to identify AβM40:AβM42 reciprocal association in the fibrils, we took into account three different possible reciprocal packing of Aβ40 and Aβ42 peptides along the fibril axis (figure 9). The first one can be excluded since in this case we would have had separated fibrils of AβM40 and of AβM42, that mean that the conformation adopted by AβM40 in the mixed fibrils should be the same of that of AβM40 fibrils alone. Experimental data obtained through SSNMR demonstrate that it is not the case. The other two models are equally possible since the experimental distance restraints can support both of them.

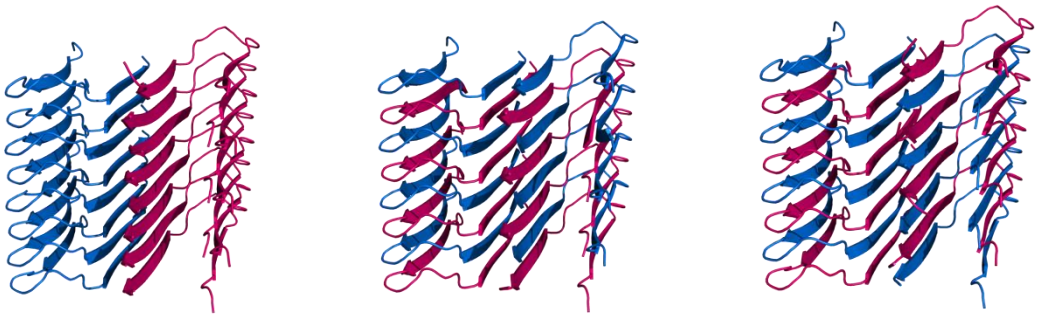

Figure 9. Putative AβM42:AβM40 reciprocal association in fibrils mixture. Pink color correspond to AβM42 and blue color correspond to AβM40 fibrils. The models were generated with HADDOCK and Modeller.

New insight in the polymorphism of Aβ peptides and the related fibrils.

The collective experimental data obtained through SSNMR and TEM demonstrate that a change in the AβM42:AβM40 reciprocal ratio induces a variation in the formed specie. From the registered spectra, we evaluated that the molar ratio 7:3 favor the presence of two specie, one corresponding to the AβM40 polypeptide with the same conformation and contacts previously characterized by Bertini et al. 2011, and a second species with a different conformation and/or contacts, whereas the molar ratio 1:1 facilitate the specific formation of only one species - aggregates of AβM40 and AβM42 together. The new conformation assumed by Aβ40 in the presence of Aβ42 reflects the dynamic behavior of these peptides. These results indicate that different relative ratios of Aβ peptides are responsible of the formation of different toxic specie correlated with the onset of the Alzheimer's disease.

References:

Ahmed M, Davis J, Aucoin D, et al (2010) Structural conversion of neurotoxic amyloid-beta(1-42) oligomers to fibrils. Nat Struct Mol Biol 17:561–567. doi: 10.1038/nsmb.1799.

Annaert W, De Strooper B (2002) A cell biological perspective on Alzheimer's disease. Annu Rev Cell Dev Biol 18:25–51. doi: 10.1146/annurev.cellbio.18.020402.142302.

Bertini I, Gonnelli L, Luchinat C, et al (2011) A new structural model of Aβ40 fibrils. J Am Chem Soc 133:16013–16022. doi: 10.1021/ja2035859.

De Vries SJ, van Dijk M, Bonvin AMJJ (2010) The HADDOCK web server for data-driven biomolecular docking. Nat Protoc 5:883–897. doi: 10.1038/nprot.2010.32.

Dominguez C, Boelens R, Bonvin AMJJ (2003) HADDOCK: A Protein−Protein Docking Approach Based on Biochemical or Biophysical Information. J Am Chem Soc 125:1731–1737. doi: 10.1021/ja026939x.

Fiser A, Šali A (2003) Modeller: Generation and Refinement of Homology-Based Protein Structure Models. In: Charles W. Carter J and RMS (ed) Methods Enzymol. Academic Press, pp 461–491.

Hellstrand E, Boland B, Walsh DM, Linse S (2009) Amyloid ?-Protein Aggregation Produces Highly Reproducible Kinetic Data and Occurs by a Two-Phase Process. ACS Chem Neurosci 1:13–18. doi: 10.1021/cn900015v.

Jan A, Gokce O, Luthi-Carter R, Lashuel HA (2008a) The Ratio of Monomeric to Aggregated Forms of Aβ40 and Aβ42 Is an Important Determinant of Amyloid-β Aggregation, Fibrillogenesis, and Toxicity. J Biol Chem 283:28176–28189. doi: 10.1074/jbc.M803159200.

Jan A, Gokce O, Luthi-Carter R, Lashuel HA (2008b) The Ratio of Monomeric to Aggregated Forms of Aβ40 and Aβ42 Is an Important Determinant of Amyloid-β Aggregation, Fibrillogenesis, and Toxicity. J Biol Chem 283:28176–28189. doi: 10.1074/jbc.M803159200.

Jan A, Hartley DM, Lashuel HA (2010) Preparation and characterization of toxic Aβ aggregates for structural and functional studies in Alzheimer's disease research. Nat Protoc 5:1186–1209. doi: 10.1038/nprot.2010.72.

Keller R (2003) CARA.

Kim J, Onstead L, Randle S, et al (2007) Abeta40 inhibits amyloid deposition in vivo. J Neurosci Off J Soc Neurosci 27:627–633. doi: 10.1523/JNEUROSCI.4849-06.2007.

Kirschner DA, Abraham C, Selkoe DJ (1986) X-ray diffraction from intraneuronal paired helical filaments and extraneuronal amyloid fibers in Alzheimer disease indicates cross-beta conformation. Proc Natl Acad Sci U S A 83:503–507.

Kuperstein I, Broersen K, Benilova I, et al (2010) Neurotoxicity of Alzheimer's disease Aβ peptides is induced by small changes in the Aβ42 to Aβ40 ratio. EMBO J 29:3408–3420. doi: 10.1038/emboj.2010.211.

Lopez del Amo JM, Schmidt M, Fink U, et al (2012) An Asymmetric Dimer as the Basic Subunit in Alzheimer's Disease Amyloid β Fibrils. Angew Chem Int Ed 51:6136–6139. doi: 10.1002/anie.201200965.

Marley J, Lu M, Bracken C (2001) A method for efficient isotopic labeling of recombinant proteins. J Biomol NMR 20:71–75. doi: 10.1023/A:1011254402785.

Nielsen JT, Bjerring M, Jeppesen MD, et al (2009) Unique identification of supramolecular structures in amyloid fibrils by solid-state NMR spectroscopy. Angew Chem Int Ed Engl 48:2118–2121. doi: 10.1002/anie.200804198.

Paravastu AK, Leapman RD, Yau W-M, Tycko R (2008) Molecular structural basis for polymorphism in Alzheimer's β-amyloid fibrils. Proc Natl Acad Sci 105:18349–18354. doi: 10.1073/pnas.0806270105.

Pauwels K, Williams TL, Morris KL, et al (2012) Structural basis for increased toxicity of pathological aβ42:aβ40 ratios in Alzheimer disease. J Biol Chem 287:5650–5660. doi: 10.1074/jbc.M111.264473.

Petkova AT, Ishii Y, Balbach JJ, et al (2002) A structural model for Alzheimer's β-amyloid fibrils based on experimental constraints from solid state NMR. Proc Natl Acad Sci 99:16742–16747. doi: 10.1073/pnas.262663499.

Petkova AT, Yau W-M, Tycko R (2006) Experimental Constraints on Quaternary Structure in Alzheimer's β-Amyloid Fibrils†. Biochemistry (Mosc) 45:498–512. doi: 10.1021/bi051952q.

Qiang W, Yau W-M, Luo Y, et al (2012) Antiparallel β-sheet architecture in Iowa-mutant β-amyloid fibrils. Proc Natl Acad Sci U S A 109:4443–4448. doi: 10.1073/pnas.1111305109.

Qiang W, Yau W-M, Tycko R (2011) Structural Evolution of Iowa Mutant β-Amyloid Fibrils from Polymorphic to Homogeneous States under Repeated Seeded Growth. J Am Chem Soc 133:4018–4029. doi: 10.1021/ja109679q.

Sali A, Blundell TL (1993) Comparative protein modelling by satisfaction of spatial restraints. J Mol Biol 234:779–815. doi: 10.1006/jmbi.1993.1626.

Walsh DM, Hartley DM, Kusumoto Y, et al (1999) Amyloid β-Protein Fibrillogenesis STRUCTURE AND BIOLOGICAL ACTIVITY OF PROTOFIBRILLAR INTERMEDIATES. J Biol Chem 274:25945–25952. doi: 10.1074/jbc.274.36.25945.

Walsh DM, Thulin E, Minogue AM, et al (2009) A facile method for expression and purification of the Alzheimer's disease-associated amyloid beta-peptide. FEBS J 276:1266–1281. doi: 10.1111/j.1742-4658.2008.06862.x.

Wang R, Wang B, He W, Zheng H (2006) Wild-type Presenilin 1 Protects against Alzheimer Disease Mutation-induced Amyloid Pathology. J Biol Chem 281:15330–15336. doi: 10.1074/jbc.M512574200.

Yoshiike Y, Chui D-H, Akagi T, et al (2003) Specific compositions of amyloid-beta peptides as the determinant of toxic beta-aggregation. J Biol Chem 278:23648–23655. doi: 10.1074/jbc.M212785200.

“Lipoic derivatives in synergistic treatment of human superoxide dismutase with cisplatin”

Lucia Banci [a,c], *Francesca Cantini* [a,c], *Leonardo Gonelli* [a,b], *Magdalena Korsak* [a,b], *Cristina Nativi*[c,d]

[a]Magnetic resonance Center (CERM), University of Florence, Via L. Sacconi 6, 50019 Sesto Fiorentino, Italy

[b]Giotto Biotech, Via Madonna del Piano 6, 50019 Sesto Fiorentino, Italy

[c]Fondazione Farmacogenomica FiorGen onlus, Via L. Sacconi 6, 50019 Sesto Fiorentino, Italy

[d]Department of Chemistry “Ugo Schiff”, University of Florence, Via della Lastruccia 3, 50019 Sesto Fiorentino, Italy

(Manuscript in preparation)

Lipoic derivatives in synergistic treatment of human superoxide dismutase with cisplatin.

Human superoxide dismutase 1 (hSOD1) is strongly implicated in the onset of amyotrophic lateral sclerosis (ALS), a neurodegenerative disease characterized by the progressive dysfunction and loss of motor neurons (Bruijn et al. 2004; Valentine et al. 2005). The causes of motor neuron death are poorly understood, but a prominent hypothesis involves the formation of protein aggregates containing misfolded hSOD1 as the main component in amyloid-like deposits which have been widely found both in the spinal cords of ALS patients (Jonsson et al 2004; Shibata et al. 1996) and in transgenic mice developing ALS (Bruijn et al. 1997; Johnston et al. 2000; Wang et al. 2002; Watanabe et al. 2001). The precursors of these protein aggregates are believed to be soluble oligomeric intermediates of the hSOD1 aggregation process. These oligomers are thought to be responsible for the toxic gain of function, similar to what has been proposed for other neurodegenerative diseases (Mulligan & Chakrabartty 2013; Ross & Poirier 2004).

hSOD1 is ubiquitously expressed in human cells where it mainly localizes in the cytosol and in the mitochondria intermembrane space (IMS) at micromolar concentrations (Okado-Matsumoto & Fridovich, 2011; Sturtz et al. 2001). At lower levels has been also found in the nucleus and in the peroxisomes.

hSOD1 is a homodimeric metalloprotein harboring in each subunit, a catalytic copper ion and a structural zinc ion, an intrasubunit disulfide bond between a highly conserved pair of cysteine (Cys-57 and Cys-146) and two free cysteines (Cys-6 and Cys-111). Functionally hSOD1 is responsible for protecting cells from oxidative damage by eliminating superoxide ions through disproportionation (Bertini et al. 1998; Fridovich 1978).

The early species of the maturation process (i.e. misfolded SOD1 lacking metal ions) have been shown to have high tendency to oligomerize in vitro, while the mature form of hSOD1 is not prone to aggregation (Banci et al. 2007; Furukawa et al. 2008; Lindberg et al. 2002; Oztug Durer et al. 2009). Previous studies have shown that in the apo hSOD1 the two free cysteines (Cis-6 and Cys-111) become solvent accessible and form intermolecular disulfide bonds which cross-link the molecules into high-molecular-weight oligomers under physiological conditions (37°C, pH 7, and 100 μM protein concentration) (Banci et al. 2007; 2009). These oligomers of high molecular weight (over MDa) are remarkably stable, persisting in the soluble state for months and exhibit positive Tht binding response (Banci et al. 2007; 2009). An experimental mutation at Cys-111 (C111S) inhibited the aggregation of

ALS-mutant SOD1s in human and mouse neuronal cell lines (Karch et al. 2008; Cozzolino et al. 2008). Moreover, mice expressing a metal deficient variant where all copper- and zinc-binding histidine residues were mutated, together with Cys-111 and Cys-6 (H43R/H46R/H48Q/H63G/H71R/H80R/H120G/C6G/C111S), did not develop pathologic symptoms of ALS on the contrary to the expected due to the lack of any metal binding (Prudencio et al. 2012). In addition, such variant was not found in detergent-insoluble fractions of either mouse spinal cords or cell models, suggesting that it has a low aggregation propensity. Since the mutant protein created by converting residues at position 6 and 111 back to cysteine exhibited a remarkably increased aggregation propensity (Sheng et al. 2012), the lack of aggregation propensity of the previously mentioned variant likely resulted from the absence of Cys-6 and Cys-111. These findings further confirm the important role of the two non-conserved cysteine residues in modulating SOD1 aggregation and in particular of Cys-111. Cys- 111 is also critical for mutant SOD1 to associate with mitochondria and thus has been proposed to be a key mediator of mitochondrial dysfunction caused by aggregation of mutant SOD1 in the mitochondrial compartment (Ferri et al. 2006).

A recent study has shown that cis-diamminedichloroplatinum (II) (cisplatinum) can be selected as potential leading compound for blocking hSOD1 oxidative oligomerization (Banci et al. 2012). Cisplatinum is a small chemotherapeutic drug molecule with very high binding affinity toward thiol groups in proteins (Wang & Lippard, 2005). It has been proved that cisplatinum inhibits the oligomerisation of hSOD1 *in vitro* and *in vivo* by covalently binding to the solvent exposed Cys-111 of the apo-form of the enzyme and leads also to the dissociation of already formed apo hSOD1 oligomers without affecting the normal hSOD1 enzymatic activity (Banci et al. 2012). Nevertheless clinical use of this chemotherapeutic agent is severely limited by the development of side effects including nephrotoxicity, emetogenesis, ototoxicity and neurotoxicity (Kelland 2007; Wang & Lippard 2005). The peripheral neuropathy associated with these neurotoxic effects can be prolonged, severe and very often responsible for therapy interruption. Recent data have suggested that cisplatin also induces the formation of reactive oxygen species (ROS) that can trigger cell death (Brozovic et al. 2010; Casaress et al. 2012; Marullo et al. 2013).

It is thus clear that the availability of safe and effective analgesic drugs, able additionally to reverse or counterbalanced the toxic effects of cisplatinum related to the formation of ROS is a target of high interest. Such presumed candidates in suppression of neuropathic pain are two molecules ADM_09 and ADM_12 (Nativi et al. 2013). ADM_09 and ADM_12 are structurally new compounds obtained from synthesis of commercially

available (±) α-lipoic acid with proved antioxidative and analgesic properties (Parcker et al. 1995) and L-carnosine witch has been proven to scavenge reactive oxygen species (ROS) (Hipkiss, 2009), in which a synergic combination of features of theirs two substrates was coupled in order to enhance theirs antioxidative and analgesic properties. It has been proved by in vivo experiments that ADM_09 is able to effectively revert neuropathy pain induced by oxaliplatin (OXA) without eliciting the commonly observed negative side effects (Nativie et. al. 2013). *In vitro* tests clearly showed the absence of any toxic effect of this compound (Nativi et al. 2013). Patch-clamp recordings demonstrated that ADM_09 is an effective antagonist of the nociceptive sensor channel TRPA1 (Nativi et al. 2013). The TRPA1 channel is activated by several mechanisms and has been actively investigated as a target to control neuropathic pain (Karashima et al. 2009; Nilius et al. 2012). This channel has been reported to mediate in OXA-evoked allodynia (pain evoked by an innocuous stimulus) and neuropathic pain (NeP) in rats by activation likely caused by glutathione-sensitive molecules (Nassini et al. 2011). A chemical activation mechanism of TRPA1 as a nociceptive sensor involves the interaction of its cysteine residues (that constitute the nucleophilic sites of disulphide bond formation) with reactive compounds, which activate the nociceptive response and causes the opening of the channel. For ADM_09 it has been proposed a dual-binding mode of action, in which a synergic combination of calcium-mediated binding of the carnosine residue and disulphide-bridge-forming of the lipoic acid residue accounts for the observed persistent blocking activity toward the TRPA1 channel (Nativi et al. 2013).

Current study was undertaken to determine the anti-oxidative propensity of two molecules, ADM_09 and ADM_12, as well as to establish the ability of these two molecules to revert side effects caused by cisplatinum. We found that these compounds do not change the biochemistry of cisplatin and its interaction with hSOD1. Oligomerization of hSOD1 wt in the presence of cisplatinum together with small molecules (ADM_09 and ADM_12) is still inhibited, what means that the molecules does not modify the behavior of cisplatin and do not disrupt cisplatin to bind SOD1. ADM_09 and ADM_12 are detectable antioxidative agents and might be remarkably effective in the treatment of cisplatinum-induced neuropathy.

Results

To investigate the properties of these molecules towards cisplatinum we incubated ADM_09 and ADM_12 (1 mM) under physiological conditions in the presence of the 0,8 mM cisplatin. Apo hSOD1 in the absence of cisplatinum shows a progressive enhancement of Tht

fluorescence signal, consistent with previous finding (Banci et al. 2007). Cisplatinum efficiently inhibits the oligomerization of SOD1 showing slower increase in intensity in Tht fluorescence over time, as already have been reported (Banci et al. 2012). Oligomerization of hSOD1 in the presence of cisplatinum together with small molecules (ADM_09 and ADM_12) is still inhibited, what means that the molecules do not modify the behavior of cisplatin and do not disrupt cisplatin to bind SOD1 (fig. 1).

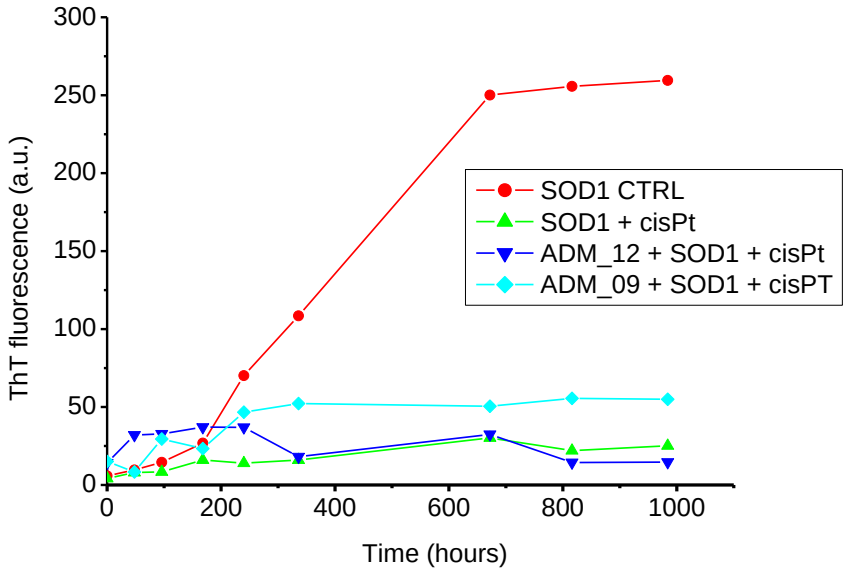

Figure 1. Fluorescence due to ThT binding to hSOD1. Plot of intensity of fluorescence versus time (h) for oxidized form of apo hSOD1 WT incubated with small molecules: ● hSOD1 control, ▲ hSOD1+cisPt 0,8mM, ▼ hSOD1+ADM_12 1mM +cisPt 0.8 mM, ♦ hSOD1+ADM_09 1mM +cisPt 0.8 mM.

Antioxidative properties.

The antioxidant profile of ADM_09 and ADM_12 was evaluated *in vitro* by measuring the oxidation of nitro blue tetrazolium (NBT) after 30 min, in the absence and in the presence of an increasing concentration of ADM_09 and ADM_12 (Table 1). In the absence of small molecules, superoxide anion (O_2^-) generated by the hypoxanthine – xanthine oxidase system increased the oxidized NBT level from 100 (basal) to around 4000 A.U. While in the presence of ADM_09 in the reaction mixture, the oxidation of NBT was inhibited in a concentration-dependent manner (Table 1). For example, 100 μM ADM_09 decreased the oxidized NBT from 4000 to 3200 A.U., indicating a detectable antioxidative activity. However, comparing the efficacy of ADM_09 with other commonly employed

antioxidants, including lipoic acid, it is easily appreciated that its antioxidative properties are only moderate and, notably, markedly less effective than the parent lipoic acid (Nativi et al. 2013). Apparently, coupling of lipoic acid with carnosine affected the antioxidative capability of the former residue, inducing a significant loss of acivity.

The antioxidative properties of ADM_12 are much more potent. The presence of ADM_12 in the reaction mixture inhibits the oxidation of NBT and reveal the strong antioxidative activity of ADM_12, that is comparable to its parent substrate – lipoic acid.

Control	Oxidation	**ADM_09** *concentration (μM)*					
		0.1	1	3	30	100	1000
100 ± 15	4069 ± 184	3842 ± 180	3753 ± 138	3764 ± 141	3704 ± 118*	3216 ± 133**	3159 ± 65**

Control	Oxidation	**ADM_12** *concentration (μM)*					
		0.1	1	3	30	100	1000
100 ± 16	3996 ± 81	3753 ± 116	3790 ± 70	3629 ± 56*	3611 ± 112*	2844 ± 42**	109 ± 37**

Table 1. Evaluation of the antioxidative properties of ADM_09 and ADM_12 by the NBT assay. O_2^- generated by hypoxanthine-xanthine oxidase reaction was used to oxidize NBT (*Nitro Blue Tetrazolium*). The oxidation kynetic was spectrophotometrically measured at 560 nm in the absence or in the presence of tested compounds. Values are expressed as absorbance arbitrary units (A.U.). Control was arbitrarily fixed at 100 A.U. *P<0.01 with respect to the Oxidation value.

The antioxidative properties of ADM_12 were also tested *in vivo* in rat cortical astrocytes. Because glial cells exert a pivotal role in the development of neuropatic pain, astrocytes from primary cultures were used in the antioxidative tests, as these are directly related to normal tissues. In primary cultures of astrocytes, the neurotoxic compound oxaliplatin (100 μM) induced a significant increase of SOD-inhibitable superoxide anion after 4 h of incubation, as evaluated by the cytochrome C assay (Fig. 2). Co-incubation with 100 μM ADM_12 inhibited the O_2^- formation by over 50% with respect to the untreated culture. This test was performed towards oxaliplatin since this chemotherapeutics agent has similar neurotoxicity profiles to cisplatinum, however is has much more clinical use.

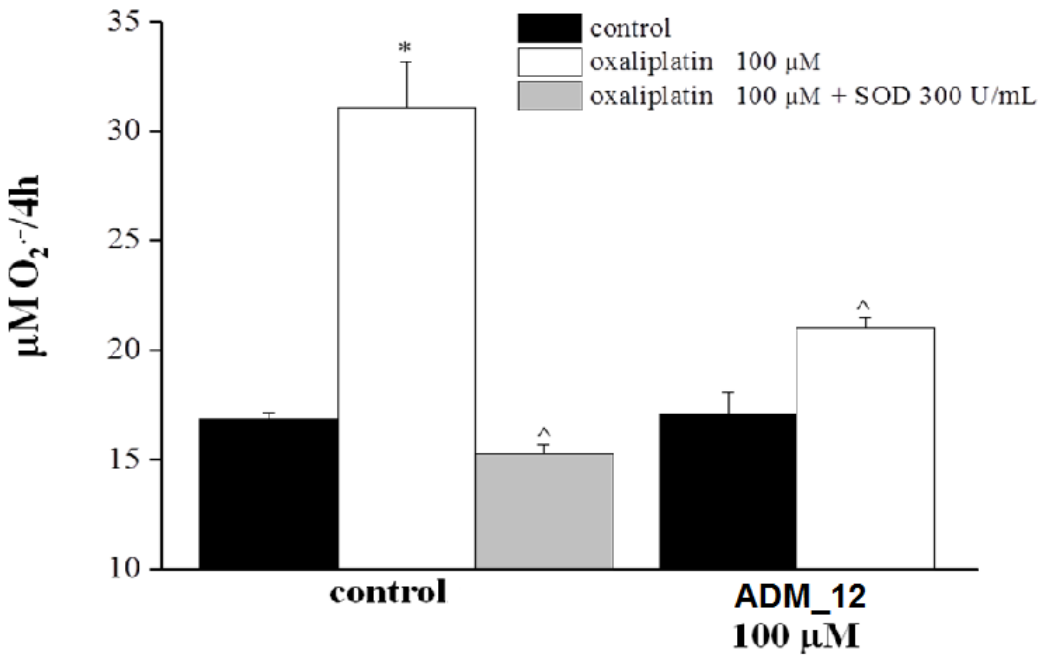

Figure 2. SOD – inhibitable superoxide anion levels in astrocyte cell lines. Astrocytes ($5*10^5$ cells/well, 3 control wells and 2 wells pre-treated with ADM_12) were exposed to 100 µM OXA for 4h. The effect of 100 µM ADM_12 co-incubation on SOD-inhibitable superoxide anion levels are depicted. The non specific absorbance measured in the presence of SOD was subtracted to the total value. Values are expressed as mean ± s. e. m. of 3 experiments. *P<0.01 vs control and ^P<0.01 vs OXA treatment.

Overall, these data indicate that ADM_09 and ADM_12 in particular, possess antioxidative properties that may be beneficial for the cisplatinum – induced oxidative stress. We found that these compounds do not change the biochemistry of cisplatin and its interaction with hSOD1. Previously published data (Nativi et al. 2013), suggest that ADM_09 and ADM_12 might be possible candidates in suppression of neuropathic pain induced also by cisplatinum. Antihyperalgesic properties of those compounds toward cisplatinum require confirmation by *in vivo* tests, which are in progress by now and are very promising. These findings might open a door toward a novel synergistic therapeutic strategies in amyotrophic lateral sclerosis (ALS), since the clinical use of cisplatin is still limited cause of the development of neurotoxicity and others undesirable effects.

Support materials:

Sample preparation:

Superoxide dismutase (SOD1) wt was overexpressed in the BL21 DE3 Origami plys *E. coli* strain. The fusion protein was obtained by growing the cells in minimal medium in shaking flasks at 37°C until OD_{600} reached 1 and then induced with 0.5 mM IPTG for 12 h at 25°C. Protein was isolated by sonication in 20 mM Tris-HCl, 100 mM NaCl, 5 mM imidazole buffer at pH 8 and centrifuged at 40 000 RPM for 20 min. Purification was performed by affinity chromatography using a nickel chelating (His-Trap) column and digestion with AcTEV protease. Final step of purification was gel filtration, which was performed using the preparative column Sephadex 75 HiLoad 26/60 to separate the cleaved tag-protein. Protein purity was checked on a 17% polyacrylamide gel, and concentration was determined by optical spectroscopy. Demetallated hSOD1 was obtained by dialysis against 10 mM EDTA in 50 mM sodium acetate pH 3.8. The chelating agent was removed by extensive dialysis against 100 mM NaCl in the same buffer and then against acetate buffer alone, gradually increasing the pH from 3.8 to 5.5.

Cis-diamminedichloroplatinum (II) (cisplatin) was purchased from Sigma-Aldrich.

Spectroscopic characterization:

Apo hSOD1 at 100 μM concentration (as dimer) was incubated alone, in the presence of cisplatinum and in the presence of cisplatinum together with small molecules (ADM_09 and ADM_12 at 1 mM concentration) at 37°C in 20mM phosphate buffer at pH 7.0. The protein:cisplatinum ratio was 1:8, the protein:cisplatinum:small molecules ratio were 1:8:10. To monitor the formation of oligomeric species fluorescence spectroscopy was used and described in Banci et al. 2007 and Banci et al. 2008. The solution fluorescence emission was measured, over time of incubation, with a Cary 50 Eclipse spectrophotometer supplied with a single-cell Peltier thermostated cell holder regulated at 37˚C. Fluorescence was followed with ThT, a dye that binds to extended β-sheets, which is typical structural feature of amyloids (Biancalana & Shohei 2010; Naiki et al.1989). Free ThT has excitation and emission maxima at 350 and 450 nm, respectively. However, upon binding to amyloid-oligomers, the excitation and emission wavelengths change to 450 and 485 nm, respectively. Fifty-four microliter aliquots of sample were added to 646 μl of a 215 μM Tht solution in a 20 mM phosphate buffer at pH 7.0. The background fluorescence spectrum of the buffer was subtracted. The

excitation wavelength was 446 nm (bandwidth, 10nm), and the emission was recorded at 480 nm (bandwidth, 10 nm). Fluorescence intensity at 483 nm was plotted against the time of incubation.

Synthesis of the N-hydroxysuccinimido ester of α-lipoic acid (Nativi et al. 2013):

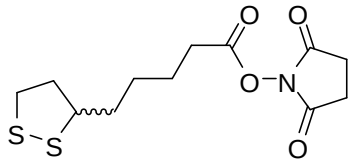

To a solution of lipoic acid (6.00 g, 29.1 mmol) and N-hydroxysuccinimide (4.02 g, 34.9 mmol) in THF (150 mL) was added dropwise at 0 C° and under vigorous stirring, a solution of dicyclohexylcarbodiimide (DCC) (7.20 g, 34.9 mmol) in THF (15 mL). The addition was completed in 15 min, after which the reaction mixture was allowed to warm to room temperature and stirred for 15 h. The precipitate obtained was filtered and the solution evaporated. The solid obtained by evaporation was suspended in ethyl acetate (100 mL) and the insoluble dicyclohexylurea was filtered off. Evaporation of the organic phase gave a yellow solid (9.03 g) that was treated with 80 mL of a mixture of hexane/ethyl acetate 1:1 to precipitate the N-hydroxysuccinimido ester of lipoic acid. The solid was collected by filtration (7.96 g, 90%) and was used in the next step without further purification.

Synthesis of (2S)- 2-(3-(5-(1,2-dithiolan-3-yl)pentanamido)propanamido)-3-(4H-imidazol-5-yl)-propanoic acid – [ADM_09] (Nativi et al. 2013):

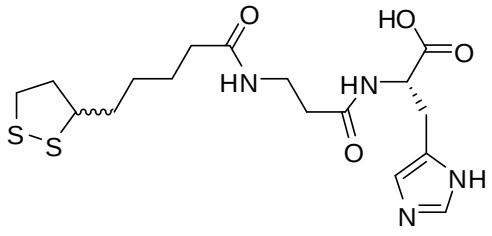

To a cooled (0 C°) and well stirred suspension of L-Carnosine (6.06 g, 26.8 mmol) and $NaHCO_3$ (2.25 g, 26.8 mmol) in DMF/H_2O 1:1 (100 mL) a solution of N-hydroxysuccinimido ester of lipoic acid (7.75 g, 25.5 mmol) in DMF (40 mL) was added dropwise in 30 min. The reaction mixture was allowed to warm to room temperature and stirred for 3 h. A TLC control

showed the complete consumption of the reagent and the reaction was stopped and the organic solvent evaporated. The yellow solid obtained was suspended in toluene (110 mL), filtered, and dried on a G3 gooch by suction. The crude (10.7 g) was purified through flash column chromatography on silica gel (CH_2Cl_2/EtOAc/MeOH 2:1:1, then MeOH/ EtOAc 2:1) to give (2*S*)-2-(3-(5-(1,2-dithiolan-3-yl)pentanamido)propanamido)-3-(4H-imidazol-5-yl)-propanoic acid (8.51g, 20.5 mmol, 81%) as a pale yellow solid.

In vitro tests:

Nitro Blue Tetrazolium (NBT) oxidation test.

Superoxide anion was generated as reaction product between ipoxanthine (600 mM) and xanthine oxidase (10 mU/ml). The oxidation kynetic of nitro blue tetrazolium (NBT, 10 mM) was spectrophotometrically measured at 560 nm in the absence or in the presence of ADM_09 and ADM_12 (0-1000 μM). Value are expressed as absorbance arbitrary units (A.U.) and the basal value of NBT oxidation was normalized to 100 U.A. (Ciuffi et al. 1998)

Cell cultures.

Primary cultures of astrocytes were obtained according to the method described by McCarthy e De Vellis (Bennett & Xie, 1988). Briefly, the cerebral cortex of newborn (P1-P3) Sprague Dawley rats (Harlan, Italy) were dissociated in Hanks' balanced salt solution (HBSS) containing 0.5% trypsin/EDTA and 1% DNAse (Sigma, Germany) for 30 minutes at 37° C. The suspension was mechanical homogenized and filtered. Cells were plated in DMEM high glucose with 20% FBS. Confluent primary glial cultures were used to isolate astrocytes removing microglia and oligodendrocytes by shaking. The purity of astrocyte cultures were determined immunocytochemically by staining for GFAP (Dako, Denmark). Cells were fixed in 4% paraformaldehyde, then incubated with the antibody (1:200) and visualized using Alexafluor conjugated secondary antibody. Nuclei were stained with 4,6-diamidino-2-phenylindole dihydrochloride (DAPI). GFAP-p ositive cells were 95-98% in astrocyte cultures. Experiments were performed 21 days after cell isolation.

SOD-inhibitable superoxide anion (O_2^-) production evaluated by cytochrome C assay.

Astrocytes were plated in 6-well plates ($5 \cdot 10^5$/well) and grown in until confluence. Cells were then incubated with or without 100 μM oxaliplatin in serum-free DMEM

containing cytochrome C (1 mg/mL) for 4 hours at 37 °C, in the absence or presence of 10 μM ADM_12. Non-specific cytochrome C reduction was evaluated carrying out tests in the presence of bovine superoxide dismutase (SOD; 300 mU/mL). The supernatants were collected, and the optical density was spectrophotometrically measured at 550 nm. After subtracting the non-specific absorbance, the SOD-inhibitable O_2^- amount was calculated by using an extinction coefficient of $2.1 \cdot 10^4\ M^{-1}cm^{-1}$ and expressed as μM/mg proteins/4 hours. The 4 hour incubation interval was chosen on the basis of preliminary experiments which showed poor reliability for longer cytochrome C exposure to the cellular environment.

References:

Banci, L. I. Bertini, A. Durazo, S. Girotto, E.Butler Gralla, M. Martinelli, J. Selverstone Valentine, M. Vieru, J. P. Whitelegge, 2007. *Biophysics.* 104(27):11263-7.

Banci L., Bertini I., Boca M., Girotto S., Martinelli M., Valentine J. S., Vieru M. 2008. *PLoS One.* 3(2):e1677.

Banci L., Bertini I., Boca M., Calderone V., Cantini F., Girotto S., Vieru M. 2009. *Proc Natl Acad Sci U S A.* 28 ;106(17).

Banci L., Bertini I., Blaževitš O., Calderone V., Cantini F., Mao J., Trapananti A., Vieru M., Amori I. Cozzolino M., Carrì M. T. 2012. *J Am Chem Soc.* 25;134(16):7009-14.

Bennett G. J., Xie Y. K. A. 1988. *Pain* 33:87-107.

Bertini I., Mangani S., Viezzoli M. S., 1998. *Academic Press*, pp 127-250.

Biancalana M. and Shohei Koide S. 2010. *Biochim Biophys Acta*.1804(7):1405-12.

Brozovic A., Ambriović-Ristov A., Osmak M. 2010. *Crit Rev Toxicol.* 40(4):347-59.

Bruijn L. I., Becher M. W., Lee M. K., Anderson K. L., Jenkins N. A., Copeland N. G., Sisodia S. S., Rothstein J. D., Borchelt D. R., Price D. L., Cleveland D.W. 1997. *Neuron.* 18(2):327-38.

Bruijn L. I., Miller T. M., Cleveland D. W. 2004. *Annu Rev Neurosci.* 27:723-49.

Casares C., Ramírez-Camacho R., Trinidad A., Roldán A., Jorge E., García-Berrocal J. R. 2012. *Eur Arch Otorhinolaryngol.* 269(12):2455-9.

Ciuffi M. et al. 1998. *Pharmacol Res.* 38:279–287.

Cozzolino, M.; Amori, I.; Pesaresi, M. G.; Ferri, A.; Nencini, M.; Carri, M. T., 2008. *J Biol Chem*, 283 (2), 866-74.

Ferri, A.; Cozzolino, M.; Crosio, C.; Nencini, M.; Casciati, A.; Gralla, E. B.; Rotilio, G.; Valentine, J. S.; Carri, M. T., 2006. *Proc Natl Acad Sci U S A*,103 (37),13860-5.

Fridovich I. 1978. *Science*, 201: 875-879.

Furukawa Y., Kaneko K., Yamanaka K., O'Halloran T. V., Nukina N. 2008. *J Biol Chem*.; 283(35):24167-76.

Hipkiss, A. R. 2009. *Adv. Food Nutr. Res*.57, 87–154.

Johnston J. A., Dalton M. J., Gurney M. E., Kopito R. R. 2000. *Proc Natl Acad Sci* USA. 97(23):12571-6.

Jonsson P. A., Ernhill K., Andersen P. M., Bergemalm D., Brännström T., Gredal O., Nilsson P., Marklund S. L. 2004. *Brain.*127(Pt 1):73-88.

Karashima Y. *et al.* 2009. *Proc. Natl. Acad. Sci USA*. 106, 1273–1278.

Karch, C. M.; Borchelt, D. R., 2008. *J Biol Chem,* 283 (20), 13528- 37.

Kelland L. 2007. *Nat Rev Cancer*. 7(8):573-84.

Lindberg M. J., Tibell L., Oliveberg M. 2002. *Proc. Natl. Acad. Sci. USA*. 99 (26), 16607-16612.

Marullo R., Werner E., Degtyareva N., Moore B., Altavilla G., Ramalingam S. S., Doetsch P. W. 2013. *PLoS One.* 8(11):e81162.

Mulligan V.K., Chakrabartty A. 2013. *Proteins.* (8):1285-303.

Naiki H., Higuchi K., Hosokawa M., Takeda T. 1989. *Anal Biochem.* 177(2):244-9.

Nassini R. *et al.* 2011. *Pain.* 152, 1621–1631.

Nativi C., Gualdani R., Dragoni E., Di Cesare Mannelli L., Sostegni S., Norcini M., Gabrielli G., la Marca G., Richichi B., Francesconi O., Moncelli M. R., Ghelardini C., Roelens S. 2013. *Sci Rep.*3:2005.

Nilius B., Appendino G. & Owsianik G. 2012. *Pflugers Arch –Eur J Physiol*. 464, 425–458.

Okado-Matsumoto A., Fridovich I. 2001. *J Biol Chem.* ,276(42):38388-93.

Oztug Durer Z. A., Cohlberg J. A., Dinh P., Padua S., Ehrenclou K., Downes S., Tan J. K., Nakano Y., Bowman C. J., Hoskins J. L., Kwon C., Mason A. Z., Rodriguez J. A., Doucette P. A., Shaw B. F., Valentine J. S. 2009. *PLoS One.* 4(3):e5004.

Parcker, L., Witt, E. H. & Tritschler, H. J. 1995. *Free Radical Biol. Med*. 19, 227–250.

Prudencio, M.; Lelie, H.; Brown, H. H.; Whitelegge, J. P.; Valentine, J. S.; Borchelt, D. R., 2012. J Neurochem, 121 (3), 475-85.

Ross C. A., Poirier M. A. 2004. *Nat Med.* 10 Suppl:S10-7.

Sheng Y., Chattopadhyay M., Whitelegge J., Valentine J. S. 2012. *Current Topics in Medicinal Chemistry*, Vol. 12, No. 22.

Shibata N., Hirano A., Kobayashi M., Siddique T., Deng H. X., Hung W. Y., Kato T., Asayama K. 1996. *J Neuropathol Exp Neurol.* 55(4):481-90.

Sturtz L. A., Diekert K., Jensen L. T., Lill R., Culotta V. C. 2001. *J Biol Chem*. 276(41):38084-9.

Valentine J. S., Doucette P. A., Zittin Potter S. 2005. *Annu Rev Biochem*. 74:563-93.

Wang J., Xu G., Borchelt D.R. 2002. *Neurobiol. Dis.* 9, 139-148.

Wang, D., Lippard, S. J. 2005. *Nat. Rev. Drug Discov*. 4, 307-320.

Watanabe M., Dykes-Hoberg M., Culotta V. C., Price D. L., Wong P. C., Rothstein J. D. 2001. *Neurobiol Dis.* 8(6):933-41.

Chapter 13

"Beta amyloid hallmarks: from intrinsically disordered proteins to Alzheimer's disease.

A brief review."

Magdalena Korsak [a,b], Tatiana Kozyreva [b]

[a]Magnetic resonance Center (CERM), University of Florence, Via L. Sacconi 6, 50019 Sesto Fiorentino, Italy

[b]Giotto Biotech, Via Madonna del Piano 6, 50019 Sesto Fiorentino, Italy

(Book chapter as a part of *"Intrinsically disordered protein by NMR"* book, Springer 2014)

(In preparation)

Chapter 13
Beta amyloid hallmarks: from intrinsically disordered proteins to Alzheimer's disease. A brief review.

From the clinical basis of neurodegeneration to the molecular level of Alzheimer's disease.
A history of the discovery of beta amyloid protein and its proteolytic biogenesis.

Polymorphism widely observed for Aβ amyloidal aggregates in vitro.

Overview of functional polymorphism and structural models of amyloidal fibrils.

Review of the methods for immobilizing and investigating amyloidal intermediate species.

Association between neurotoxicity and different ratios of Aβ40 to Aβ42.

Conclusions.

Short summary of expression and purification procedures for the preparation of Aβ peptides.

References.

Beta amyloid hallmarks: from intrinsically disordered proteins to Alzheimer's disease.

A brief review.

From the clinical basis of neurodegeneration to the molecular level of Alzheimer's disease. A history of the discovery of beta amyloid protein and its proteolytic biogenesis.

"You have to begin to lose your memory, if only in bits and pieces, to realize that memory is what makes our lives. Life without memory is no life at all, just as an intelligence without the possibility of expression is not really an intelligence. Our memory is our coherence, our reason, our feeling, even our action. Without it, we are nothing."

Luis Bunuel

Over 600 disorders afflict the nervous system (European Commission website 2014). Neurodegenerative diseases are defined as hereditary and sporadic conditions that are characterized by progressive nervous system dysfunction. These disorders are often associated with atrophy of the affected central or peripheral structures of the nervous system. They include diseases such as Alzheimer's disease (AD) and other dementias, brain cancer, degenerative nerve diseases, encephalitis, epilepsy, genetic brain disorders, head and brain malformations, hydrocephalus, stroke, Parkinson's disease, multiple sclerosis, amyotrophic lateral sclerosis (ALS or Lou Gehrig's Disease), Huntington's disease, and prion diseases.

Neuroscientific research has enjoyed rapid progress fuelled by technologically sophisticated, multidisciplinary approaches. If we consider the vast amount of literature published on the subject of neurodegeneration just in the last years, we could notice a substantial progress in

understanding the molecular basis of these terrifying diseases, but what we know is still a drop in the bucket, and the main question remains: what causes neurodegeneration and how can we cope with it?

In this short review we illustrate the emerging trend of defining several human neurodegenerative disorders as syndromes of protein folding and oligomerization through the example of AD. AD is recognized as a major public health problem in developed countries, and knowledge of its causes and mechanisms has grown enormously in the past decade. This insidious and devastating brain degeneration that robs its victims of their memory, reasoning, abstraction, and language abilities affects one in four individuals over 85 years of age. According to the World Alzheimer Report, the disease is expected to affect 115.4 million people by the year 2050 (Alzheimer's Disease International website 2014). From an economic point of view, AD is one of the most expensive diseases because it usually spans many years and patients require intense daily care.

Symptoms associated with the illness include cognitive dysfunction and neuronal death in the brain, both of which are indicative of a significant progressive neurodegenerative disease (Walsh and Selkoe, 2004). No effective treatments for AD are currently available and not even its pathogenesis is fully understood. The current limited number of treatments for Alzheimer's disease merely address symptoms rather than the root cause. The so-called "amyloid hypothesis" has come to dominate explanations for the damage that occurs to the brain. The presence of amyloid plaques and congophilic angiopathy in the brain cortex and hippocampus is considered to be a major pathological feature of AD (Evin and Weidemann, 2002). Almost nine decades passed from the moment when Alois Alzheimer peered through a microscope at the brain of his first patient and prophetically wrote, "scattered through the entire cortex … one found miliary foci that were caused by the deposition of a peculiar substance …" (Selkoe D. J. 1994) and when neuroscientists isolated and chemically

characterized the nature of the amyloid material found in the senile plaque, revealing the Aβ protein (Glenner and Wong, 1984; Masters et al. 1985) and its precursor APP (amyloid precursor protein) (Kang et al. 1987; Evin and Weidemann, 2002). They observed that amyloid peptides constitute ~90% of the plaque material (Glenner and Wong, 1984; Masters et al. 1985; Kang et al. 1987), while the remaining 10% of amyloid plaques are composed of proteins from the apolipoprotein E class, lipids from membranes of degenerated portions of the intercommunicated nerve extensions called axons, metal ions such as Cu, Zn, Fe and Al, and traces of other components from the extracellular liquid. Transmission electron microscopy of amyloid plaques revealed numerous unbranched filaments, representing amyloid fibrils, surrounded by amorphous aggregates of diffuse amyloid. Amyloid plaques fall into two broad morphological categories: diffuse and neuritic. Both plaque types are detectable with anti-Aβ antibodies, but only neuritic plaques are prominently stained by sheet-binding dyes such as Congo red and thioflavin S. Neuritic dystrophies are swollen and distorted processes of axonal or dendritic origin that radiate from the core of a neuritic plaque. They are detectable with antibodies against APP, phospho-tau, neurofilaments and ubiquitin, indicating a disruption of protein transport and attempts to degrade this blockage (Dickson et al. 1999). Progressive neuritic plaque deposition is a hallmark of AD. Neuritic plaque formation commonly begins in the neocortex and later affects the hippocampus and amygdala. By the end stage of the disease, neuritic plaques are present in the brainstem and other subcortical structures (Thal et al. 2002). It has been suggested that the presence and a substantial increase in diffuse plaque is associated with the preclinical stages of AD (Knopman et al. 2003; Vlassenko et al. 2011). The surprising and totally unexpected observation that Aβ is produced constantly throughout life as a physiologically normal metabolite generated in healthy people changed the common concept of AD (Hardy and Selkoe, 2002). Plaques have also been found in cognitively normal individuals, and plaque

burden does not correlate with memory decline. Moreover, successful removal of amyloid plaques by immunotherapy fails to improve cognition (Haass, 2010). Additionally, Dobson and co-workers have shown that virtually any protein can be induced into forming amyloid, suggesting that amyloid is a primordial, highly stable polypeptide form that had to be overcome by evolution in order to create functional globular proteins (Dobson, 2003). Soluble Aβ oligomers are now believed to act as neurotoxic entities rather than amyloid plaques.

It appears that the soluble Aβ monomers require conversion to a largely β-pleated sheet conformation and subsequent aggregation before they can confer neurotoxicity *in vitro* (Lorenzo et al. 1994; Howlett et al. 1995). The production of the toxic species – soluble Aβ oligomers – and their subsequent ability to cause neuronal injury depends on the precision of an intramembranous proteolytic cleavage of APP (Haass and Selkoe 2007). Proteolytic processing of APP protein involves three types of proteases.

APP is a member of an evolutionarily conserved gene family with two mammalian homologs, amyloid precursor-like proteins (APLP) 1 and 2 (Wasco et al. 1992, 1993). These proteins contain highly similar sequences in their ectodomains and intracellular carboxy-termini, but the transmembrane region comprising the Aβ peptide is unique to APP (Bayer et al. 1999). Although its primary physiological function remains unclear, APP has been implicated in a variety of processes such as intracellular signalling, synapse adhesion, trophic support, axon remodelling and apoptosis (Zheng and Koo, 2011).

APP is ubiquitously expressed. There are three major APP isoforms resulting from alternative splicing of its 18 exon gene: APP695, APP751 and APP770 (Yoshikai et al. 1990). APP751 and APP770 are the main transcripts found in non-neuronal tissue. APP695 is the most abundant isoform in the brain, where its expression is primarily limited to neurons. Brain region-specific variation in APP695 expression occurs in both mouse and human, with the highest transcript levels found in the cortex, hippocampus and cerebellum (Sola et al. 1993).

APP is processed via two major pathways that utilize different enzymes and result in distinct cleavage products. The non-amyloidogenic pathway precludes the formation of Aβ due to constitutive α-secretase-mediated cleavage in the middle of the Aβ domain (Esch et al. 1990). It was initially proposed that a zinc-dependent, transmembrane protease served as α-secretase (Roberts et al. 1994). Three members of the A disintegrin and metalloproteinase (ADAM) family were later found to possess α-secretase activity: ADAM-10, ADAM-17, and ADAM-9 (Lammich et al. 1999). More recent evidence, however, suggests that ADAM-10 serves as the primary α-secretase in neurons (Kuhn et al. 2010). Alpha-cleavage of APP occurs mainly at the plasma membrane, releasing a soluble α-APP fragment (sAPP α) into the lumen/extracellular space and creating a membrane-bound, 83-residue C-terminal fragment (C83) (Sisodia, 1992). Subsequent intramembranous cleavage of C83 by γ-secretase liberates a soluble, 3 kDa fragment (p3) and the APP intracellular domain (AICD) (Zheng and Koo, 2011). The p3 fragment is rapidly degraded, while AICD may act as a transcriptional regulator (Haass et al. 2007).

The amyloidogenic processing of APP primarily occurs in the endocytic pathway. β-secretase initiates the sequence of amyloidogenic cleavage events. Cleavage of APP at the β-site generates a soluble amino-terminal fragment (sAPP β) and a membrane-associated, 99-residue C-terminal fragment (C99). γ-secretase then performs a stepwise, intramembrane cleavage of the C99 fragment, liberating Aβ and AICD. Aβ peptides range from 37 to 43 amino acids in length; however, under physiological conditions, the majority of Aβ produced is 40 amino acids long (Aβ40). The 42 amino acid variant (Aβ42) normally only comprises a minor fraction of the total Aβ. Nevertheless Aβ42 has a more hydrophobic nature, and its aggregative ability and neurotoxicity are therefore much greater than those of Aβ40; both of these forms (Aβ40 and Aβ42) are therefore targets of intense study (Haass et al. 2010). β-site cleaving enzyme 1 (BACE1) was identified as the enzyme responsible for APP β–cleavage.

BACE1 is a type 1 membrane-bound aspartyl protease with its active site facing the lumen. It is capable of cleaving APP at two positions: the aspartate at position 1 of the Aβ sequence or the glutamate at position 11. BACE1 is found in a variety of tissues, but is predominantly expressed in neurons (Sinha et al. 1999). Intracellularly, BACE1 mainly localizes to the trans-Golgi network and endosomes. However, BACE1 is also trafficked between the Golgi and the plasma membrane, where it is enriched in lipid rafts. From the plasma membrane, BACE1 is internalized and sorted into endosomes or recycled to the trans-Golgi network (Walter et al. 2001). It serves as the primary β-secretase and is the rate-limiting enzyme in Aβ production. There are currently four known components of γ-secretase: presenilin (PS1 or PS2), nicastrin, anterior pharynx defective 1 (APH1) and presenilin enhancer 2 (PEN-2). These proteins assemble into the γ–secretase complex while cycling through the endoplasmic reticulum/Golgi (Edbauer et al. 2003). Once mature, γ-secretase is primarily found at the plasma membrane and in the endosomal/lysosomal system. Although PS, nicastrin, APH1 and PEN-2 are all required for γ-secretase activity, PS contains the catalytic active site needed for γ-cleavage of APP (Edbauer et al. 2003).

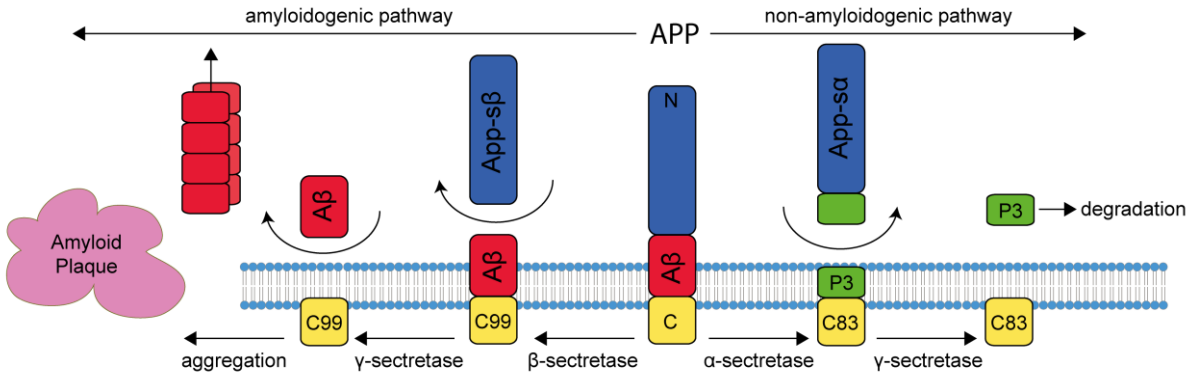

Figure 13.1. APP metabolism by the secretase enzymes (Barrantes et al. 2010).

Polymorphism widely observed for Aβ amyloidal aggregates in vitro.

Aβ molecules can spontaneously self-aggregate *in vitro* into different species (Jan et al. 2010) under distinct conditions. Aβ peptides can form soluble oligomers and protofibrils, which could be intermediates of a fibrillation process (Fig. 13.2) (Benilova et al. 2012). Studies have revealed the high neurotoxicity of these species and their close links with AD (Benilova et al. 2012; Chimon et al. 2007; Hoshi et al. 2003; Krafft and Klein, 2010; Kirkitadze et al. 2002; Lambert et al. 1998; Lesne´ et al. 2006; Noguchi et al. 2009; Selkoe, 2008). Instead, the formation of amyloidal deposits consisting of Aβ fibrils is a pathological hallmark of AD. Although mature amyloid fibrils are sometimes described as being predominantly neutral (Aksenov et al. 1996), there is evidence in some recent reports that Aβ fibrils are also neurotoxic and that the progression of AD symptoms is correlated with the amount of these insoluble Aβ assemblies (Chimon et al. 2007; Lorenzo et al. 1994; Meyer-Luehmann et al. 2008; Petkova et al. 2005; Qiang et al. 2012; Selkoe et al. 2004; Walsh et al. 1999).

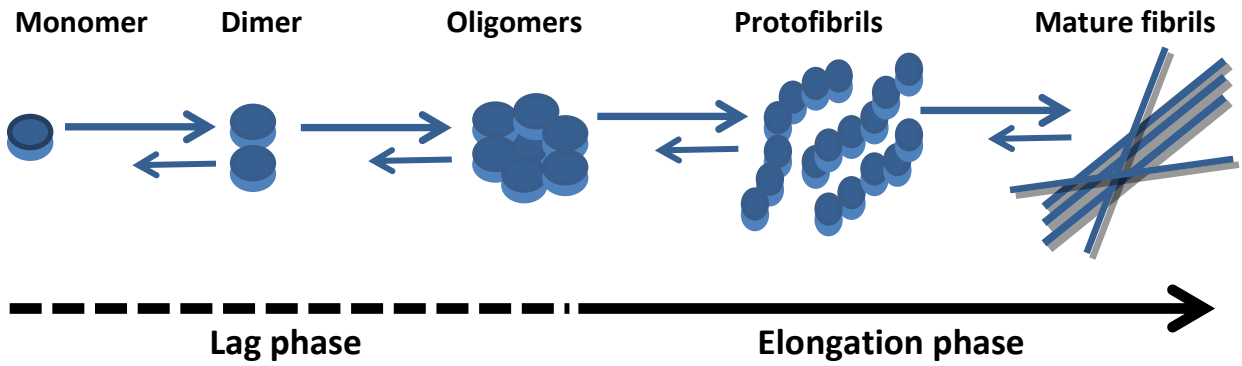

Figure 13.2. A putative schematic of aggregation of Aβ with two kinetic phases. In the lag phase, monomers slowly form oligomers (dashed lines). In the elongation phase, oligomers promote fibril formation via protofibrils (straight line) (Kumar et al. 2011).

Besides the different types of aggregates, the morphology of the same type of Aβ assemblies can also vary significantly depending on different aggregation conditions. This phenomenon is typically called polymorphism and has also been found in samples derived from AD patient brain tissues (Paravastu et al. 2009; Lu et al. 2013). Furthermore, it has been shown that different morphologies of Aβ fibrils can cause changes in neurotoxicity (Petkova et al. 2005).

Overview of functional polymorphism and structural models of amyloidal fibrils.

The polymorphism of Aβ fibrils has been determined *in vitro* by numerous different structural studies such as cryo-electron microscopy (cryo-EM) (Fändrich et al. 2011; Meinhardt et al. 2009), which revealed a large spectrum of Aβ40 fibril polymorphisms, and solid-state nuclear magnetic resonance (SSNMR) (Benzinger et al. 1998; Bertini et al. 2011; Lansbury et al. 1995; Paravastu et al. 2008; Petkova et al. 2002, 2005, 2006; Qiang et al. 2011) in particular.

SSNMR is one of the best techniques for obtaining atomic resolution structures of amyloid fibrils sufficient for the development of full molecular models (Tycko, 2010; Wasmer et al. 2008), as X-ray crystallography is limited to small amyloidogenic peptides and cryo-EM is hindered by its relatively low spatial resolution. SSNMR has allowed for substantial advancement in understanding the structure of amyloid fibrils. Dipole-dipole couplings and chemical shift anisotropies are not averaged due to the absence of isotropic tumbling in solid-state samples. As a result, linewidths in SSNMR spectra are broadened relative to solution-state NMR, resulting in lower resolution. On the other hand, the absence of tumbling enables the study of the effects of anisotropic or orientation-dependent interactions. Cross polarization (CP), high-power proton decoupling, and magic-angle spinning (MAS) are used as standard techniques to obtain high-resolution SSNMR spectra. The isotropic chemical shift values obtained from CP-MAS experiments can be used to determine site-specific secondary structures. In fibrillar samples, CP-MAS is useful for observing rigid fibrillar parts, while

dipolar-dephasing MAS is used to detect soluble components of mobile parts (Naito et al. 2004). Rational resonance is used for determining homonuclear-internuclear distances, and rational echo double resonance (REDOR) is used to determine heteronuclear-internuclear distances (Tycko and Ishii, 2003). Other techniques, such as radiofrequency-driven recoupling and dipolar-assisted rational resonance, are useful for obtaining folding information on amyloid fibrils (Balbach et al. 2002).

The only restriction of high-resolution studies of Aβ assemblies by SSNMR is the requirement for highly ordered and homogeneous samples. However, in amyloid systems it is rather common that several differently shaped aggregates coexist in a mixture, making preparation of the samples very difficult. This limitation can be overcome by programmed isotopic labelling schemes or sequence truncation, but each of these methods hampers complete structural analysis by SSNMR. Another strategy to overcome this restraint is the so-called seeding procedure, which leads not only to an improvement in the homogeneity of Aβ fibrils, but also permits insights into the molecular structures of amyloid fibrils developing in human tissue. This tactic is feasible after reconstruction of isotope enriched *in vivo* fibrils using brain tissues as seeds from patients with AD (Paravastu et al. 2009). This approach is made possible by the fact that *in vitro* studies have shown that the seeding procedure allows fibrils to be obtained that exactly retain the same molecular structures, corresponding to the seeds from the brain of patients with AD (Paravastu et al. 2008; Petkova et al. 2005). This strategy also has many drawbacks because the sample obtained in this way might contain significant contamination from many tissue components such as lipids. However, it allows the restoration of pathological samples from AD patients and the obtainment of high-resolution structural characterizations of these assemblies.

As heterogeneity also depends heavily upon different aggregation conditions, several different factors must be taken into consideration. One important key factor is the purity of the starting

materials. The presence of pre-existing aggregates can result in a lack of reproducibility, as well as in changes of kinetics, fibrillogenesis processes, and neurotoxic activity (Fezoui et al. 2000). Several different protocols have been developed in order to solve this issue, resulting in standardized aggregate-free Aβ peptide samples (Broersen et al. 2011, Jao et al. 1997, Fezoui et al. 2000). Disaggregation of the Aβ assemblies involved the use of the structure-breaking organic solvents hexafluoroisopropanol (HFIP) and dimethyl sulfoxide (DMSO), trifluoroacetic acid (TFA) pre-treatment, and pre-dissolution of the peptide in a dilute base solution (e.g. NaOH). Each of these approaches allows aggregate-free material to be obtained. Another significant aspect is represented by the conditions of the fibrillation protocols such as concentration, pH, ionic strength, and temperature. The incubation of the sample in quiescent conditions leads to fibrils with the "twisted pairs" morphology (Paravastu et al. 2008), while gentle agitation results in striated ribbons (Petkova et al. 2006) or "flat" striated bundles (Bertini et al. 2011). The appropriate selection of the fibrillation strategy is essential for obtaining high quality samples for high resolution SSNMR.

Aβ40 amyloid fibrils have been widely investigated and several structural models have recently been proposed using SSNMR (Bertini et al. 2011; Paravastu et al. 2008; Petkova et al. 2002, 2006), A structural model of Aβ42 fibrils was proposed based on solution NMR and mutagenesis (Lührs et al. 2005).

In all these fibrillar assemblies Aβ molecules are densely packed in extended β-sheets (ladders) but exhibit polydispersed morphology and differ from one another in length and bundle width. Mature fibrils are characterized by a specific filamentous structure and usually contain 2–6 protofilaments that are more than 1 μm long and 8–12 nm in diameter. They display a cross-β X-ray fibre diffraction pattern as well as stainability with Congo red, resulting in green birefringence; they also bind Thioflavin-T (Merz et al. 1983; Petkova et al. 2005; Serpell, 2000). It is widely accepted that amyloid fibrils are insoluble deposits, but

recent studies have shown that many biochemical factors, e.g. biological lipids, are able to efficiently revert the fibrillation process and convert these insoluble assemblies into soluble, highly toxic intermediate species that retain the same biochemical and biophysical properties (Martins et al. 2008).

The distinct polymorphism of fibrillar assemblies is reflected in variations in overall structural symmetry and differences in specific aspects of structural elements and various residue sites, as well as in the nature of β-sheet structures including topologies of the β1-turn-β2 motif and inter-protofilament contacts (Ahmed et al. 2010; Bertini et al. 2011; Lührs et al. 2005; Paravastu et al. 2008; Petkova et al. 2006) (Fig. 13.3). Recent studies have also shown that, in Aβ fibrils carrying mutants, both parallel and anti-parallel registry can occur (Qiang et al. 2011).

Although the structural polymorphism of Aβ40 fibrils was initially described as taking place mainly at the supramolecular level (Paravastu et al. 2008), a recent structural model of mature Aβ fibrils (Bertini et al. 2011) suggests that polymorphism can already originate at the level of the zipper of the β1-turn-β2 motif, the inter-protofilament interface and the N-terminal conformation. The N-terminal part of the peptide in the fibril model can adapted β_N-strand, but there is also evidence in the literature that a disordered conformation on the N-terminal part in some other Aβ fibrils is also possible (Paravastu et al. 2008; Petkova et al. 2006; Sachse et al. 2008, 2010). It can therefore be concluded that the N-terminal part of Aβ40 peptides can adopt distinct conformations and thereby also contribute to structural diversity.

It is reasonable to speculate that the folding of the monomer and supramolecular packing (within and among protofilaments) are linked or even define the morphology of amyloid fibrils through structural duplication/propagation along the fibril axis similar to the growth of 1D nanomaterials (Bertini et al. 2011).

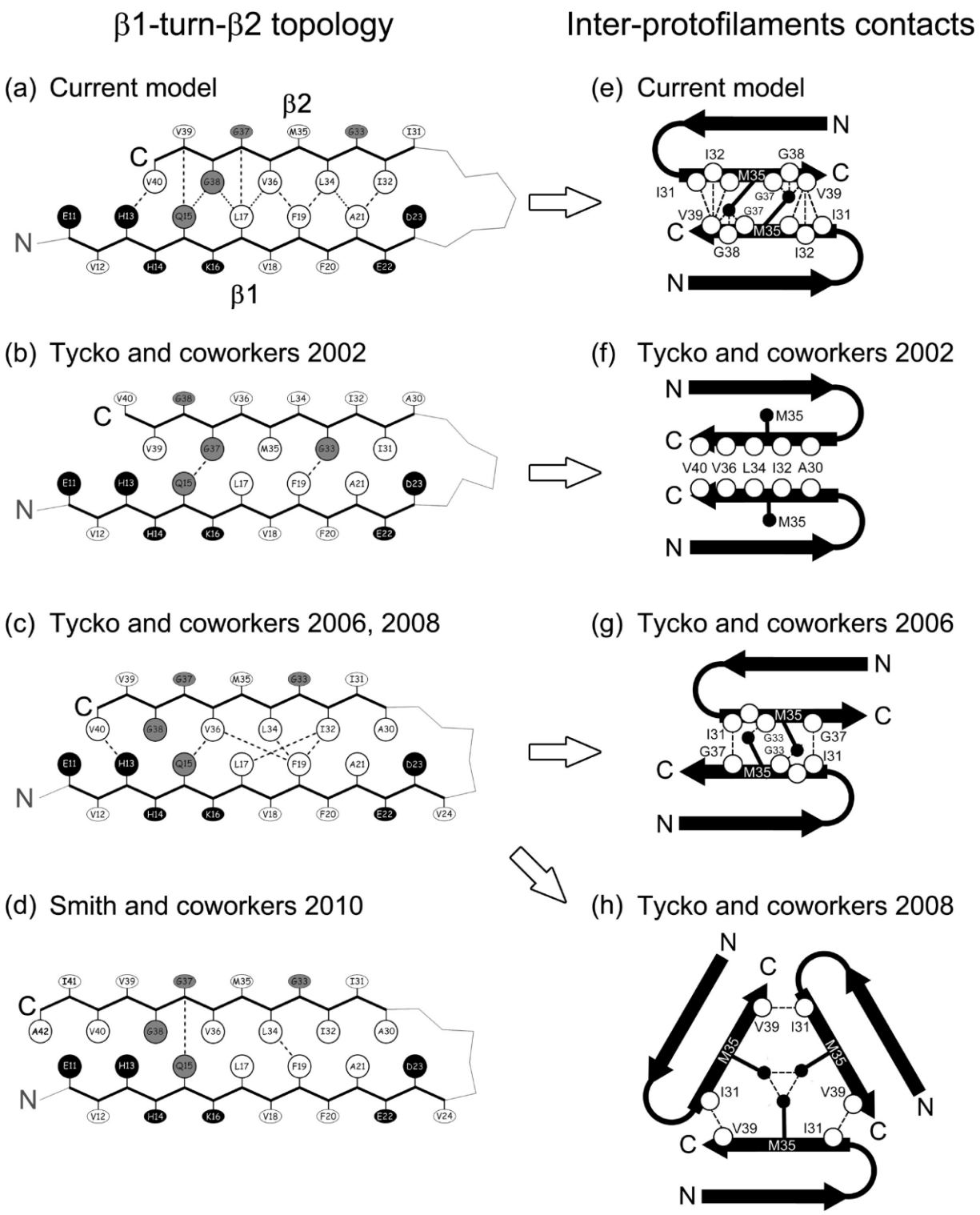

Figure 13.3. Different topologies of β1-turn-β2 motif (left column) and inter-protofilament contacts (right column) in various SSNMR-derived structural models of Aβ fibrils ((a) Bertini et al. 2011; (b) Petkova et al. 2002; (c) Petkova et al. 2006; Paravastu et al. 2008; (d) Ahmed et al. 2010)). Adapted from (Bertini et al. 2011).

Review of the methods for immobilizing and investigating amyloidal intermediate species

Since various studies had reported that the neurotoxicity of Aβ peptides might be ascribed to pre-fibrillar assemblies (i.e. not necessarily fibrils (Benilova et al. 2012; Chimon et al. 2007; Hoshi et al. 2003; Kirkitadze et al, 2002; Krafft and Klein, 2010; Lambert et al. 1998; Lesne´ et al. 2006; Noguchi et al. 2009; Selkoe, 2008)), the high-resolution structural characterisation of these soluble species has become an overarching objective for understanding Aβ aggregation pathways and the complex molecular mechanism of AD (Benilova et al. 2012).

Several *in vitro* SSNMR studies established an initial high-resolution insight into certain non-fibrillar (Ahmed et al. 2010; Chimon et al. 2005, 2007; Lopez del Amo et al. 2012) and protofibrillar (Qiang et al. 2012; Scheidt et al. 2011) Aβ aggregates. Several other experimental and theoretical methods have also been used to obtain residue-specific information on prefibrillar Aβ aggregates and on structural persistence in the monomer (Bernstein et al. 2009; Bertini et al. 2013; Danielsson et al. 2006; Fändrich et al. 2012; Fawzi et al. 2011; Gallion 2012; Haupt et al. 2012; Kheterpal et al. 2006; Pan et al. 2011).

These prefibrillar intermediate assemblies, e.g. oligomers, protofibrils, and Aβ-derived diffusible ligands (ADDLs), as well as Aβ annular assemblies, are likely involved in amyloid fibril formation. All of these assemblies are rich in β-sheet structure and bind Congo red and Thioflavin-T, although more weakly than mature fibrils (Jan et al. 2010).

However, an investigation of these prefibrillar deposits faces many obstacles. As they are often thermally unstable compared to mature fibrils, many different methods to immobilize and study these species have been developed in recent years and each strategy has its own advantages and disadvantages.

Pioneering work in this direction has been performed by the groups of Smith and Ishii (Ahmed et al. 2010; Chimon et al. 2005, 2007), who focused on the Aβ oligomeric form. Taking advantage of the fact that various proteins including Aβ retain their structures after lyophilisation (Benzinger et al. 1998; Petkova et al. 2002; Studelska et al. 1997), many groups trap the thermally labile intermediate by freeze-trapping and subsequent lyophilisation. Different methods of trapping oligomeric and protofibrillar Aβ species were used such as filtration through low molecular weight cut off filters (Bitan et al. 2005), photo-induced crosslinking of unmodified proteins (Bitan et al. 2003), organic solvents (Haupt et al. 2012), density gradient centrifugation (Ward et al. 2000), size exclusion chromatography (SEC) (Bitan et al. 2003; Hartley et al. 1999; Jan et al. 2010; Walsh et al. 1997) and interaction partners (Bieschke et al. 2012; Lopez del Amo et al. 2012; Scheidt et al. 2011).

A method termed sedimented solute NMR (sedNMR) has recently been developed and allows Aβ aggregates to be collected and trapped in a fully hydrated environment without adding cosolvents or interaction partners, therefore providing a unique way to access the formation kinetics and structural features of these species with reduced perturbations (Bertini et al. 2013).

In this method, solid-state NMR (SSNMR) experiments are used to observe proteins that are sedimented from solution using an ultracentrifugal field (Bertini et al. 2011, 2012, 2012, 2013; Gardiennet et al. 2012; Polenova 2011; Ravera et al. 2013). The application of SSNMR is possible, as it has been reported (Ahmed et al. 2010; Bernstein et al. 2009; Fawzi et al. 2011; Kirkitadze et al. 2002; Lee et al. 2011) that Aβ peptides in aqueous solutions spontaneously form soluble aggregates of high molecular weight (50–200 kDa) that are large enough to sediment and thus become visible by SSNMR.

Sedimented solute NMR relies on the fact that sedimented macromolecules may be rotationally impaired by self-crowding, thus giving rise to solid-state NMR spectra. The

sedimentation of macromolecules into this type of solid-like phase can be achieved in two different ways. One way is direct *in situ* sedimentation by magic angle spinning (MAS) of the NMR rotor (MAS-induced sedimentation), which acts as an ultracentrifuge (Bertini et al. 2011) (Fig. 13.4A). *In situ* SedNMR can be used to address the kinetics of formation of soluble Aβ assemblies by simultaneously monitoring the disappearance of the monomer and the appearance of the oligomers. Another method is *ex situ* sedimentation by common ultracentrifuge (UC-induced sedimentation) (Bertini et al. 2012; Gardiennet et al. 2012) with the help of devices designed to pack NMR rotors with precipitates or microcrystals (Böckmann et al. 2009) (Fig. 4B). *Ex situ* sedNMR allows one to select different oligomeric species by changing experimental conditions such us ultracentrifugation frequency or time and the initial Aβ peptide concentration.

Sedimentation through ultracentrifugation, either by magic angle spinning (*in situ*) or preparative ultracentrifugation (*ex situ*), can be used to immobilize and characterize oligomeric species, measure their formation kinetics, selectively sediment some of these species by their different molecular weights, and reveal the atomic-level structural features of soluble Aβ assemblies.

The collective data obtained from all of these methods demonstrate probable pathways from these fibril precursors to terminal fibrillar states and also provide evidence that these prefibrillar assemblies already contain β-strand structures but with different supramolecular organizations and reduced structural order and periodic symmetry, which might define the structures of the multiple conformers in fibrils in amyloid misfolding. However, some authors have suggested that certain oligomers that do not further aggregate to amyloid fibres and that have different secondary structures exist among different Aβ intermediate species.

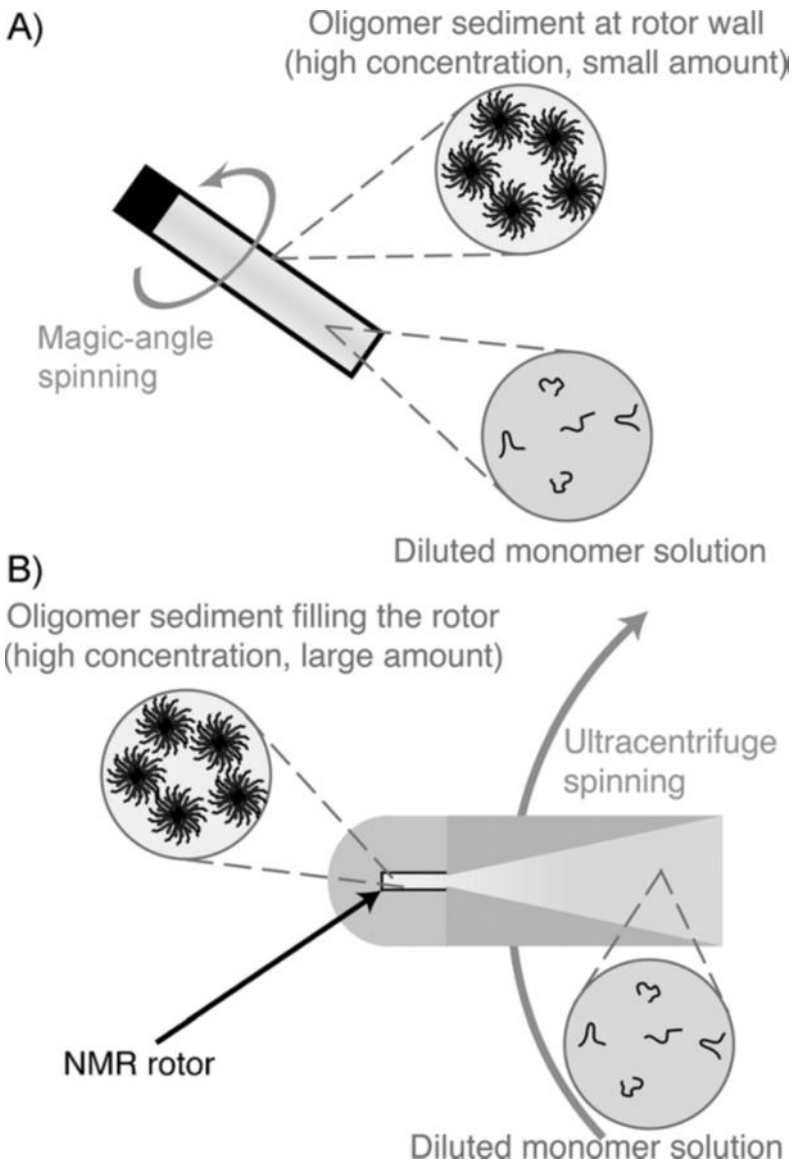

Figure 13.4. Representation of the sedimentation process. In magic angle spinning-induced (*in situ*) sedimentation (top), the sediment is created in a thin layer at the rotor walls (the width of the sediment layer is greatly exaggerated). Sedimentation induced by preparative ultracentrifugation (*ex situ*) (bottom) can be used to effectively fill the rotor with sediment. Adapted from (Bertini et al. 2013).

Association between neurotoxicity and different ratios of Aβ40 to Aβ42

Aside from the fact that neurotoxicity can be induced by intermediate deposits, recent studies have established that the ratio of Aβ40 to Aβ42 is an important factor for providing stability to intermediate, neurotoxic species and affecting aggregation kinetics (Frost et al. 2003; Herzig et al. 2004; Jan et al. 2008, 2010; Kim et al. 2007; Kuperstein et al. 2010; Pauwels et al. 2012; Snyder et al.; Wang et al. 2006; Yan and Wang, 2007; Yoshiike et al. 2003; Younkin et al. 1995; Zou et al. 2003).

Aβ42 and Aβ40 alloforms co-exist in a molar ratio of 1:9 under normal physiological conditions in the brain. In patients with familial AD this ratio is shifted to a higher level of Aβ42, corresponding to a ratio of 3:7. Investigations of the properties of the Aβ40/Aβ42 mixture by different groups have clearly shown that these two species interact and change each other's dynamic behaviour. Even minor alterations in the relative amount of the Aβ42/Aβ40 ratio dramatically affect the biophysical and biological properties of the Aβ mixtures reflected in their aggregation kinetics by altering the pattern of oligomer formation. It has been shown that Aβ40 delays Aβ42 aggregation, while Aβ42 has an opposite effect and induces Aβ40 aggregation. This observation was also confirmed by *in vivo* studies, which have shown that a higher percentage of Aβ40 peptides in the brain might be protective (Kim et al. 2007; Wang et al. 2006).

Although it is generally assumed that alterations in ratios of the Aβ40 and Aβ42 mixture can stabilize distinct intermediate species associated with toxicity, the possibility that neurotoxicity is induced by a number of different conformations should not be neglected. This possibility can be explained by the fact that those toxic intermediate deposits might exist in dynamic equilibrium through their assembly and disassembly.

Since neurotoxic conformation(s) might by induced by a particular ratio of Aβ40 to Aβ42 a detailed structural characterization of Aβ40:Aβ42 mixed fibrils is needed. Investigation of the structure of Aβ40:Aβ42 mixed fibrils in different molar ratios might shed light on the processes related to the onset of the disease and on their correlation with Aβ peptides reciprocal ratios.

Conclusions

Although the direct involvement of Aβ peptides in AD is well documented, the toxic Aβ species and the precise mechanism of its neurotoxicity remain unclear. Moreover, there is still a significant gap between site-specific structural information and the complex structural diversity of Aβ amyloids. A detailed structural and functional characterization of fibrillar assemblies as well as the various prefibrillar intermediates is crucial for understanding Aβ aggregation pathways and identifyingtoxic Aβ species. The recognition of the real culprit for AD onset is fundamental for the design of new, effective therapeutic strategies targeted at preventing the formation or impairing the activity of toxic Aβ assemblies involved in AD.

Short summary of expression and purification procedures for the preparation of Aβ peptides

Below we describe the methods of sample preparation of different kinds of Aβ peptides for NMR investigations.

The AβM40 and AβM42 peptides without any fusion tags, as well as Aβ40 and Aβ42 without the starting methionine fused with an N-terminal hexahistidine affinity tag were expressed as inclusion bodies in *E. coli*. Although inclusion bodies are usually undesirable due to problems with protein refolding, they are a good alternative in the case of intrinsically disordered proteins because their separation from the cell lysate is an easy and efficient protein purification method.

Aβ peptides with Met

The cDNA of AβM40/AβM42 was cloned in the pET3a vector using the NdeI and BamHI restriction enzymes. The peptides were expressed in the BL21(DE3)pLys *E. coli* strain. The presence of an exogenous N-terminal methionine, due to the translation start codon, as reported in the literature (Walsh et al. 2009), does not affect the fibrillation kinetics or morphology of the fibrils formed by AβM40 or AβM42.

Many papers report the expression conditions for Aβ peptide production as follows: 8 to 16 h of incubation after induction with the addition of 0.8 – 1 mM of isopropyl β-D-1-thiogalactopyranoside (IPTG) and a temperature of 25-27˚C (Long, Cho, and Ishii 2011; Zhang et al. 2009). In order to increase the protein yield, especially in terms of labelled protein production, we tried to increase the variable cell culture parameters as much as possible, boosting protein expression as an insoluble fraction. Expression of the fusion

constructs under control of the T7 promoter/lac operator in *E. coli* BL21(DE3) cells provides high yields of the fusion proteins, which accumulate in inclusion bodies.

In the case of AβM40/AβM42 the growth was performed using the Marley method (Marley, Lu, and Bracken 2001). The cells transformed with the AβM40/AβM42 expression plasmid were predominately grown in rich medium at 37°C until OD600 reached 0.6, then centrifuged and exchanged into an isotopically defined minimal media enriched with ($^{15}NH_4$)2SO_4 (1 g/L) and (^{13}C) glucose (4 g/L). The peptide expression was induced with 1.2 mM IPTG and the cells were harvested after 4 hours of incubation at 39°C.

The peptides were purified as reported (Bertini et al. 2011; Hellstrand et al. 2010; Jan, Hartley, and Lashuel 2010; Walsh et al. 1997; 2009) with some modifications using a combination of anion exchange and size exclusion chromatography. All the manipulations were performed at slightly alkaline pH in order to avoid the formation of structural contaminants produced by isoelectric precipitation.

There are some reports in the literature regarding possible aggregation and as a consequence a decrease in protein yield in pre-packed purification columns versus free resin (Walsh et al. 2009; Zhang et al. 2009). We also observed that purification of AβM40 and AβM42 by ion exchange chromatography in column mode (diethylaminoethyl (DEAE) cellulose column) led to much lower yields of monomeric peptide than in batch mode because of protein precipitation and aggregation.

The inclusion bodies were first solubilized with 8 M urea and then purified by ion exchange chromatography performed in batch mode. For this purpose DE52 resin on a Büchner funnel with filter paper on a vacuum glass bottle was used. Elution was performed using different concentrations of NaCl buffer. The protein was eluted with a 125 mM concentration of the salt. In the case of AβM42, the protein was also present in 20 mM, 150 mM, 200 mM and 1M fractions, probably due to progressive sample aggregation. All the obtained fractions of

diluted protein were concentrated to the final volume using an Amicon device. We examined a number of methods to concentrate the Aβ solution. Although several different methods within the 3 kDa molecular mass cut-off for centrifugal devices proved useful, the Amicon device was the best solution for highly concentrated proteins.

This two-step purification allows a highly pure product to be obtained with a yield of about 10 mg of AβM40 and 5-10 mg of AβM42 per litre of culture.

Aβ peptides without Met

Aβ40 and Aβ42 were produced in *E. coli* cytoplasm as fusion proteins with N-terminal hexahistidine affinity tags. The fusion construct consists of a soluble polypeptide segment comprised of 19 repeats of the tetrapeptide sequence NANP, a TEV protease cleavage site (sequence ENLYFQ), dipeptide linker sequences and the Aβ sequence.

We applied a similar approach for the expression and purification of Aβ peptides (Aβ40 and Aβ42) without methionine. Cells were grown in rich medium (lysogeny broth (LB) or Terrific Broth (TB)) until they reached high OD values. Peptide expression was induced with 1-1.2 mM IPTG and cells were harvested after 4 hours incubation at 39°C. After the removal of the soluble proteins the inclusion bodies were solubilized with 20 mM TRIS pH 8, 8M and purified by affinity chromatography using a nickel chelating (His-Trap) column under denaturating conditions, followed by digestion with AcTEV protease. In order to avoid protein aggregation and improve the separation of cut/uncut protein, 8 M urea or 6 M guanidine hydrochloride was introduced in two affinity column steps.

As a final purification step for both peptide families (Aβ40,42; AβM40,42), a gel filtration in 50 mM ammonium acetate pH 8.5 using a Superdex 75 26/60 column was used. It is important to keep the pH of the solution over 4-7, the pH range where aggregation is maximized.

The aggregation of Aβ peptides is strongly influenced by the presence of structural and chemical impurities; therefore, before proceeding with SEC, all samples were denatured using 6 M guanidine hydrochloride as described previously (Walsh et al. 1997).

The protein obtained was dialysed in water and lyophilised.

In the case of Aβ42 peptides and even more so with their mutants, due to problems with tag digestion, we have to adopt a different purification procedure, introducing organic solvents.

The inclusion bodies were solubilized with 6 M guanidinium chloride and the protein was purified by metal chelating affinity chromatography on Ni2+-nitrilotriacetic acid agarose in the presence of 6 M guanidinium chloride, thus lowering the pH. The fusion proteins were further purified via reversed phase high-performance liquid chromatography (RP-HPLC) using a semi-preparative Zorbax SB300 C8 column (Agilent), lyophilized from aqueous acetonitrile and directly used for TEV protease cleavage. A cleavage efficiency of about 70% was achieved after incubation at pH 8.0 and 4°C for 16 h at a protein concentration of 100 μM in the presence of 5 μM TEV protease. The cleavage mixture was subsequently applied to RP-HPLC, which allowed quantitative separation of the hydrophobic Aβ42 peptide from the other, more hydrophilic components in the cleavage reaction. The final yield of purified Aβ40 was 20 mg/L of culture.

Another problem encountered was associated with solubilisation of lyophilised protein in water. Because the Aβ peptides undergo time- and concentration-dependent aggregation in acetonitrile-water (Shen and Murphy 1995), the dry, purified peptides adopt different structures and aggregation states (Soto et al. 1995). Depending on the peptide batch and the particular aggregation conditions, considerable discrepancies exist across different laboratories as well as within the same laboratory over time. In addition, numerous studies have established that neurotoxicity and the kinetics of aggregation are directly related to assembly state in solution. Therefore, direct solubilisation of the Aβ peptides in aqueous

media should always be avoided because it generates batch-dependent mixtures of aggregates and structures (Hou et al. 2004).

A couple of procedures have been proposed to disaggregate the Aβ and generate a monomeric random coil structure: pre-dissolution of the peptide in dilute base solution, and pre-dissolution in TFA and HFIP solvents (Jao et al. 1997). Finally, we applied a protocol that has already been reported (Broersen et al. 2011) for the solubilisation of Aβ peptide that involves sequential solubilisation using the structure-breaking organic solvents HFIP and DMSO followed by column purification and results in standardized aggregate-free Aβ peptide. As was reported in pure DMSO, Aβ appears to be monomeric and lacks any β-sheet character (Shen and Murphy 1995).

REFERENCES:

Ahmed Mahiuddin, Davis Judianne, Aucoin Darryl, Sato Takeshi, Ahuja Shivani, Aimoto Saburo, Elliott James I, Van Nostrand William E, Smith Steven O. 2010. "Structural conversion of neurotoxic amyloid-beta(1-42) oligomers to fibrils." *Nature Structural & Molecular Biology* 17 (5), 561–567.

Aksenov Micheal Y., Aksenova Marina V., Butterfield D.A., Hensley Kenneth, Vigo-Pelfrey Carmen, Carney John M. 1996. "Glutaminesynthetase-induced enhancement of beta-amyloid peptide A beta (1–40) neurotoxicity accompanied by abrogation of fibril formation and A beta fragmentation." *Journal of Neurochemistry* 66: 2050–2056.

Balbach JJ, A.T. Petkova, N.A. Oyler, O.N. Antzutkin, D.J. Gordon, S.C. Meredith, R. Tycko, 2002. 'Supramolecular Structure in Full-Length Alzheimer's β -Amyloid Fibrils: Evidence for a Parallel β -Sheet Organization from Solid-State Nuclear Magnetic Resonance', Biophys. J., 83, 1205–1216.

Barrantes Francisco J., Virginia Borroni, Sofía Vallés. 2010 .Neuronal nicotinic acetylcholine receptor–cholesterol crosstalk in Alzheimer's disease *FEBS Lett.* May 3;584(9):1856-63.

Bayer, T. A., Cappai, R., Masters, C. L., Beyreuther, K., and Multhaup, G. 1999. It all sticks together the APP-related family of proteins and Alzheimer's disease. *Molecular psychiatry*, 4(6):524{8.

Benilova Iryna, Karran Eric, De Strooper Bart. 2012. "The toxic Aβ oligomer and Alzheimer's disease: an emperor in need of clothes." *Nature Neuroscience* 15(3):349-57.

Benzinger Tammie L.S., Gregory David M., Burkoth Timothy S., Miller-Auer Helene, Lynn David G.,Botto Robert E., and Meredith Stephen C.1998. " Propagating structure of Alzheimer'sb-amyloid(10-35) is parallel b-sheet with residues in exact register." *Proceedings of the National Academy of Sciences USA* 95 (23), 13407–13412.

Bernstein Summer L., Dupuis Nicholas F., Lazo Noel D.,Wyttenbach Thomas, Condron Margaret M., Bitan Gal, Teplow David B., Shea Joan - Emma, Ruotolo Brandon T., Robinson Carol V., Bowers Michael T. 2009. "Amyloid-β protein oligomerization and the importance of tetramers and dodecamers in the aetiology of Alzheimer's disease." *Nature Chemistry* 1 (4), 326– 331.

Bertini Ivano, Leonardo Gonnelli, Claudio Luchinat, Jiafei Mao, and Antonella Nesi. 2011. "A New Structural Model of Aβ40 Fibrils." *Journal of the American Chemical Society USA* 133(40): 16013–22.

Bertini Ivano, Luchinat Claudio, Parigi Giacomo, Ravera Enrico, Reif Bernd, Turano Paola. 2011. "Solid-state NMR of proteins sedimented by ultracentrifugation." *Proceedings of the National Academy of Sciences USA*108 (26), 10396 –10399.

Bertini Ivano, Engelke Frank, Luchinat Claudio, Parigi Giacomo, Ravera Enrico, Camila Rosa, Paola Turano. 2012. "NMR properties of sedimented solutes.'' Physical Chemistry Chemical Physics14 (2), 439 –447.

Bertini Ivano, Engelke Frank, Gonnelli Leonardo, Knott Benno, Luchinat Claudio, Osen David, Ravera Enrico. 2012. "On the use of ultracentrifugal devices for sedimented solute NMR." *Journal of Biomolecular NMR* 2012, 54 (2), 123 –127.

Bertini Ivano, Luchinat Claudio, Parigi Giacomo, Ravera Enrico. 2013. "SedNMR: On the Edge between Solution and Solid-State NMR." *Accounts of Chemical Research*46(9):2059-69.

Bertini Ivano, Gallo Gianluca, Korsak Magdalena, Luchinat Claudio, Mao Jiafei, Ravera Enrico**.** 2013. " Formation Kinetics and Structural Features of Beta- Amyloid Aggregates by Sedimented Solute NMR".*European Journal of Chemical Biology*14(14):1891-7.

Bieschke Jan, Herbst Martin, Wiglenda Thomas, Friedrich Ralf P., Boeddrich Annett, Schiele Franziska, Kleckers Daniela, Lopez del Amo Juan Miguel, Grüning Björn A, Wang Qinwen, Schmidt Michael R, Lurz Rudi, Anwyl Roger, Schnoegl Sigrid, Fändrich Marcus, Frank Ronald F., Reif Bernd, Günther Stefan, Walsh Dominic M., Wanker Erich E., 2012. "Small-molecule conversion of toxic oligomers to nontoxic β-sheet-rich amyloid fibrils. *Nature Chemical Biology* 8 (1), 93–101.

Bitan Gal, Kirkitadze Marina D., Lomakin Aleksey, Vollers SS, Benedek George B., Teplow David B. 2003."Amyloid beta -protein (Abeta) assembly: Abeta 40 and Abeta 42 oligomerize through distinct pathways." *Proceedings of the National Academy of Sciences USA*100 (1), 330–335.

Bitan Gal, Teplow David B. 2005. "Preparation of aggregate-free, low molecular weight amyloid beta for assembly and toxicity assays." *Methods in Molecular Biology* 299, 3–9.

Bockmann Anja, Gardiennet Carole, Verel Rene, Hunkeler Andreas, Loquet Antoine, Pintacuda Guido, Emsley Lyndon, Meier Beat H., Lesage Anne, 2009. "Characterization of different water pools in solid-state NMR protein samples." *Journal of Biomolecular NMR* 45 (3), 319 – 327.

Broersen, Kerensa, WimJonckheere, JefRozenski, AnneliesVandersteen, Kris Pauwels, Annalisa Pastore, Frederic Rousseau, and JoostSchymkowitz. 2011. "A Standardized and Biocompatible Preparation of Aggregate-Free Amyloid Beta Peptide for Biophysical and Biological Studies of Alzheimer's Disease." *Protein engineering, design &selection : PEDS* 24(9): 743–50.

Chimon Sandra, IshiiYoshitaka. 2005. "Capturing intermediate structures of Alzheimer's β-amyloid, Aβ1−40, by solid state NMR spectroscopy." *Journal of the American Chemical Society USA*127 (39) :13472–73

Chimon Sandra, Shaibat Medhat A., Jones Christopher R., CaleroDianaC., Aizezi Buzulagu , Ishii Yoshitaka. 2007."Evidence of fibril-like b-sheet structures in a neurotoxic amyloid intermediate of Alzheimer's b-amyloid" *Nature Structural & Molecular Biology*14, 1157–1164.

Danielsson Jens, Andersson August, Jarvet Juri, Gräslund Astrid. 2006. "15N relaxation study of the amyloid beta-peptide: structural propensities and persistence length." *Magnetic Resonace in Chemistry* 44, S114– S121.

Dobson C.M., 'Protein Folding and Misfolding'.2003.*Nature*, 426, 884–890.

Esch, F. S., Keim, P. S., Beattie, E. C., et al. 1990. Cleavage of amyloid beta peptide during constitutive processing of its precursor.*Science* (New York, N.Y.), 248(4959):1122{4.

Geneviève Evin, Andreas Weidemann. 2002. Biogenesis and metabolism of Alzheimer's disease Aβ amyloid peptides, *Peptides* 23 1285–1297.

Glenner GG, Wong CW.1984 Alzheimer's disease: initial report of the purification and characterization of a novel cerebrovascular amyloid protein. *Biochem Biophys Res Commun*. 16;120(3):885-90.

Fändrich Marcus, Schmidt Matthias and Grigorieff Nikolaus. 2011. "Recent progress in understanding Alzheimer's β-amyloid structures." *Trends in Biochemical Sciences*36, 338-345.

Fändrich Marcus. 2012. "Oligomeric intermediates in amyloid formation: structure determination and mechanisms of toxicity."*Journal of Molecular Biology* 421 (4-5), 427– 440.

Fawzi Nicolas L., Ying Jinfa, Ghirlando Rodolfo, Torchia Dennis A. Clore Marius G. 2011.''Atomic-resolution dynamics on the surface of amyloid-β protofibrils probed by solution NMR.'' *Nature,* 480 (7376), 268-272.

Fezoui Youcef, Hartley Dean M., Harper James D., Khurana Ritu, Walsh Dominic M., Condron Margaret M., Fink Anthony L., Teplow David B. 2000. ''An improved method of preparing the amyloid beta-protein for fibrillogenesis and neurotoxicity experiments.''*Amyloid*7(3):166-78.

Frost David, Gorman Paul M., Yip Christopher M., Chakrabartty Avijit. 2003. "Co-incorporation of A beta 40 and A beta 42 to form mixed pre-fibrillar aggregates." *European Journal of Biochemistry*270(4):654-63.

Gallion Steven L.,2012.'' Modeling amyloid-beta as homogeneous dodecamers and in complex with cellular prion protein.''*PLoS ONE*7(11):e49375.

Gardiennet Carole, Schutz Anne K., Hunkeler Andreas, Kunert Britta, Terradot Laurent, A. Bockmann Anja, Meier Beat H.2012. "A sedimented sample of a 59 kDa dodecameric helicase yields high-resolution solid-state NMR spectra." *Angewandte Chemie International Edition* 51 (31), 7855 –7858.

Haass Christian nitiation and propagation of neurodegeneration. 2010. *Nat Med.* Nov;16(11):1201-4.

Haass Christian, Selkoe Dennis J. 2007. Soluble protein oligomers in neurodegeneration: lessons from the Alzheimer's amyloid beta-peptide.*Nat Rev Mol Cell Biol*. Feb;8(2):101-12.

Hartley Dean M., Walsh Dominic M., Chian Ping, Diehl Thekla S.,Vasquez S., Vassilev Peter M., Teplow David B., Selkoe Dennis J. 1999. "Protofibrillar intermediates of amyloid beta-protein induce acute electrophysiological changes and progressive neurotoxicity in cortical neurons." *The Journal of Neuroscience* 19 (20), 8876–8884.

Haupt Christian, Leppert Jorg, Ronicke Raik, Meinhardt Jessica, Yadav Jay K., Ramachandran Ramadurai, Ohlenschoger Oliver, Reymann Klaus G., Gorlach Matthias, Fandrich Marcus. 2012. "Structural basis of β-amyloid-dependent synaptic dysfunctions." *Angewandte Chemie International Edition* 2012, 51 (7), 1576 – 1579.

Hellstrand, Erik, Barry Boland, Dominic M Walsh, and Sara Linse. 2010. "Amyloid B-Protein Aggregation Produces Highly Reproducible Kinetic Data and Occurs by a Two-Phase Process." *ACS chemical neuroscience* 1(1): 13–18.

Herzig Martin C., Winkler David T., Burgermeister Patrick, Pfeifer Michelle, Kohler Esther, Schmidt Stephen D., Danner Simone, Abramowski Dorothee, Stürchler-Pierrat Christine, Bürki Kurt,

Van Duinen Sjoerd G., Maat-Schieman Marion L.C., Staufenbiel Matthias, Mathews Paul M., Jucker Mathias.2004. “Abeta is targeted to the vasculature in a mouse model of hereditary cerebral hemorrhage with amyloidosis.” *Nature Neuroscience* 7 (9), 954–960.

Hardy John and Dennis J. Selkoe 2002 The Amyloid Hypothesis of Alzheimer’s Disease: Progress and Problems on the Road to Therapeutics. *Science* 297: 353–356

Hoshi Minako,Sato Michio, Sato Michio, Matsumoto Shinichiro, Noguchi Akihiko, Yasutake Kaori, Yoshida Natsuko, Sato Kazuki. 2003. “Spherical aggregates of (b-amyloid (amylospheroid) show high neurotoxicity and activate tau protein kinase I/glycogen synthase kinase-3b.” *Proceedings of the National Academy of Sciences USA* 100, 6370–6375 (2003).

Hou, Liming, Haiyan Shao, Yongbo Zhang, Hua Li, Nanda K Menon, Elizabeth B Neuhaus, John M Brewer, In-Ja L Byeon, Dale G Ray, Michael P Vitek, Takashi Iwashita, Ronald A Makula, Alan B Przybyla, and Michael G Zagorski. 2004. “Solution NMR Studies of the a Beta(1-40) and a Beta(1-42) Peptides Establish That the Met35 Oxidation State Affects the Mechanism of Amyloid Formation.” *Journal of the American Chemical Society* 126(7): 1992–2005.

Howlett DR1, Jennings KH, Lee DC, Clark MS, Brown F, Wetzel R, Wood SJ, Camilleri P, Roberts GW. 1995. Aggregation state and neurotoxic properties of Alzheimer beta-amyloid peptide. *Neurodegeneration*. Mar;4(1):23-32.

Jan Asad, Gokce O, Luthi-Carter R, Lashuel Hilal A. 2008. ’’The ratio of monomeric to aggregated forms of Abeta40 and Abeta42 is an important determinant of amyloid-beta aggregation, fibrillogenesis, and toxicity.” *The Journal of Biological Chemistry* 283(42):28176-89.

Jan Asad, Dean M Hartley, and Hilal A Lashuel. 2010. “Preparation and Characterization of Toxic Abeta Aggregates for Structural and Functional Studies in Alzheimer's Disease Research.” *Nature protocols* 5(6): 1186–1209.

Jao, Shu-Chuan, Kan Ma, Joseph Talafous, Ron Orlando, and Michael G Zagorski. 1997. “Trifluoroacetic Acid Pretreatment Reproducibly Disaggregates the Amyloid B-Peptide.” Amyloid: *International Journal of Experimental & Clinical Investigation* 4(4): 240–52.

Kang J., H.G. Lemaire, A. Unterbeck, J.M. Salbaum, C.L. Masters, K.H. Grzeschik et al. 1987, The precursor of Alzheimer’s disease amyloid A4 protein resembles a cell surface receptor *Nature*, 325 pp. 733–736.

Kheterpal Indu, Chen Maolian, Cook Kelsey D., Wetzel Ronald. 2006. “Structural differences in Abeta amyloid protofibrils and fibrils mapped by hydrogen exchange--mass spectrometry with on-line proteolytic fragmentation.” *Journal of Molecular Biology* 361 (4), 785 – 795.

Kim Jungsu, Onstead Luisa, Randle Suzanne, Price Robert, Smithson Lisa, Zwizinski Craig, Dickson Dennis W., Golde Todd, McGowan Eileen. 2007. ’’Abeta40 inhibits amyloid deposition in vivo.’’ *Journal of Neuroscience* 27(3):627-33.

Kirkitadze Marina D, Bitan, Gal, Teplow David B. 2002,” Paradigm shifts in Alzheimer's disease and other neurodegenerative disorders: the emerging role of oligomeric assemblies.”*Journal of Neuroscience Research*69, 567-577.

Krafft Grant A., Klein William L. 2010. “ADDLs and the signaling web that leads to Alzheimer’s disease.” *Neuropharmacology* 59 (4-5), 230–242.

Kumar Sathish, Rezaei-Ghaleh Nasrollah, Terwel Dick, Thal Dietmar R, Richard Mélisande, Hoch Michael, Mc Donald Jessica M, Wüllner Ullrich, Glebov Konstantin, Heneka Michael T, Walsh Dominic M, Zweckstetter Markus, Walter Jochen. 2011.“Extracellular phosphorylation

of the amyloid β-peptide promotes formation of toxic aggregates during the pathogenesis of Alzheimer's disease". *European Molecular Biology Organization Journal* 30(11):2255-65.

Kuperstein Inna, Broersen Kerensa, BenilovaIryna, Rozenski Jef, Jonckheere Wim, Debulpaep Maja, Vandersteen Annelies, Segers-Nolten Ine, Van Der Werf Kees, Subramaniam Vinod, Braeken Dries, Callewaert Geert, Bartic Carmen, D'Hooge Rudi, Martins Ivo Cristiano, Rousseau Frederic, Schymkowitz Joost, De Strooper Bart. 2010. "Neurotoxicity of Alzheimer's disease Aβ peptides is induced by small changes in the Aβ42 to Aβ40 ratio." *European Molecular Biology Organization Journal* 29(19):3408-20.

Lambert Mary P., Barlow A. K., Chromy Brett A., Edwards C., Freed Rachel M., Liosatos Magdaline, Morgan Todd E., Rozovsky Irina, Trommer Barbara L., Viola Kirsten, P Wals, Zhang C., Finch C. E., Krafft Grant A., Klein William L. 1998. "Diffusible, nonfibrillar ligands derived from Ab1–42 are potent central nervous system neurotoxins." *Proceedings of the National Academy of Sciences USA* 95, 6448–6453.

Lammich, S., Kojro, E., Postina, R., et al. 1999.Constitutive and regulated alpha-secretase cleavage of Alzheimer's amyloid precursor protein by a disintegrin metalloprotease.*Proceedings of the National Academy of Sciences of the United States of America*, 96(7):3922{7.

Lansbury Peter T., Costa Philip R., Griffiths Janet M., Simon Eric J., Auger Michele, Halverson Kurt J., Kocisko David A., Hendsch Zachary S., Ashburn Ted T., Spencer Richard G.S. 1995. "Structural model for the b-amyloid fibril based on interstrand alignment of an antiparallel-sheet comprising a C-terminal peptide." *Nature Structural & Molecular Biology* 2 (11),990–998.

Lee Jiyong, Culyba Elisabeth K., Powers Evan T., Kelly Jeffery W. 2011. "Amyloid-β forms fibrils by nucleated conformational conversion of oligomers." *Nature Chemical Biology* 7 (9), 602–609.

Lesne´ Sylvain, Koh Ming Teng, Kotilinek Linda, Kayed Rakez, Glabe Charles G., Yang Austin, Gallagher Michela, Ashe Karen H. 2006. "A specific amyloid-b protein assembly in the brainimpairs memory." *Nature* 440 (7082), 352–357.

Long, Fei, Wonhwa Cho, and Yoshitaka Ishii. 2011. "Expression and Purification of 15N- and 13C-Isotope Labeled 40-Residue Human Alzheimer's B-Amyloid Peptide for NMR-Based Structural Analysis." *Protein expression and purification* 79(1): 16–24.

Lopez del Amo Juan Miguel, Fink Uwe, Dasari Muralidhar, Grelle Gerlinde, Wanker Erich E., Bieschke Jan, Reif Bernard. 2012. "Structural properties of EGCG-induced, nontoxic Alzheimer's disease Aβ oligomers.'' *Journal of Molecular Biology* 421 (4-5), 517–524.

Lorenzo Alfredo, Yankner Bruce A. 1994. "Beta-amyloid neurotoxicity requires fibril formation and is inhibited by Congo red." *Proceedings of the National Academy of Sciences USA*91(25), 12243–12247.

Lu Jun-Xia, Qiang Wei, Yau Wai-Ming, Schwieters Charles D, Meredith Stephen C, Tycko Robert.2013. "Molecular structure of b-amyloid fibrils in Alzheimer's Disease Brain Tissue".*Cell* 154(6):1257-68.

Lührs Thorsten, Ritter Christiane, Adrian Marc, Riek-Loher Dominique, Bohrmann Bernd, Dobeli Heinz ,Schubert David, Riek Roland. 2005. "3D structure of Alzheimer's amyloid beta (1-42) fibrils." *Proceedings of the National Academy of Sciences USA*102(48), 17342–17347.

Martins Ivo Cristiano, Kuperstein Inna, Wilkinson Hannah, Maes Elke, Vanbrabant Mieke, Jonckheere Wim, Van Gelder Patrick, Hartmann Dieter, D'Hooge Rudi, De Strooper Bart, Schymkowitz Joost, Rousseau Frederic 2008. "Lipids revert inert Abeta amyloid fibrils to

neurotoxic protofibrils that affect learning in mice.'' *European Molecular Biology Organization Journal* 27(1):224-33.

Marley, Jonathan, Min Lu, and Clay Bracken. 2001. "A Method for Efficient Isotopic Labeling of Recombinant Proteins." *Journal of biomolecular NMR* 20(1): 71–75.

Masters CL, Multhaup G, Simms G, Pottgiesser J, Martins RN, Beyreuther K. 1985 Neuronal origin of a cerebral amyloid: neurofibrillary tangles of Alzheimer's disease contain the same protein as the amyloid of plaque cores and blood vessels. *EMBO J*. Nov;4(11):2757-63.

Masters CL, G. Simms, N.A. Weinman, G. Multhaup, B.L. McDonald, K. Beyreuther. 1985. Amyloid plaque core protein in Alzheimer disease and Down syndrome *Proc. Natl. Acad. Sci. U.S.A.*, 82 pp. 4245–4249.

Meinhardt Jessica, Sachse Carsten, Hortschansky Peter, Grigorieff Nikolaus, Fändrich Marcus. 2009. "Abeta(1-40) fibril polymorphism implies diverse interaction patterns in amyloid fibrils."*Journal of Molecular Biology* 386 (3), 869-877.

Merz Patrizia A.,Wisniewski Henryk M., Somerville R. A., Bobin S. A. , Masters Colin L., Iqbal Khalid.1983. "Ultrastructural morphology of amyloid fibrils from neuritic and amyloid plaques." *Acta Neuropathologica* 60(1-2):113-24.

Meyer-Luehmann Melanie, Spires – Jones Tara L., Prada Claudia, Garcia – Alloza Monica, de Calignon Alix, Rozkalne Anete, Koenigsknecht-Talboo Jessica, Holtzman David M., Bacskai Brian J., Hyman Bradley T. "Rapid appearance and local toxicity of amyloid-beta plaques in a mouse model of Alzheimer's disease." *Nature* 2008, 451, 720-7U5.

Naito A., M. Kamihira, R. Inoue, H. Saito, 2004.'Structural Diversity of Amyloid Fibril Formed inHuman Calcitonin as Revealed by Site-Directed 13C Solid-State NMR Spectroscopy', *Magn. Reson. Chem*., 42, 247–257.

Noguchi Akihiko, Matsumura Satoko, Dezawa Mari, Tada Mari, Yanazawa Masako, Ito Akane, Akioka Manami, Kikuchi Satoru, Sato Michio, Ideno Shouji. 2009. " Isolation and characterization of patient-derived, toxic, high mass amyloid b-protein (Abeta) assembly from Alzheimer disease brains." *Journal of Biological Chemistry* 284 (47), 32895–32905.

Pan Jingxi, Han Jan, Borchers Christoph H., Konermann Lars. 2011. "Conformer-specific hydrogen exchange analysis of Aβ(1-42) oligomers by top-down electron capture dissociation mass spectrometry." *Analytical Chemistry*83 (13),5386 –5393.

ParavastuAnant K, Leapman Richard D., Yau Wai-Ming, Tycko Robert 2008. "Molecular structural basis for polymorphism in Alzheimer's b-amyloid fibrils." *Proceedings of the National Academy of Sciences USA* 105 (47), 18349–18354.

Paravastu Anant K., Quhwash Isam, Leapman Richard D., Meredith Stephen C., Tycko Robert. 2009. "Seeded growth of beta-amyloid fibrils from Alzheimer's brain-derived fibrils produces a distinct fibril structure." *Proceedings of the National Academy of Sciences USA* 106 (18), 7443-7448.

Pauwels K., Williams T.L., Morris K.L., Jonckheere W., Vandersteen A., Kelly G., Schymkowitz J., Rousseau F., Pastore A., Serpell L.C, Broersen K. 2012. ''Structural basis for increased toxicity of pathological aβ42:aβ40 ratios in Alzheimer disease.''*The Journal of Biological Chemistry* 287(8):5650-60.

Petkova Aneta T., IshiiYoshitaka, Balbach, J. J., Antzutkin Oleg N., Leapman Richard D., Delaglio, F., Tycko Robert. 2002. "A structural model for Alzheimer's beta -amyloid fibrils based on experimental constraints from solid state NMR." *Proceedings of the National Academy of Sciences USA* 99 (26), 16742–16747.

Petkova Aneta T., Leapman Richard D., Guo, Zhihong H., Yau Wai-Ming, Mattson Mark P., and Tycko Robert. 2005. “Self-propagating, molecular-level polymorphism in Alzheimer’s b-amyloid fibrils”.*Science* 307(5707):262-5.

Petkova Aneta T, Yau Wai-Ming, Tycko Robert. 2006. “Experimental constraints onquaternary structure in Alzheimer’s b-amyloid fibrils.” *Biochemistry* 45 (2),498–512.

Polenova Tatyana. 2011. “Protein NMR spectroscopy: spinning into focus.” Nature Chemistry 3 (10), 759– 760.

Qiang Wei, Yau Wai-Ming, Tycko Robert. 2011. “Structural evolution of Iowa mutant b-amyloid fibrils from polymorphic to homogeneous states under repeated seeded growth.” *Journal of the American Chemical Society* 133 (11), 4018–4029.

Qiang Wei, Yau Wai-Ming, Luo Youngquan, Mattson Mark P., Tycko Robert 2012. “Antiparallelb-sheet architecture in Iowa-mutant b-amyloid fibrils.” *Journal of the American Chemical Society USA* 109 (12), 4443–4448.

Ravera Enrico, Corzilius Bjorn, Michaelis Vladimir K., Rosa Camila,Griffin Robert G., Luchinat Claudio, Bertini Ivano. 2013. “Dynamic Nuclear Polarization of Sedimented Solutes’’. *Journal of the American Chemical Society USA* 135 (5), 1641– 1644.

Roberts, S. B., Ripellino, J. A., Ingalls, K. M., Robakis, N. K., and Felsenstein, K. M. 1994. Nonamyloidogenic cleavage of the beta-amyloid precursor protein by an integral membrane metalloendopeptidase.*The Journal of biological chemistry*, 269(4):3111{6.

Sachse Carsten, Fändrich Marcus, Grigorieff Nikolaus. 2008. ’’Paired beta-sheet structure of an Abeta(1-40) amyloid fibril revealed by electron microscopy.’’*Proceedings of the National Academy of Sciences USA*105(21):7462-6.

Sachse Carsten, Grigorieff Nikolaus, Fändrich Marcus. 2010. ’’Nanoscale flexibility parameters of Alzheimer amyloid fibrils determined by electron cryo-microscopy.’’ *Angewandte Chemie International Edition*49(7):1321-3.

Scheidt Holger A., Morgado Isabel, Rothemund Sven, Huster Daniel, Fändrich Marcus. 2011. “Solid-state NMR spectroscopic investigation of Ab protofibrils: implication of a b-sheet remodeling upon maturation into terminal amyloid fibrils.” *Angewandte Chemie International Edition*50 (12), 2837–2840.

Shen, C L, and R M Murphy. 1995. “Solvent Effects on Self-Assembly of Beta-Amyloid Peptide.” *Biophysical journal* 69(2): 640–51.

Selkoe, Dennis J. M.D. 1994. "Alzheimer's Disease: A Central Role for Amyloid". Journal of Neuropathology & Experimental Neurology, 53 (5), 438-447.

Selkoe Dennis J. 2004. “Cell biology of protein misfolding: the examples of Alzheimer’s and Parkinson’s diseases.” *Nature Cell Biology* 6(11), 1054–1061.

Selkoe Dennis J. 2008. “Soluble oligomers of the amyloid b-protein impair synaptic plasticity and behavior.” *Behavioural Brain Research* 192 (1), 106–113.

Serpell Louise C. et al. 2000. “Alzheimer's amyloid fibrils: structure and assembly.”*Biochimica et Biophysica Acta*1502(1):16-30.

Sinha, S., Anderson, J. P., Barbour, R., et al. 1999.Puri_cation and cloning of amyloid precursor protein beta-secretase from human brain.*Nature*, 402(6761):537{540.

Sisodia, S. S. 1992.Beta-amyloid precursor protein cleavage by a membrane-bound protease.*Proceedings of the National Academy of Sciences of the United States of America*, 89(13):6075{9.

Sola, C., Mengod, G., Probst, A., and Palacios, J. M. 1993. Di_erential regional and cellular distribution of beta-amyloid precursor protein messenger RNAs containing and lacking the Kunitz protease inhibitor domain in the brain of human, rat and mouse. *Neuroscience*, 53(1):267{295.

Soto, Claudio, Eduardo M Castaño, R Asok Kumar, Ronald C Beavis, and Blas Frangione. 1995. "Fibrillogenesis of Synthetic Amyloid-B Peptides Is Dependent on Their Initial Secondary Structure." *Neuroscience Letters* 200(2): 105–8.

Studelska Daniel R, McDowell Lynda M., Espe M. P., Klug Christopher, Schaefer Jacob.1997. "Slowed enzymatic turnover allows characterization of intermediates by solid-state NMR." *Biochemistry* 36 (50), 15555–15560.

Tycko Robert. 2010. "Solid-State NMR Studies of Amyloid Fibril Structure".*Annual Review of Physical Chemistry*62:279-99.

Tycko Robert, Y. Ishii, 2003. 'Constraints on Supramolecular Structure in Amyloid Fibrils from Two-Dimensional Solid-State NMR Spectroscopy with Uniform Isotopic Labeling', *J. Am. Chem. Soc*., 125, 6606–6607.

Walsh Dominic M, Lomakin Aleksey, Benedek George B., Condron Margaret M., Teplow. David B. 1997. "Amyloid B-Protein Fibrillogenesis Detection of a Protofibrilar Intermediate." *The Journal of biological chemistry* 272(35): 22364–72.

Walsh Dominic M., Hartley Dean M., Kusumoto Y., Fezoui Youcef, Condron Margaret M., Lomakin Aleksey, Benedek George B., Selkoe Dennis J., Teplow David B. 1999. "Amyloid b-protein fibrillogenesis. Structure and biological activity of protofibrillar intermediates." *The Journal of Biological Chemistry* 274 (36), 25945–25952.

Walsh, Dominic M, Eva Thulin, Aedín M Minogue, NiklasGustavsson, Eric Pang, David B Teplow, and Sara Linse. 2009. "A Facile Method for Expression and Purification of the Alzheimer's DiseaseAssociated Amyloid Beta Peptide." 276(5): 1266–81.

Walter, J., Fluhrer, R., Hartung, B., et al. 2001. Phosphorylation regulates intracellular traficking of beta-secretase. The Journal of biological chemistry, 276(18):14634{41.

Wang Runsheng, Wang Baiping, He Wanxia, Zheng Hui. 2006. ''Wild-type presenilin 1 protects against Alzheimer disease mutation-induced amyloid pathology.'' *The Journal of Biological Chemistry*281(22):15330-6.

Ward RobinV.,Jennings Kevin H., Jepras Robert, Neville William, Owen Davina E., Hawkins Julie, Christie Gary, Davis John B., George Ashley, Karran Eric H., Howlett David R. 2000. "Fractionation and characterization of oligomeric, protofibrillar and fibrillar forms of beta-amyloid peptide." *Biochemical Journal* 348 (Pt 1): 137–144.

Wasco, W., Bupp, K., Magendantz, M., et al. 1992. Identification of a mouse brain cDNA that encodes a protein related to the Alzheimer disease-associated amyloid beta protein precursor. *Proceedings of the National Academy of Sciences of the United States of America*, 89(22):10758{62.

Wasco, W., Gurubhagavatula, S., Paradis, M. D., et al. 1993.Isolation and characterization of APLP2 encoding a homologue of the Alzheimer's associated amyloid beta protein precursor.*Nature genetics*, 5(1):95{100.

Wasmer Chritian, Lange Adam, Van Melckebeke Helene, Siemer Ansgar B., Riek Roland, Meier Beat H. 2008. "Amyloid fibrils of the HET-s(218-289) prion form a beta solenoid with a triangular hydrophobic core." *Science* 319 (5869), 1523-1526.

Yan Yilin, Wang Chunyu. 2007. "Abeta40 protects non-toxic Abeta42 monomer from aggregation." *The journal of Molecular Biology* 369(4):909-16.

Yoshiike Yuji, Chui De-Hua, Akagi Takumi, Tanaka Nobuo, Takashima Akihiko. 2003. ''Specific compositions of amyloid-beta peptides as the determinant of toxic beta-aggregation.'' *The Journal of Biological Chemistry* 278(26):23648-55.

Yoshikai, S., Sasaki, H., Doh-ura, K., Furuya, H., and Sakaki, Y. 1990.Genomic organization of the human amyloid beta-protein precursor gene.*Gene*, 87(2):257{63.

Younkin Steven G.1995. " Evidence that A beta 42 is the real culprit in Alzheimer's disease." *Annals of Neurology* 37 (3), 287–288.

Zhang, Li, Huixin Yu, Cuicui Song, Xiufeng Lin, Bo Chen, Chen Tan, Guoxian Cao, and Zhengwu Wang. 2009. "Expression, Purification, and Characterization of Recombinant Human B-Amyloid42 Peptide in Escherichia Coli." *Protein expression and purification*64(1): 55–62.

Zheng, H. and Koo, E. H. 2011. Biology and pathophysiology of the amyloid precursor protein.*Molecular neurodegeneration*, 6(1):27.

Zou Kun , Kim Daesung, Kakio Atsuko, Byun Kyunghee, Gong Jian-Sheng, Kim Jaewoo, Kim Myeungju, Sawamura Naoya, Nishimoto Sei-ichi, Matsuzaki Katsumi, Lee Bonghee, Yangisawa Katsuhiko, Michikawa Makoto. 2003. " Amyloid beta-protein (Abeta)1–40 protects neurons from damage induced by Abeta1–42 in culture and in rat brain." *Journal of Neurochemistry* 87 (3), 609–619.

European Commission (2014) Neurodegenerative Disorders. http://ec.europa.eu/health/major_chronic_diseases/diseases/brain_neurological/index_en.htm. Accessed 26 October 2014.

Alzherimer's Disease International (2014) World Alzheimer's Reports. http://www.alz.co.uk/research/world-report. Accessed 26 October 2014.

Chapter 5

"Recombinant IDPs for NMR. Tips and tricks"

Eduardo Calcada [a], Magdalena Korsak [a,b], Tatiana Kozyreva [b]

[a]Magnetic resonance Center (CERM), University of Florence, Via L. Sacconi 6, 50019 Sesto Fiorentino, Italy

[b]Giotto Biotech, Via Madonna del Piano 6, 50019 Sesto Fiorentino, Italy

(Book chapter as a part of *"Intrinsically disordered protein by NMR"* book, Springer 2014)

(In preparation)

Chapter 5
Recombinant IDPs for NMR
Tips and tricks

Recombinant IDPs for NMR

Tips and tricks

It is becoming evident that intrinsically disordered proteins (IDPs) are not fully disordered, but have all sorts of transient, short, and long-range structural organisations that are function-related.

The structural and functional study of biomolecules is a highly interdisciplinary field that requires a correlation between different biophysical techniques. Although at first glance the study of IDPs seems very similar to the traditional analysis of structured proteins, specific skills and different approaches are needed to undergo IDP characterization (Uversky 2011). Structural biology requires a large number of steps to convert DNA sequence information into protein samples, including cloning, expression and purification strategy. The following is intended to assist in the sample preparation of IDPs from genome browsing to sample preparation and analysis. Different methodologies will be addressed with special tips and tricks highlighted that are helpful for overcoming common drawbacks/barriers usually found when working with IDPs.

Genome browsing and bioinformatics analysis

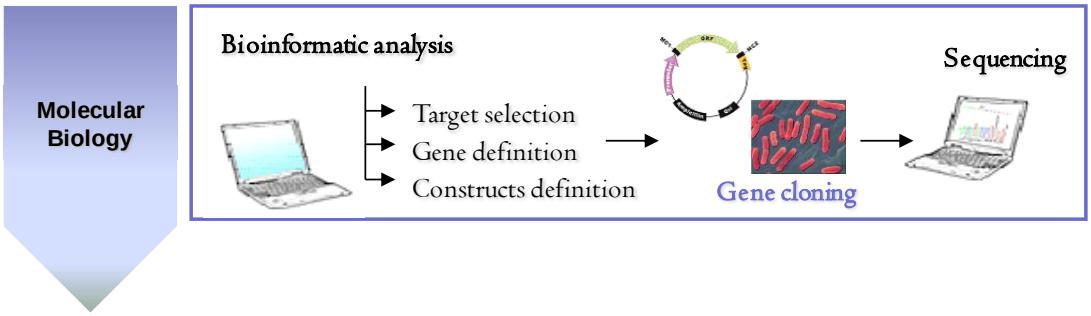

Intrinsic structural disorder is a widespread phenomenon, especially in eukaryotes, where conservative bioinformatics predictions suggest that 5%–15% of proteins are IDPs, and about 35-50% of proteins have intrinsically disordered regions (IDRs) longer than 30 residues (Ward et al. 2004). It has been accepted that disorder is needed for signalling among various living systems, and increases with organism complexity (Dunker and Obradovic 2001). Indeed, 75% of the signalling proteins in mammals are predicted to contain long disordered regions (Dunker et al. 2008).

The web tools currently available are incredibly easy to use and, in most cases, very accurate information can be obtained quickly. Advanced genome tools for studying biology made an incredible amount of biological data available with a concomitant proliferation of biological databases and web software tools, i.e. data banks containing information on DNA, protein sequences, expression profiles, protein ensembles and structures. One example is the recently created protein ensemble database for IDPs (Varadi et al. 2013).

The first step to start the work with a new protein is the sequence analysis, both if you are a protein hunter looking for an interesting target to study, as well if you've just joined a scientific work already ongoing. First of all analysis of the DNA sequence through bioinformatic tools might be helpful to order the synthetic gene of your target protein specifically adapted to the expression system of choice. Later on you can analyze the domain

composition, presence of signal peptide and inert-membrane helixes, as well as disorder regions in order to create suitable expression constructs. Even if the bioinformatic analysis is just the prediction, anyway it can be useful in order to get the preliminary information of the target protein. In case of IDPs the prediction of disorder domains is essential.

A number of approaches have been developed to predict regions of protein disorder. These methods can be broadly classified into several different categories: *ab initio*, clustering and meta or consensus.

The majority of these predictors are available through public servers, and links to many of them can be found in the "Disordered Protein Database" (Disprot)[1], (Sickmeier et al. 2007), the "Database of Disordered Protein Prediction" (D^2P^2)[2] (Oates et al. 2013), and in the recently created IDPbyNMR website[3]

The big group of a prediction methods belong to the ab initio group and depend almost exclusively on sequence information. In other words, nothing more than the primary sequence is needed in order to make a prediction. Disordered regions in proteins are predicted using features extracted from the primary sequence in conjunction with statistical models. In clustering methods, tertiary structure models are predicted for the target protein, and then these models are superimposed by carrying out structural alignments.

The generation of disorder prediction tools started from a comparison between the amino acid sequences of IDPs and those of structured globular proteins, which resulted in a number of significant differences including amino acid composition, sequence complexity, hydrophobicity, aromaticity, charge, and flexibility (Dunker et al. 2001). For example, IDPs are significantly depleted in hydrophobic (Ile, Leu, and Val) and aromatic (Trp, Tyr, and Phe)

[1] http://www.dabi.temple.edu/disprot/index.php
[2] http://d2p2.pro
[3] http://www.idpbynmr.eu/home

amino acid residues, which form and stabilize the hydrophobic core of folded globular proteins. These residues are called order-promoting amino acids. On the other hand, IDPs/IDRs are substantially rich in polar (Arg, Gln, Glu, Lys, and Ser) and structure-breaking (Gly and Pro) disorder-promoting amino acid residues (Dunker et al. 2001; Radivojac et al. 2007). Among the twenty common amino acid residues, proline is the most disordered-promoting (Theillet et al. 2013). The accuracy of predictors is regularly assessed as part of the Critical Assessment of Structure Prediction (CASP) experiment (Monastyrskyy *et al*., 2011). It is therefore now possible to predict the tendency of a polypeptide chain to be disordered based on its primary sequence with an approximate accuracy of 80% (He *et al*., 2009).

To obtain more accurate disorder predictions, a good option is the use of meta predictors such as PONDR-FIT (Xue *et al*., 2010), which combine the output of several individual predictors.

After obtaining the preliminary view of your sequence with information about folded and unfolded regions, you can think about creating the set of constructs, omitting unfolded regions, shortening the last ones, or simply substituting some amino acid so as to increase order.

Tip 1 – Consider the possibility of creating different domain constructs as well as the full-length construct.

IDPs are often able to bind to different partners or to act as hub proteins, and in this way play an important role in a variety of different processes. IDPs are particularly relevant for viruses, which need to exploit simple amino acid sequences (short linear motifs, SLiMs), which are well-exposed and ready to function, in order to interact with crucial key proteins from the host organism. They are also known as molecular recognition features **(**MoRFs) and different tools

for their prediction are available such as SLiMfinder[4] (Davey et al. 2010), MoRFpred[5] (Disfani et al. 2012) and Anchor[6] (Mészáros, Simon, and Dosztányi 2009).

Using the BLAST alignment it is possible to establish the homology of the target protein with some proteins with known three-dimensional structure. In this case one can consider the use of the MODELLER software to generate a homology comparative structural model of the target protein. The development of comparative software allows the study of the homology modelling of the protein's three-dimensional structures (Eswar et al. 2006). With this tool, the user provides a sequence alignment of the protein of interest and obtains a model based on known related Protein Data Bank (PDB) structures. For example, a model containing all of the non-hydrogen atoms calculated by comparative protein structure modelling based on the satisfaction of spatial restraints can be obtained using MODELLER (Šali and Blundell 1993). MODELLER also performs *de novo* modelling of loops in protein structures, multiple alignments of protein sequences and structures, optimization of various models of protein structure with respect to a defined objective, searching of sequence databases, clustering, comparison of protein structures, and so on.

Once the protein sequence has been defined, the easiest way to obtain the corresponding gene is by ordering the synthesized gene of interest suitable for your expression system. With the development of new instruments that facilitate the production of biological material, the synthesis of genes containing the DNA sequence of a target protein is now feasible. Many companies such as Invitrogen's GenArt®, OriGene, Eurofins MWG Operon, GenScrip, and DNA2.0 among others provide web tools to order these genes, with several possibilities and strategies, including the optimization of the codons for the specific expression organism. It is important to highlight that the over-expression of human proteins in *E. coli* systems could be

[4] http://bioware.ucd.ie/~compass/biowareweb/Server_pages/slimfinder.php
[5] http://biomine-ws.ece.ualberta.ca/MoRFpred/index.html
[6] http://anchor.enzim.hu

compromised, resulting in low expression yields, if the open reading frame (ORF) of the protein contains codons infrequently used by *E. coli*, the so-called "rare codons". In particular, codons for arginine (AGG, AGA, CGA), isoleucine (ATA), leucine (CTA) and proline (CCC) should be avoided (Schenk et al. 1995). Different web tools, such as those offered by Genscript[7] and the United States National Institutes of Health (NIH)[8], are available to check the presence of rare codons related to the desired expression system. Nevertheless, the gene of interest can be directly cloned from the organism cDNA, if available. The cloning strategy should be designed carefully, as it could be the basis of a successful work.

Tip 2 – IDPs usually have a high proline content. Avoid rare codons in the DNA sequence, as they could lead to a low expression yields.

Expression plasmid generation

The standard procedure to express a recombinant protein is to carry out a screening of different constructs to identify the most efficient conditions for downstream purposes. The first step of the cloning process consists of the amplification of the target gene from a DNA template or plasmids through a polymerase chain reaction (PCR) using specific primers. After purification, the amplified product is inserted into a specific expression vector. Different vectors may be selected in order to obtain native protein or protein fused with different tags. The tags vary in size starting from 6-His to fusion proteins of 10-20 kDa o even 40 kDa proteins such as maltose-binding protein (MBP). They can enhance the expression level, increase solubility, and be very useful for the subsequent purification procedure due to their chemical properties (Esposito and Chatterjee 2006). Later on these tags may be removed by

[7] http://www.genscript.com/cgi-bin/tools/rare_codon_analysis
[8] http://nihserver.mbi.ucla.edu/RACC/

proteolytic cleavage with specific enzymes such as factor Xa, enterokinase (EK) or tobacco etch virus (TEV) protease (Arnau et al. 2006; Malhotra 2009).

Tip 3 – Even if the tags are considered a good strategy, always consider expressing the native protein sequence.

The classic method to insert an amplified PCR product into a vector is to use restriction enzymes that cleave DNA at specific recognition sites. Both the DNA and the cloning vector have to be treated with two restriction enzymes that create compatible ends. Later on these ends are joined together by a ligation reaction performed by the bacteriophage T4 DNA ligase. Finally an aliquot of the product of the reaction is transformed in DH5α *E. coli* competent cells and positive clones are screened by PCR screening followed by DNA sequencing. However, the classic cloning strategy is sometimes not feasible for the preparation of different constructs in parallel due to the lack of the suitable restriction sites common for the target gene and available vectors. Together with low efficiency and false positive clones, this technique is not the best for high-throughput cloning. Therefore, other cloning strategies have been developed that exploit ligation-independent cloning such as Gateway® (Invitrogen) and most recently Electra™ (DNA2.0) (Katzen 2007).

Tip 4 – Many companies offer the possibility to clone the synthetic gene directly into a desired expression plasmid.

Gateway® cloning technology has been one of the most used strategies and enables rapid and highly efficient simultaneous transfer of DNA sequences into multiple vector systems for protein expression and functional analysis while maintaining orientation and reading frame. It basically consists of the generation of an expression silent entry clone that can be further recombined in the several expression vectors without the use of any restriction enzyme, taking advantage of the site-specific recombination properties of bacteriophage lambda. There are

many ways to create an entry clone but the most straightforward method is directional TOPO® cloning. The ligation reaction of the PCR product to the pENTR vector is accomplished by topoisomerase I. After isolation of the entry clone, the second step is to generate an expression vector. This is done by recombination of the gene on the entry clone with the final expression vector, performed by LR Clonase®. The different antibiotic resistances of the vectors allow fast clone selection. A large selection of Gateway expression vectors is available for the expression of native proteins as well as proteins fused with tags. One of the versions of the Gateway Cloning System is pENTR/TEV/D-TOPO. This version of the Gateway Cloning System includes the TEV recognition site on the N-terminus of the protein. The following expression destination vectors can be used in order to create the expression clones: pDEST-17 (conferring 6x histidine N-terminus), pETG-30A (conferring GST plus 6x histidine N-terminus), and pDEST-His-MBP (conferring MBP plus 6x histidine N-terminus), pETG-20A (conferring Trx plus 6x histidine N-terminus), and pTH34 (conferring GB1 plus 6x histidine N-terminus), among others. It is important to highlight that the use of this methodology will result in the expression protein including extra residues on the N-terminus. For example, using the expression vector pDEST-17 that contains the 6xHis tag, the expressed and purified target protein will have 44 extra amino acids. After tag removal using TEV protease, the final construct will contain 4 extra residues on the N-terminus, GSFT.

Tip 5 – Added fusion tags can be removed upon protease cleavage, but many of them can result in the addition of an extra amino acid sequence.

Site-directed mutagenesis is a standard technique used to make point mutations, replace amino acids, and delete or insert single or multiple adjacent amino acids. Point mutations in which a single nucleotide is exchanged but the new codon specifies the same amino acid are called silent mutations. They basically code for the same amino acid, and are an easy way to avoid the "rare codons" that may decrease expression yield. This method uses the double-

stranded DNA vector template containing the target gene and two complementary synthetic oligonucleotide primers, both containing the desired mutation. The primers are mixed with the DNA vector template and extended during PCR cycles performed by a high fidelity DNA polymerase. The PCR product is then treated with DpnI, an endonuclease that will digest the DNA template due to its high specificity to Dam methylated and hemimethylated DNA isolated from *E. coli* strains. The new copies of the DNA PCR product were never methylated and are thus not digested. The digested solution is then transformed into XL1-Blue super-competent cells and subsequently subjected to sequencing analysis.

Tip 6 – Use site-directed mutagenesis to create silent mutations of rare codons, increasing the expression yield.

Protein expression

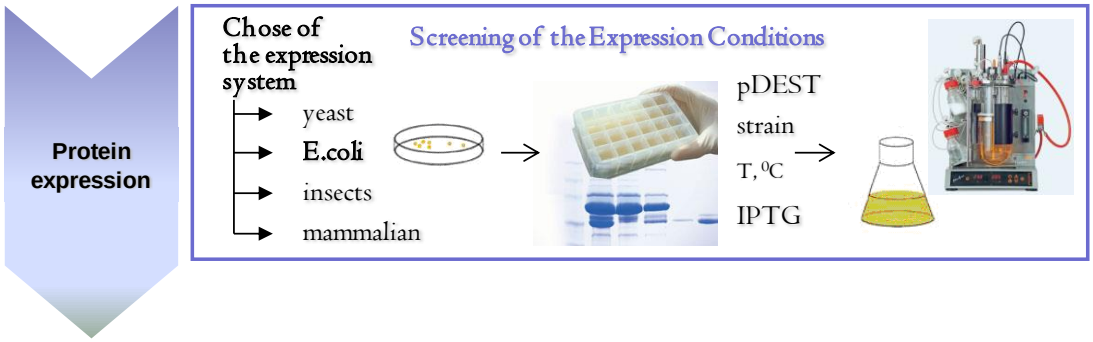

Several host systems are available for protein production including fungi, plant, bacteria, insect, yeast and mammalian cells (Shatzman 1995). The choice of the expression system for the high-level production of recombinant proteins depends on many factors, including biological activity of the target protein, post-translational modifications, cell growth features, intracellular and extracellular characteristics, and expression levels. The many advantages of the use of *Escherichia coli* (*E. coli)* have ensured that it has remained a valuable organism for the high-level production of recombinant proteins; it is the easiest, quickest and cheapest

expression system (Tong, Yamamoto, and Tanaka 2008). Protein expression using the yeast expression system is also a good solution; however, for ^{13}C labelling, which requires a correct promoter for the carbon source (Weinhandl et al. 2014), it can be an expensive solution compared with the *E. coli* expression system for isotopic proteins. A wealth of biochemical and genetic knowledge of *E. coli* has driven the development of a variety of strategies for achieving high-level protein expression. The major challenges for obtaining high protein yields at low cost involve several aspects such as expression vector design, gene dosage, transcriptional regulation (promoter), mRNA stability, translational regulation (initiation and termination), host design considerations, codon usage, and the fermentation factors available for manipulating the expression conditions (Jana and Deb 2005).

Tip 7 – Expression of isotopically labelled proteins in *E. coli* is much cheaper as comparing to yeast due to carbon source costs.

The expression condition should be tested once the expression system has been selected. Therefore, the best approach is to use parallel test expression strategies (Lesley 2009). A preliminary expression test can be performed using a small volume in order to find the best conditions to be reproduced in large volumes to obtain soluble recombinant protein. It is important to take the following factors into consideration for protein expression: culture medium, temperature, optical density, isopropyl β-D-1-thiogalactopyranoside (IPTG) inducer concentrations and induction time. A library of different *E. coli* strains possessing various properties that could be advantageous in the expression of a certain protein is available. Common examples are the *E. coli* strains BL21(DE3) (the standard version) or some variants such as BL21(DE3)pLysS, which encode the T7 lysozyme to decrease the background expression level of target genes under the control of the T7 promoter, but do not interfere with expression levels following induction by IPTG, Rosetta(DE3) and Codon Plus for genes

containing rare codons, Origami(DE3) for proteins containing disulfide bridges, and Gold(DE3) for increasing expression yields.

Depending on the research purpose the cells can be grown in different types of media: rich media, lysogeny broth (LB), 2x yeast extract and tryptone broth (YT), Terrific broth, NZY and the minimal media M9. When labelled protein is necessary, the M9 is supplemented with [C^{13}] and [N^{15}] sources. In order to increase the expression yield of isotopically labelled protein, one good solution could be the use of the Marley method (Marley, Lu, and Bracken 2001). The cells transformed with the expression plasmid are initially grown in rich medium until high optical densities, and are then centrifuged and exchanged into an isotopically defined minimal media enriched with $(^{15}NH_4)_2SO_4$ (1 g/L) and (^{13}C) glucose (4 g/L). Labelled protein can also be produced in commercially available and isotopically enriched rich media, e.g. Silantes. This could be particularly advantageous for the expression of deuterated labelled protein in terms of a simplified cell adaptation process. Small-scale test expression is the first step in the expression of the target protein; it is important to reproduce the expression conditions required for large-scale production as much as possible.

Tip 8 – In some cases the isotopically labelled carbon and nitrogen sources may give different expression yields and protein solubility. Consider a small test expression using isotopically labelled nutrients.

Zinc is essential for many cellular processes, including DNA synthesis, transcription, and translation, but an excess can be toxic (Babich and Stotzky 1978; Kindermann et al. 2005). In order to find the optimal amount of zinc additive, different trials should be performed using controlled minimal media instead of rich LB (Outten and O'Halloran 2001). The amount of zinc can be tested by comparing zinc-depleted cultures at a concentration range of 10 - 400 μM of $ZnCl_2$ and $ZnSO_4$ addition.

Tip 9 – When working with a metalloprotein, the expression tests should be performed taking into account the concentration of the required metal.

In order to avoid hundreds of different screening conditions, one can start with a couple of conditions and alter specific conditions if needed and according to the preliminary results obtained. Three different *E. coli* strains induced at a single optical density of 0.6, using a single IPTG concentration of 0.5 mM, three different expression temperatures (17, 30 and 37ºC) and two expression times (4 h and 16 h) will result in 18 different conditions. In case of non-satisfactory results, one can try different *E. coli* strains, optical densities or IPTG concentrations. Cells should be harvested, disrupted and normalized to the final optical density. The presence of soluble protein is checked with sodium dodecyl sulfate polyacrylamide gel electrophoresis (SDS-PAGE).

One important aspect of IDPs when running an SDS-PAGE is abnormal protein size. IDPs typically run on SDS-PAGE as though they exhibit a higher molecular mass. This aberrant migration occurs due to the different amino acid composition caused by the high acidic residue content of some IDPs (Armstrong and Roman 1993; Graceffa, Jancsó, and Mabuchi 1992).

Tip 10 – In some cases the isotopically labelled carbon and nitrogen sources may give different expression yields and protein solubility. Consider a small test expression using isotopically labelled nutrients.

If all the trials to obtain soluble protein fail, the insoluble fraction can be recovered in the refolding process.

Protein purification

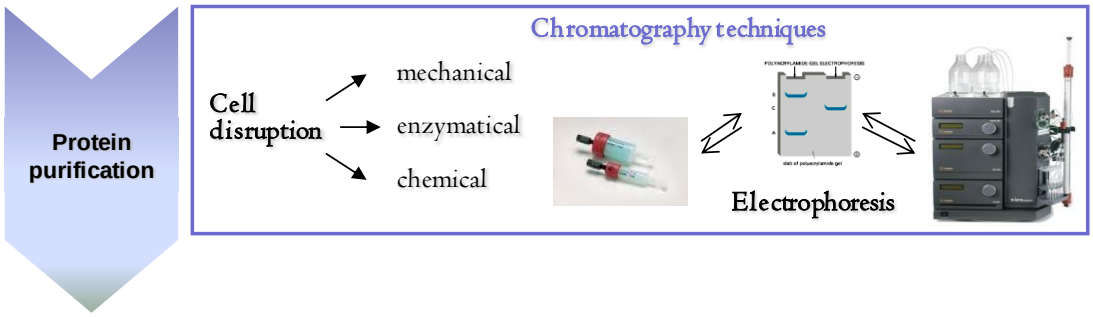

The protein purification strategies rely on the biophysical and biochemical properties of each specific protein. The purification strategy could be summarized in three main steps (Figure 5.1), which may or may not be performed depending on the required purity of the final sample. In the first step the target protein is isolated from the cells and protected from possible degradation. The main bulk of impurities could then be removed by heating, passing the lysate through ion exchange or affinity columns. In the final step the samples could undergo size exclusion or high-resolution chromatography for the removal of trace impurities.

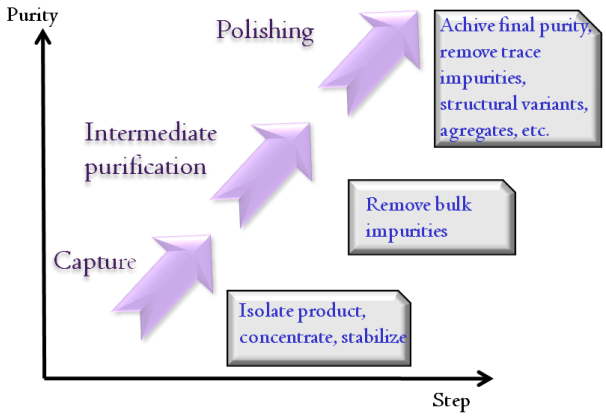

Figure 5.1. Three step purification strategy

The peculiar amino acid composition of IDPs will contribute to specific biophysical properties that are completely different from those of folded proteins. A set of preliminary experimental trials should be performed to learn which reagents might be present during the

purification, which must be avoided, and under which conditions the protein has to be stored. Designing the protein purification strategy for a new protein from scratch requires a preliminary bioinformatics study to predict several biochemical and biophysical characteristics as well as the study of previously published purification strategies (Hunt 2005). Several factors should be taken into account for both soluble and unsoluble proteins, including: ionic strength, pH, temperature, oxygen concentration, and protein concentration. For example, if the protein contains several free cysteine residues, anaerobic purification methods and the use of reducing agents may be required to avoid the formation of non-physiological multimers and oligomers. The localization of the expressed protein within the cell (soluble in cytoplasm or periplasm, or present in inclusion bodies (IBs)) makes a strong contribution to the choice of the purification strategy (Linn 2009). In each case the isolation is performed in different ways. Assuming the protein was not excreted into the growth medium, cell lysis is the first step for protein purification. The disruption of the cells can be performed through several techniques, ranging from mechanical to detergent-based methods. For instance, the French press is an efficient method, though it heats the final lysate, while freeze-thaw or enzymatic and detergent lysis are considered mild methods but less efficient. In the present work, the cell disruption was performed by sonication, which comprises pulsed, high frequency sound waves to mechanically agitate and lyse the cells. The isolation of proteins using sonication should be done carefully because the mechanical wave energy will heat the sample. To avoid sample warming, sonication should be performed using an ice bath and with short pulses, with intervals to allow the temperature to decrease. Sonication methods can be also performed inside an anaerobic chamber (glove box) for anaerobic purification strategies. If degradation of the protein target has been observed during the purification steps, different cocktails of protease inhibitors can be directly added to the lysis buffer.

IDPs are prone to degradation due to their intrinsically disordered properties, which make the amino acid chain fairly exposed and allow easy access to proteases. The use of protease inhibitor cocktails starting from the first step of protein purification may be a good solution to avoid IDP degradation. Working at low temperatures may also help decrease protease activity. Conversely, some IDPs are thermo-stable at high temperatures, which can be used as an initial purification step. By warming the cell extract, several folded proteins including proteases will precipitate and can be easily separated by centrifugation. High temperature can cause some conformational changes in protein structure. Comparison of the pure protein sample obtained with and without heating should be performed by using circular dichroism (CD), dynamic light scattering (DLS) and nuclear magnetic resonance (NMR). Different temperatures and durations of sample exposure to the heat can be checked in order to find the optimal conditions where the IDP can be isolated without being damaged.

Tip 11 – Check how thermo-stable your IDP is. It may be helpful for the purification steps.

Once the protein fraction is isolated from the cells, the following purification step can be performed in a multitude of chromatography runs. The methodology should always be optimized to reach an efficient protocol in terms of yield, speed and costs. Among all the different chromatography techniques, we will describe the three most used ones: immobilised metal ion affinity chromatography (IMAC), ion exchange chromatography (IEX) and size exclusion chromatography (SEC).

Immobilized metal ion affinity chromatography (IMAC) is currently the most used affinity technique exploiting the interaction between chelated transition metal ions (such as Zn^{2+} or Ni^{2+}) and the side chains of specific amino acids (such as histidines) on the protein.

Tip 12 – Take advantage of the specific metal affinity of your protein in the choice of metal ions for IMAC.

In basic terms, by using IMAC the target protein is tightly bound to the resin matrix and the impurities are washed out with increasing concentrations of imidazole, which acts as a competitive agent. At higher imidazole concentrations the target protein is eluted at an almost pure concentration (Block et al. 2009).

Fused proteins can be separated by enzymatic digestion to cleave the tags. After tag cleavage the separation of tag and target protein can be accomplished by the second IMAC chromatography step.

Tip 13 –To avoid imidazole during the IMAC protein elution process, an elution buffer with low pH could be used.

IEX separates proteins on the basis of a reversible interaction between the polypeptide chain and a specific charge ligand attached to a chromatographic matrix. The isoelectric point (pI) of the target protein must be known. The sample is loaded in conditions that favour specific binding such as calibrated pH and low ionic strength salt concentration in order to enhance the interaction between the target protein and column matrix. The unbound impurities are washed out and the bound protein is eluted by changing the pH or ionic strength of the elution buffer. If the overall net charge of the protein is positive, a cationic IEX resin must be used, while if it is negative, an anionic IEX resin must be used. The buffer pH should be at least ± 1 unit different from the protein pI.

SEC is a separation technique based on the hydrodynamic radius of the proteins. The column matrix is composed of precisely sized beads containing pores of given sizes. Larger proteins whose hydrodynamic dimensions are too big to fit inside any pore will only have access to the

mobile phase between the beads, and will be excluded as they will just follow the solvent flow and reach the end of the column before molecules of a smaller size. Proteins with smaller hydrodynamic dimensions will be drawn into the pores by diffusion, and have access to the mobile phase inside and between the beads. Therefore, smaller molecules will have a long distance to cross with several small retention times between the diffusion movements through the bead pores. Due to larger retention, smaller hydrodynamic molecules will elute last during the size exclusion separation. SEC can be used to separate proteins by size and shape, to exchange the buffer, and also to isolate protein mixtures and separate monomers, multimers or oligomers. In the case of folded proteins, it can also be used to determine the molecular mass by performing a molecular weight distribution analysis using available standards.

Tip 14 - Hydrodynamic volume is one of the most important IDP biophysical parameters to be taken into consideration.

SEC profiles are therefore dependent on the hydrodynamic volume of a protein, which is one of the most important and fundamental structural parameters of a protein molecule. Hydrodynamic volume is a prerequisite for an accurate classification of a protein conformation. It changes dramatically depending on whether the protein hydrodynamic dimension is compact like a folded protein or extended or partially extended like an IDP.

Tip 15 – Comparison between the protein in native conditions and in the presence of a chaotropic agent allows a better understanding of how compact or extended the IDP hydrodynamic volume is. A comparative analysis can easily be addressed by SEC, CD, DLS and SAXS.

Comparing two proteins with the same molecular weight, a well-folded protein will have a smaller hydrodynamic radius while an IDP will have a bigger one, behaving like a large folded protein with SEC. The SEC retention times for a folded protein and an IDP of the same

molecular mass will therefore be different and the IDP will elute first. SEC has been used for over three decades for the separation of unfolded and folded proteins (Gupta 1983). However, due to the particular characteristics of IDPs, SEC can be used for the analytical study of the conformational IDP properties in solution where the size and shape of molecules are the prime separation parameters (Uversky 2013). SEC is usually performed as the last purification step for the preparation of high purity samples. A column of at least one meter high connected to a water thermostatic cooling system at 4ºC can be one of the best solutions for separating proteins with large hydrodynamic volumes.

Tip 16 – When using analytical SEC for IDP studies, it is important to use standard IDPs such as α-synuclein in the same buffer conditions and temperatures as the target IDP.

Purifying and refolding a protein from the insoluble fraction could be a challenging task and should be planned carefully. The strategy can be based on a previous bioinformatics analysis of the target protein combined with knowledge of the state-of-the-art of similar protein systems. Although many protocols have already been published and summarized in many reviews and book chapters (Burgess, Richard, and Murray 2009; Cowieson et al. 2006; Qoronfleh, Hesterberg, and Seefeldt 2007; Singh et al. 2005; Vincentelli et al. 2004), each protein is unique and requires a specific approach to the refolding process.

The first step in refolding is solubilisation of the inclusion bodies. The solubilising agent/denaturant could be a chaotropic agent such as GuHCl and urea, or a detergent, and should be prepared in a controlled pH buffer. As for the other techniques already described in this work, the key concept for refolding is the systematic, parallel screening of multiple refolding conditions. Many additives may prove useful in refolding, but preventing aggregation and precipitation upon refolding is crucial for refolding at low protein concentrations. However, many variables in refolding should be controlled such as pH,

temperature, salt concentration, redox environment, and the presence of divalent metal ions.

Redox agents

Various redox pairs can be used including reduced and oxidized cysteine or glutathione as well as a reducing agent such as β-mercaptoethanol (BME), dithiothreitol (DTT) or tris (2-carboxyethyl) phosphine hydrochloride (TCEP) to control the oxidation state of the protein. Since the cytoplasm of *E. coli* is highly reducing, most internal proteins are in the reduced state. If the protein contains both native disulfide bonds and free cysteines, the red/ox couple should be introduced into the refolding system in order to achieve optimal native disulfide bond formation, keeping native free cysteine residues. The free cysteines might induce incorrect disulfide bridge formation, especially at high protein concentrations. It could be advantageous to use a high concentration of the reducing agents, e.g. DTT and TCEP.

Tip 17 - Consider the presence of disulfide bridges; the addition of a high concentration of the reductant can break them.

Salt concentration

To prevent undesirable hydrophobic interactions, the ionic strength of the solution could be increased by the addition of salt starting from 150 mM.

pH

In general the pH of the buffer should be at least one pH unit away from the pI in order to avoid a zero net charge of the protein, making it prone to precipitation. Some protocols rely only on a single pH refolding procedure (Coutard et al. 2012).

Temperature

Most refolding procedures are carried out at room temperature, which is low enough to

prevent thermal damage to the protein and high enough to increase the thermal motion of the molecules, an important aspect that allows them to reach their native state.

Proline and arginine

Proline is considered an osmoprotectant and has been found to be effective in increasing solubility both *in vitro* and *in vivo* (Ignatova and Gierasch 2006). Arginine can decrease aggregation by slowing the rate of protein–protein interactions by supramolecular assembly formation in solution. However, effective concentrations are reported to be in the range of 0.5–1.0 M (Das et al. 2007).

Glycerol

Glycerol has been found to be an excellent refolding additive in many cases, as is usually used in the 5–30% range.

Detergents

Detergents can increase solubility, preventing aggregation during refolding. At low concentrations they bind weakly to exposed hydrophobic regions, preventing aggregation.

As their concentration decreases they dissociate and allow reformation of the native structure. At high concentrations detergents are denaturants, but at low concentrations they can act as an artificial chaperone, promoting refolding without aggregation. One important aspect of detergents is the critical micelle concentration (CMC), the concentration at which micelles begin to form. The CMC value can be subject to buffer conditions such as pH and ionic strength. The CMC should be checked once for each buffer system as the manufacturer only provides a few values/conditions. Tables exist that report several values for each specific buffer condition (Brito and Vaz 1986; Jumpertz et al. 2011).

Once the protein of interest has been solubilised and all the refolding buffer conditions have been defined, refolding can be attempted. The refolding procedure is the removal of the denaturant agent, allowing the protein to reach its native state. Refolding can therefore be performed by dilution, multi-step dialysis, single dialysis, or with on-column refolding. Dialysis is one of the most used methods but it is time- and reagent-consuming. Affinity tagging of the recombinant protein can give the possibility of efficient and rapid on-column refolding and purification in a few steps just performing a washing series. If it doesn't precipitate inside the column, the refolded protein can be further eluted. Alternatively, dilution refolding can be performed by reverse dilution, the addition of refolding buffer to denatured protein with mixing between each addition, flash dilution, the addition of denatured protein to refolding buffer quickly, and drip dilution**,** the addition of denatured protein to refolding buffer very slowly, drop-by-drop, allowing refolding at low concentration.

Several commercial products have been developed to help identify suitable refolding conditions such as EMD/Novagen's iFOLD kits, Pierce Biotechnology's ProMatrix™ and AthenaES's QuickFold™.

Sample handling of intrinsically disordered proteins

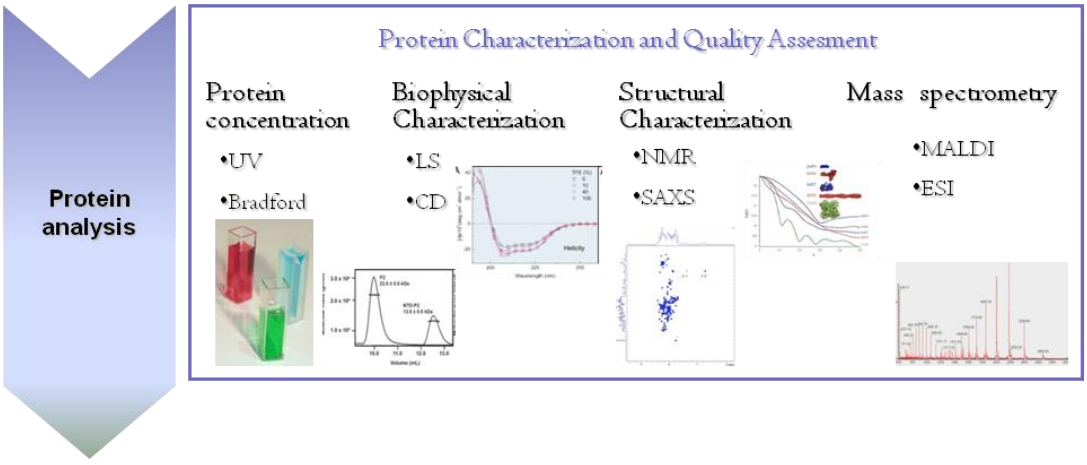

The preparation of samples for different biophysical and biochemical characterisations should be prepared according to the technical limits of each technique/method.

Stability

Stability is one of the first conditions to check. One can try to perform the degradation test at various temperatures in order to understand if the protein is susceptible to degradation.

Tip 18 – For the sake of protein long-term stability, work in the presence of protease inhibitor cocktails and at low temperatures during the purification steps.

Anaerobic purification

Proteins containing cysteine residues must be handled inside an anaerobic chamber under nitrogen atmosphere to prevent the oxidation of cysteine residues. All buffers used for the purification and sample preparation steps may be extensively degassed with nitrogen and argon. Reducing agents may be added to keep the cysteine residues reduced.

Reducing agents

Reducing agents can be exogenous sulfhydryl containing reducing agents such as DTT, or non-sulfhydryl reducing agents such as TCEP. The control of the redox state of the IDP target is crucial for a successful purification. The optimal reducing activity of DTT is in the 6.5 - 9.0 pH range, while TCEP has a wide optimal reducing activity pH range spanning from 1.5 - 9.0. In some cases TCEP was reported to be more useful than DTT for protein sample preparation (Getz et al. 1999; Krezel et al. 2003).

Once the protein sample is pure and stable conditions have been discovered, it is important to know its concentration to apply in different biophysical methods.

Methods of the protein concentration measurements

Ultraviolet (UV)–visible spectroscopy applied to the protein research field can be used for many applications including detection of eluting components in high performance liquid chromatography (HPLC), the determination of the oxidation state of a metalloprotein centre of a cofactor, as well as the determination of the maximum absorbance of proteins and DNA for measurement of their concentrations. DNA quantification is based on purine and pyrimidine absorption, which is maximum around 260 nm. Proteins contain aromatic amino acid residues, which absorb light in the UV-range with absorption maxima around 280 nm. These amino acids are tryptophan (Trp), tyrosine (Tyr), and phenylalanine (Phe). The Trp, Tyr, and Phe absorption spectra of IDPs can be compromised as typically IDPs are depleted of these residues (Dunker et al. 2001).

The concentrations can be calculated using the Beer-Lambert law, $A = \varepsilon cl$, where A is the absorbance value at the chosen wavelength, c is the sample concentration (M) and l is the length of the light path through the sample (cm). The absorption spectrum of a protein is usually normalized to a concentration unit and cell width, and thus depends on the protein specific molar absorption coefficient ε and the measured wavelength λ absorption values. The theoretical molar extinction coefficient can be calculated, for example using the ExPASyProtparam[9] tool (Gasteiger et al. 2005).

Tip 19 - Some reagents used during the purification procedures such as imidazole or DTT exhibit absorbance at 280 nm. Remember to use the blank sample containing the same concentration of these reagents that is present in your sample.

When the IDP doesn't contain any aromatic residues, a refractometer instrument can be a good option for measuring protein concentration. This method is very sensitive to buffer

[9] http://web.expasy.org/ protparam/

conditions, so a standard curve should be created in the exact same buffer as the protein of interest. The preparation of a similar buffer will not work. The last step dialysis buffer, or even better the flow-through buffer, should be used when concentrating a pure protein sample. The same buffer should be used for the preparation of the bovine serum albumin (BSA) or lysozyme solutions in order to create a standard curve measured on the refractometer instrument. The target protein concentration can then be measured with high accuracy by interpolation.

Tip 20 – A refractometer is very useful for IDPs that lack aromatic residues, but a standard curve should be created with exactly the same buffer as the one of the target IDP.

Complementary biophysical techniques

NMR is known as the best technique to study IDPs at atomic level, providing detailed residue-specific information. However, it is useful to complement the information obtained from NMR with other biophysical methodologies to better understand all kinds of function-related transient, short, and long-range structural organisations.

Depends on the specific type of information, needed to complete NMR data, different biophysical methods can be implemented. Among many various techniques, mass spectrometry (MS), Small Angle X-ray Scattering (SAXS), Circular Dichroism (CD) as well as Dynamic Light Scattering (DLS) are the excellent complementation of NMR data. In this section we will focus our attention on IDP sample preparation for different biophysical techniques.

Mass spectrometry (MS) is an important emerging method for the protein characterization. The two primary methods for soft ionization of whole proteins are electrospray ionization (ESI) and matrix – assisted laser desorption/ionization (MALDI) (Romanova et al. 2009). They are strategies that can be used to retrieve accurate molecular weight measurements,

determine the purity of a sample, verify amino acid substitutions, detect post-translational modifications, calculate the number of disulphide bridges, analyze intermolecular interactions (e.g. protein-protein binding). Application of hydrogen-deuterium exchange mass spectroscopy can provide valuable information about localization of flexible regions and protein folding (Bobst and Kaltashow, 2012). Ion – mass spectrometry (IMS-MS) can be successfully applied for the identification of different aggregated assemblies and characterization of various conformation forms of the protein, which is especially important in terms of IDPs (Vlad et all 2012). This technology has the potential to separate and discern different conformational families even for IDPs, that the conformational properties of different forms of the same protein can be compared and structural events taking place during the transition from co-populated conformations can be monitored, giving interesting insights into their respective conformational behavior patterns (Knapman et al. 2013).

Tip 21 – Use MS as one of the complementary techniques to characterize the different conformational states of IDPs.

CD is an excellent tool that allows the quick determination of secondary structure and folding properties (e.g. arrangement of peptide bonds in secondary structure elements such as helices and strands) of proteins or nucleic acids in solution and is based on differential absorption of left- and right-handed circularly polarized light.

In proteins the major optically active groups are the amide bonds of the peptide backbone (peptide bond: absorption below 240 nm, aromatic amino acid side chains: absorption in the range 260 to 320 nm, and disulphide bonds: weak broad absorption bands centred around 260 nm), typically disposed in highly ordered arrays such as alpha-helices or beta-pleated sheets. All alpha- helices proteins display a strong positive band (at 191–193 nm) and an intense

negative band with two peaks at 208 and 222 nm. Beta-sheets proteins have a negative band at 210–225 nm and a stronger positive band at 190–200 nm. Instead unordered peptides and denatured proteins have a strong negative band at 195–200 nm (Martin and Schilstra, 2008).

IDPs present particular CD characteristics different from those of folded proteins and also different from random coil polypeptides, presenting specific conformational preferences and thus revealing partially populated secondary content. CD allows to analyze stability as well as alterations of these conformation under different conditions e.g. changes in pH, temperatures, salt concentrations and addition of the cosolvents.

Special care should be devoted to sample preparation. All samples prepared for CD measurements should be of the highest possible purity due to the fact that contaminations lead to deceptive results. The high concentrations of chloride and nitrate, as well as common chelators (ethylene glycol tetraacetic acid (EGTA)/ethylenediaminetetraacetic acid (EDTA)) and reducing agents (dithiothreitol and 2-mercaptoethanol) should be avoided in the buffer. It is also not advisable to use certain organic solvents (dioxane, dimethyl sulfoxide (DMSO)) and some biological buffers such as HEPES, PIPES, and MES. If the IDP target is oxygen sensitive, anaerobic conditions should be established.

The CD data can be fitted using the secondary structure estimation program K2D3[10] (Louis-Jeune, Andrade-Navarro, and Perez-Iratxeta 2012).

Tip 22 – CD allows the determination of whether or not a purified protein is folded and how sample conditions affect its conformation or stability.

Dynamic Light Scattering (DLS), also known as Photon correlation spectroscopy or Quasi-elastic light scattering is a technique which can be used to determine such molecular

[10] http://www.ogic.ca/projects/k2d3/

parameters such as size, molar mass, and intermolecular interactions, which are important to identify and characterize intrinsically disordered proteins (IDPs). Coupled together with chromatography system it provides also information about aggregation state of the proteins.

In DLS light intensity fluctuations taking place at microsecond or millisecond scales are measured. Those fluctuations are a measure of the diffusion constant (Brownian motion) of the molecules and are related to the hydrodynamic radius (RH) of a molecule, also known as the Stokes radius. Measured RH reflects the apparent size adopted by the solvated tumbling molecule and thus is possible to monitor expansion or compaction of protein molecules. This is especially important for IDPs, which can be recognized and characterized by comparing the measured RH radii with those calculated for particular reference states, such as the compactly folded or the fully unfolded states.

Tip 23 - A useful procedure to analyse the basic conformational type of a protein through DLS is to utilize IDP like protein standard e.g. α-synuclein or a protein in the compactly folded globular state under the same conditions as the target protein in order to compare the measured Stokes radius.

Essential point in sample preparation for DLS measurements is removal of the interfering dust particles, by e.g. filtration of protein solution. Is important to remove unwanted scattering events that will exclude coherence and destroy determinations of the diffusion coefficient and therefore size of the sample of interest.

Tip 24 – The use of DLS attached to a fast protein liquid chromatography (FPLC) with SEC system might be applied for the investigation of the aggregation state of the IDPs, as well as efficient separation of their different assemblies such as oligomers.

Although DLS allows an easy and quick way to determine the value of the hydrodynamic Stokes radius (R_H), obtainment of the geometric radius of gyration (R_g) through this technique is usually hampered by an excessively small size of the protein. This limitation can be overcome by utilization of SAXS. The ratio of R_g and R_H (R_g/R_H) provides useful shape information about a protein molecule, being the most informative parameter comparing SAXS and DLS data for the same IDP measured at the same buffer, temperature and concentration conditions.

Tip 25 – Among many parameters that describe a molecule's size and shape, R_H is the most important information that can be obtained from DLS measurements of IDPs. A comparison with R_g from SAXS should be made.

Small-angle X-ray scattering (SAXS), as one of the method complementary to NMR, provide low-resolution structural characterization of biological macromolecules in solution. In a SAXS experiments, samples containing dissolved proteins are exposed to an X-ray bean and the scattered intensity is recorded by a detector as a function of the scattering angle (Petoukhov and Svergun 2013).

The major advantage of the method lies in its ability to provide structural information about partially or completely disordered systems. SAXS mostly contributes to obtain information about the IDPs hydrodynamic behavior and topology of the polypeptide chain. This techniques is also employed for the validation of structural models, analysis of oligomeric states, and the estimation of volume fractions of components in mixtures..

Tip 26 – Many IDPs are prone to aggregate, making SAXS measurements a challenging task. The sample preparation conditions may need to be redesigned according to the SAXS instrumentation capabilities.

SAXS not only provides shapes, oligomeric states, and quaternary structures of folded protein complexes, but also allows for the quantitative analysis of flexible systems. This fact can be successfully used to study the conformational flexibility of IDPs (Bernadó and Svergun 2012a; Bernadó et al. 2007) and allows the exploration of different protein conformations in response to variations in external conditions such as buffer composition, ionic strength, pH, and temperature. Temperature measurements are particularly useful for studies of the thermodynamic characteristics of IDPs. However, in order to avoid radiation damage, SAXS measurements are usually made below room temperature.

Sample preparation for SAXS experiments should follow the standard guidelines (Jacques et al. 2012). SAXS experiments typically require a highly pure, monodisperse protein solution in a concentration range from 1-10 mg/ml in order to fulfil the condition of a "dilute" solution. The concentrations must be determined accurately as it is necessary to appropriately normalize the scattering data and thus to estimate the effective molecular mass of the solute. If the sample is aggregated, the scattering data will be difficult or even impossible to interpret. A typical sample volume required for each single measurement depends on the SAXS station and a volume of about 50 µl is typically required for each single measurement. Each SAXS experiment at a given condition should be prepared in at least three different concentrations. Each condition such as buffer, ionic strength, pH, and temperature therefore requires 1-2 mg of purified sample. The concentration range can be prepared by dilution of a concentrated stock, if it is known that the protein is not affected by aggregation. In case the protein tends to aggregate it is better to prepare a stock of diluted protein sample and then prepare the concentrated samples immediately before the SAXS experiments. Is important to note that for each experiment at a given condition, the scattering of the buffer is also measured by SAXS for further subtraction. Thus the buffer composition must precisely match the composition of the sample. Even a small mismatch in the chemical composition of the solvent between the

buffer and the sample may lead to difficulties during background subtraction. The best approach is to use the dialysis buffer in which the protein was prepared.

Different strategies and software packages are available for the analysis of the SAXS data. One example is the protocols based on the use of the program ATSAS, which is in use at the German Electron Synchrotron DESY (Konarev et al. 2006; Petoukhov et al. 2012). The ATSAS package also includes the Ensemble Optimization Method (EOM), which has been developed as a strategy for the structural characterization of IDPs (Bernadó et al. 2007). This program takes into consideration an infinite amount of conformations that are in fast equilibrium exchange and is especially useful for flexible systems.

References

Armstrong, D J, and A Roman. 1993. "The Anomalous Electrophoretic Behavior of the Human Papillomavirus Type 16 E7 Protein Is Due to the High Content of Acidic Amino Acid Residues." *Biochemical and Biophysical Research Communications* 192(3): 1380–87.

Arnau, José et al. 2006. "Current Strategies for the Use of Affinity Tags and Tag Removal for the Purification of Recombinant Proteins." *Protein expression and purification* 48(1): 1–13.

Babich, H, and G Stotzky. 1978. "Toxicity of Zinc to Fungi, Bacteria, and Coliphages: Influence of Chloride Ions.." *Applied and Environmental Microbiology* 36(6): 906–14.

Bermel, Wolfgang et al. 2012. "Speeding Up Sequence Specific Assignment of IDPs." *Journal of biomolecular NMR* 53(4): 293–301.

Bernadó, Pau et al. 2007. "Structural Characterization of Flexible Proteins Using Small-Angle X-Ray Scattering.." *Journal of the American Chemical Society* 129(17): 5656–64.

Bernadó, Pau, and Dmitri I Svergun. 2012a. "Analysis of Intrinsically Disordered Proteins by Small-Angle X-Ray Scattering.." *Methods in molecular biology (Clifton, N.J.)* 896: 107–22.

Bernadó, Pau, and Dmitri I Svergun. 2012b. "Structural Analysis of Intrinsically Disordered Proteins by Small-Angle X-Ray Scattering.." *Mol. BioSyst.* 8(1): 151–67.

Block, Helena et al. 2009. "Immobilized-Metal Affinity Chromatography (IMAC): a Review.." *Methods in enzymology* 463: 439–73.

Brito, R M M, and W L C Vaz. 1986. "Determination of the Critical Micelle Concentration of Surfactants Using the Fluorescent-Probe N-Phenyl-1-Naphthylamine." *Analytical biochemistry* 152(2): 250–55.

Burgess, RR, RB Richard, and PD Murray. 2009. "Refolding Solubilized Inclusion Body Proteins." *Methods Enzymol*: 259–82.

Coutard, Bruno et al. 2012. "Single pH Buffer Refolding Screen for Protein From Inclusion Bodies.." *Protein expression and purification* 82(2): 352–59.

Cowieson, Nathan P et al. 2006. "An Automatable Screen for the Rapid Identification of Proteins Amenable to Refolding." *Proteomics* 6(6): 1750–57.

Das, Utpal et al. 2007. "Inhibition of Protein Aggregation: Supramolecular Assemblies of Arginine Hold the Key" ed. Suzannah Rutherford. *PloS one* 2(11).

Davey, Norman E, Niall J Haslam, Denis C Shields, and Richard J Edwards. 2010. "SLiMFinder: a Web Server to Find Novel, Significantly Over-Represented, Short Protein Motifs.." *Nucleic Acids Research* 38(Web Server issue): W534–39.

Di Marco, Valerio B, and G Giorgio Bombi. 2006. "Electrospray Mass Spectrometry (ESI- MS) in the Study of Metal–Ligand Solution Equilibria." *Mass Spectrometry Reviews* 25(3): 347–79.

Disfani, Fatemeh Miri et al. 2012. "MoRFpred, a Computational Tool for Sequence-Based Prediction

and Characterization of Short Disorder-to-Order Transitioning Binding Regions in Proteins." *Bioinformatics (Oxford, England)* 28(12): i75–i83.

Dunker, A K et al. 2001. "Intrinsically Disordered Protein.." *Journal of molecular graphics & modelling* 19(1): 26–59.

Dunker, A K, and Z Obradovic. 2001. "The Protein Trinity - Linking Function and Disorder." *Nature biotechnology* 19(9): 805–6.

Dunker, A Keith et al. 2008. "The Unfoldomics Decade: an Update on Intrinsically Disordered Proteins.." *BMC genomics* 9 Suppl 2(Suppl 2): S1.

Esposito, Dominic, and Deb K Chatterjee. 2006. "Enhancement of Soluble Protein Expression Through the Use of Fusion Tags." *Current opinion in biotechnology* 17(4): 353–58.

Eswar, Narayanan et al. 2006. "Comparative Protein Structure Modeling Using Modeller.." *Current protocols in bioinformatics / editoral board, Andreas D. Baxevanis ... [et al.]* UNIT 5.6: Unit5.6.

Gasteiger, Elisabeth et al. 2005. *Protein Identification and Analysis Tools on the ExPASy Server*. Totowa, NJ: Humana Press.

Getz, Elise Burmeister et al. 1999. "A Comparison Between the Sulfhydryl Reductants Tris(2-Carboxyethyl)Phosphine and Dithiothreitol for Use in Protein Biochemistry." *Analytical biochemistry* 273(1): 73–80.

Graceffa, Philip, Agnes Jancsó, and Katsuhide Mabuchi. 1992. "Modification of Acidic Residues Normalizes Sodium Dodecyl Sulfate-Polyacrylamide Gel Electrophoresis of Caldesmon and Other Proteins That Migrate Anomalously." *Archives of biochemistry and biophysics* 297(1): 46–51.

Gupta, B B. 1983. "Determination of Native and Denatured Milk Proteins by High-Performance Size Exclusion Chromatography." *Journal of Chromatography A* 282: 463–75.

Hunt, Ian. 2005. "From Gene to Protein: a Review of New and Enabling Technologies for Multi-Parallel Protein Expression." *Protein expression and purification* 40(1): 1–22.

Ignatova, Zoya, and Lila M Gierasch. 2006. "Inhibition of Protein Aggregation in Vitro and in Vivo by a Natural Osmoprotectant." *Proceedings of the National Academy of Sciences* 103(36): 13357–61.

Jacques, David A, J Mitchell Guss, Dmitri I Svergun, and Jill Trewhella. 2012. "Publication Guidelines for Structural Modelling of Small-Angle Scattering Data From Biomolecules in Solution.." *Acta crystallographica. Section D, Biological crystallography* 68(Pt 6): 620–26.

Jana, S, and J K Deb. 2005. "Strategies for Efficient Production of Heterologous Proteins in Escherichia Coli." *Applied Microbiology and Biotechnology* 67(3): 289–98.

Jumpertz, Thorsten et al. 2011. "High-Throughput Evaluation of the Critical Micelle Concentration of Detergents." *Analytical biochemistry* 408(1): 64–70.

Kaltashov, Igor A, Cedric E Bobst, and Rinat R Abzalimov. 2013. “Mass Spectrometry-Based Methods to Study Protein Architecture and Dynamics..” *Protein science : a publication of the Protein Society* 22(5): 530–44.

Katzen, Federico. 2007. “Gateway ®Recombinational Cloning: a Biological Operating System.” *Expert Opinion on Drug Discovery* 2(4): 571–89.

Kelly, Sharon M, Thomas J Jess, and Nicholas C Price. 2005. “How to Study Proteins by Circular Dichroism.” *Biochimica et Biophysica Acta (BBA) - Proteins and Proteomics* 1751(2): 119–39.

Kindermann, Birgit et al. 2005. “Effects of Increased Cellular Zinc Levels on Gene and Protein Expression in HT-29 Cells.” *Biometals* 18(3): 243–53.

Knapman, T W, N M Valette, S L Warriner, and A E Ashcroft. 2013. “Ion Mobility Spectrometry-Mass Spectrometry of Intrinsically Unfolded Proteins: Trying to Put Order Into Disorder..” *Current analytical chemistry* 9(2): 181–91.

Konarev, P V, M V Petoukhov, V V Volkov, and D I Svergun. 2006. “ATSAS 2.1, a Program Package for Small-Angle Scattering Data Analysis.” *J. Appl. Crystallogr.* 39(2): 277–86.

Krezel, Artur, Rafał Latajka, Grzegorz D Bujacz, and Wojciech Bal. 2003. “Coordination Properties of Tris(2-Carboxyethyl)Phosphine, a Newly Introduced Thiol Reductant, and Its Oxide..” *Inorganic chemistry* 42(6): 1994–2003.

Lesley, Scott A. 2009. “Parallel Methods for Expression and Purification.” In *Methods in Enzymology*, Methods in Enzymology, Elsevier, 767–85.

Linn, Stuart. 2009. “Strategies and Considerations for Protein Purifications.” In *Methods in Enzymology*, Methods in Enzymology, Elsevier, 9–19.

Louis-Jeune, Caroline, Miguel A Andrade-Navarro, and Carol Perez-Iratxeta. 2012. “Prediction of Protein Secondary Structure From Circular Dichroism Using Theoretically Derived Spectra.” *Proteins* 80(2): 374–81.

Malhotra, Arun. 2009. “Tagging for Protein Expression.” In *Methods in Enzymology*, Methods in Enzymology, Elsevier, 239–58.

Mészáros, Bálint, István Simon, and Zsuzsanna Dosztányi. 2009. “Prediction of Protein Binding Regions in Disordered Proteins” ed. Rita Casadio. *PLoS computational biology* 5(5): e1000376.

Oates, Matt E et al. 2013. “D²P²: Database of Disordered Protein Predictions..” *Nucleic Acids Research* 41(Database issue): D508–16.

Outten, Caryn E, and and Thomas V O'Halloran. 2001. “Femtomolar Sensitivity of Metalloregulatory Proteins Controlling Zinc Homeostasis.” *Science (New York, N.Y.)* 292(5526): 2488–92.

Petoukhov, M V et al. 2012. “New Developments in the ATSAS Program Package for Small-Angle Scattering Data Analysis.” *J. Appl. Crystallogr.* 45(2): 342–50.

Petoukhov, Maxim V, and Dmitri I Svergun. 2013. “Applications of Small-Angle X-Ray Scattering to

Biomacromolecular Solutions..” *The international journal of biochemistry & cell biology* 45(2): 429–37.

Qoronfleh, M Walid, Lyndal K Hesterberg, and Matthew B Seefeldt. 2007. “Confronting High-Throughput Protein Refolding Using High Pressure and Solution Screens.” *Protein expression and purification* 55(2): 209–24.

Radivojac, Predrag et al. 2007. “Intrinsic Disorder and Functional Proteomics..” *Biophysical journal* 92(5): 1439–56.

Schenk, P M, S Baumann, R Mattes, and H Steinbiss. 1995. “Improved High-Level Expression System for Eukaryotic Genes in Escherichia Coli Using T7 RNA Polymerase and Rare ArgtRNAs..” *BioTechniques* 19(2): 196–200.

Shatzman, A R. 1995. 6 Current opinion in biotechnology *Expression Systems*.

Sickmeier, M et al. 2007. “DisProt: the Database of Disordered Proteins.” *Nucleic Acids Research* 35(Database): D786–93.

Singh, Surinder Mohan, Singh, Surinder Mohan, Amulya Kumar Panda, and Amulya Kumar Panda. 2005. “Solubilization and Refolding of Bacterial Inclusion Body Proteins.” *Journal of Bioscience and Bioengineering* 99(4): 303–10.

Šali, Andrej, and Tom L Blundell. 1993. “Comparative Protein Modelling by Satisfaction of Spatial Restraints.” *Journal of molecular biology* 234(3): 779–815.

Theillet, Francois-Xavier et al. 2014. “Physicochemical Properties of Cells and Their Effects on Intrinsically Disordered Proteins (IDPs).” *Chemical reviews*: 140627063652000.

Theillet, François-Xavier et al. 2013. “The Alphabet of Intrinsic Disorder I. Act Like a Pro: on the Abundance and Roles of Proline Residues in Intrinsically Disordered Proteins.” *Intrinsically Disordered Proteins* 1(1): 0–12.

Tong, Kit I, Masayuki Yamamoto, and Toshiyuki Tanaka. 2008. “A Simple Method for Amino Acid Selective Isotope Labeling of Recombinant Proteins in E. Coli.” *Journal of biomolecular NMR* 42(1): 59–67.

Uversky, Vladimir N. 2011. “Intrinsically Disordered Proteins From a to Z..” *The international journal of biochemistry & cell biology* 43(8): 1090–1103.

Uversky, Vladimir N. 2013. “A Decade and a Half of Protein Intrinsic Disorder: Biology Still Waits for Physics..” *Protein science : a publication of the Protein Society* 22(6): 693–724.

Varadi, Mihaly et al. 2013. “pE-DB: a Database of Structural Ensembles of Intrinsically Disordered and of Unfolded Proteins..” *Nucleic Acids Research*.

Vincentelli, R et al. 2004. “High-Throughput Automated Refolding Screening of Inclusion Bodies.” *Protein Science* 13(10): 2782–92.

Ward, J J et al. 2004. “Prediction and Functional Analysis of Native Disorder in Proteins From the

Three Kingdoms of Life." *Journal of molecular biology* 337(3): 635–45.

Weinhandl, Katrin, Margit Winkler, Anton Glieder, and Andrea Camattari. 2014. "Carbon Source Dependent Promoters in Yeasts.." *Microbial cell factories* 13(1): 5.

Chapter 4 Conclusions

This thesis is focused on expression, purification, as well as structural and biochemical characterization of potential amyloidogenic proteins: Aβ peptides and hSOD. Both of these proteins very often misfolds and evades normal clearance pathways, what results in pathogenic process in which the protein aggregates progressively into intracellular and/or extracellular deposits. The consequence of aggregation of Aβ peptides and hSOD in characteristic patterns and locations is Alzheimer's disease (AD) and amyotrophic lateral sclerosis (ALS), respectively. The molecular mechanism of both these neurodegenerative disorders is still unclear and unveiled and until now no efficient treatments are available for AD and ALS.

A detailed structural and functional characterization of fibrillar assemblies as well as the various prefibrillar intermediates is crucial for understanding Aβ precise mechanism aggregation pathways and identifying toxic Aβ species. Therefore we focused on the investigation of different Aβ assemblies. Section 3.1 show application of a novel method defined as sedimented solutes NMR (SedNMR) to detailed structural characterization of oligomeric and prefibrillar assemblies. We proved that SedNMR allows to trapped Aβ aggregates in a fully hydrated environment without adding cosolvents or interaction partners, therefore providing a unique way to access the formation kinetics and structural features of these species with reduced perturbations. Obtained qualitative picture of intermediates structural features provide evidence that these prefibrillar assemblies already contain β-strand structures (especially most hydrophobic regions), but with different supramolecular organizations and reduced structural order and periodic symmetry and demonstrate probable pathway from these fibril precursors to terminal fibrillar states. Section 3.2 is focused on high resolution structural characterization of AβM40 and AβM42 mixture fibrils prepared in different molar ratio related to the pathological conditions. Optimized sample preparation is crucial for obtaining high resolution SSNMR spectra on these biomacromolecular assemblies and only high homogeneity (conformational homogeneity and local order of packing) of the samples permits a full assignment of SSNMR signals. The collective data obtained through SSNMR demonstrate that a change in the AβM42:AβM40 ratio induces differences in conformational plasticity of the peptide mixtures, that clearly shown that these two species interact and change each other's dynamic behaviour. The new structural model derived from high resolution data and the identification of AβM40:AβM42 reciprocal association in the

fibrils should broaden our understanding of exacts structural properties, as well as interaction and behaviour of these components. Finally structural information of Aβ amyloid fibril formation is fundamental for the development of diagnostics and therapeutic approaches, and in addition might be valuable for elucidating fundamental mechanism of proteins folding and assembly.

Although the causes of motor neuron death in ALS are poorly understood, a prominent hypothesis for SOD1-linked familial ALS involves the formation of protein aggregates containing misfolded hSOD1 as the main component in amyloid-like deposits. Therefore many studies have been focused on the investigation of the therapeutic strategies aimed to prevent SOD1 pathogenic aggregation. One of the rational drug design was established based on previous knowledge on the chemical mechanism of apo SOD1 aggregation and the chemical reactivity of cisplatin that selectively binds to solvent exposed Cys-111 and strongly inhibits process of oligomerization. Section 3.3 demonstrates attempt of reverting side effects caused by cisplatin, since clinical use of this chemotherapeutic agent is severely limited by the development of neurotoxicity and others undesirable effects. We proposed that chemically synthesized new molecues, ADM_09 and ADM_12 are possible candidates in suppression of neuropathic pain. Although the actual mechanism of action of these molecules has yet to be established, the findings reported in this work open the way to the development of a new generation of compounds remarkably effective in the treatment of cisplatinum-induced neuropathy without eliciting the most common negative side-effects, what could open a door toward a novel therapeutic strategies in ALS.

Section 3.4 and section 3.5 are book's chapters and are integral part of *"Intrinsically disordered protein by NMR"* book. Section 3.4 comprise history of the discovery of beta amyloid protein and it's proteolytic biogenesis, polymorphism widely observed for Aβ amyloidal aggregates in vitro, overview of functional polymorphism and structural models of amyloidal fibrils, review of the methods of immobilization and investigation of amyloidal intermediate species, as well as association between neurotoxicity and different ratios of Aβ40 to Aβ42, which provide the stability to neurotoxic species. Last subsection contains materials and methods, as well as practice advice about handling with Aβ samples. Section 3.5 contains such issue as genome browsing and bioinformatics analysis, expression plasmid generation and different approaches of protein expression and purification. Last subsection is devoted to different methodologies with special highlight for tips and tricks helpful to overcome common drawbacks/barriers usually faced when working with IDPs.